# Design and validation of a non-invasive method for the treatment of varicose veins using high-intensity focused ultrasound

Nesrine Barnat

PSL UNIVERSITÉ PARIS

THÈSE DE DOCTORAT
DE L'UNIVERSITÉ PSL

Préparée à l'ESPCI Paris

# Design and validation of a non-invasive method for the treatment of varicose veins using high-intensity focused ultrasound

## Conception et validation d'une méthode non-invasive de traitement des varices par ultrasons focalisés de haute intensité


Soutenue par

**Nesrine BARNAT**

Le 29 novembre 2019


Ecole doctorale n° 564

**Physique en Ile de France**

Laboratoire

**Physique pour la Médecine Paris**

Spécialité

**Physique**

Composition du jury :

| | |
|---|---|
| Catherine, GHEZZI<br>PU, Université Joseph Fourier Grenoble | *Président* |
| Cécile, BARON<br>CR, Université Aix-Marseille - CNRS | *Rapporteur* |
| Bradley, TREEBY<br>Associate professor, University College London | *Rapporteur* |
| Arnaud, DERODE<br>PU, Institut Langevin Paris VII | *Examinateur* |
| Sylvain, YON<br>Ingénieur, THERACLION | *Examinateur* |
| Jean-François, AUBRY<br>DR, ESPCI-CNRS | *Directeur de thèse* |

Confidentielle jusqu'au 1 septembre 2025

ESPCI PARIS | PSL

*To my parents, Latifa and Mustapha, both the noor of my eyes*

*To my grandma Zouzou, who never left my mind*

*It always seems impossible until it's done.*

-Nelson Mandela-

اطلب وستنال مطالبك

*[Traduction] Désire, et tes désirs seront accomplis.*

-*La peau de chagrin,* Honoré de Balzac-

# Remerciements

C’est à la fois avec grand enthousiasme et émotion que je rédige la dernière page de mon manuscrit, mes remerciements. J’ai eu le grand privilège de faire une thèse avec un sujet qui me passionnait mais j’ai surtout eu une chance inouïe d’avoir été entourée de personnes fabuleuses et brillantes.

Mes premiers remerciements s’adressent à mon directeur de thèse, Jean-François Aubry, mon co-encadrant, Sylvain Yon et mes collègues avec qui j’ai travaillé de façon étroite durant ces trois années, Jérémie Anquez, Anthony Grisey et Björn Gerold.

Merci à Jean-François, pour la qualité de son encadrement, ses nombreuses relectures et ses corrections qui ont contribué à grandement améliorer ce manuscrit et mes articles scientifiques. En plus de son expertise internationalement reconnue, son investissement scientifique hors-norme pour faire de la belle recherche, il a tout le long de ma thèse fait preuve d’une extrême gentillesse, psychologie et empathie. Merci d’avoir accepté de m’encadrer, quel immense privilège de t’avoir eu pour directeur de thèse ! J’adresse également mes remerciements à Sylvain pour m’avoir donné les moyens et permis d’effectuer cette thèse.

Un grand merci à Jérémie, pour le partage généreux de ses connaissances et expertises en recherche préclinique, ses remarques et ses conseils toujours pertinents. Je tiens également à le remercier de m’avoir transmis son virus perfectionniste, me voilà, grâce à lui, psychopathe du détail. Merci pour ta grande sympathie, ta patience, ton écoute toujours attentive, ton soutien, tes encouragements et toutes « les remises en confiance » dans mes moments de doute.

Mes pensées s’adressent maintenant à Anthony, mon compagnon d’expériences à l’intelligence foudroyante mêlée à un enthousiasme abondant et une bienveillance intarissable. Merci pour ton aide pour les simulations, tes astuces de geek (et oui, Anthoïde..), tes relectures nourrissantes, tes nombreux enseignements allant jusqu’au combat de girafes et enfin pour les multiples conseils que tu m’as prodigués tout le long. Même si je n’ai pas suivi tes recommandations de rédaction régulière,

je dois dire que ta méthode « boulettes » bien à points, m'a bigrement aidé à rédiger correctement… c'est peut-être d'ailleurs à breveter ?

A Björn, ce collègue devenu un ami, qui en plus de ses talents de physicien, sa maîtrise courante de quatre langues et son aisance sur presque tous les terrains, sait rester humble. Merci pour ton écoute, tes relectures et tes retours. Je retiendrai ton franc-parler qui m'a aidé à plusieurs reprises à améliorer mes présentations et mes rédactions.

J'exprime toute ma gratitude envers les membres du jury de ma thèse, en particulier Cécile Baron et Bradley Treeby, pour avoir accepté de rapporter ce travail. Merci à Catherine Ghezzi de m'avoir fait l'honneur de présider mon jury de soutenance ainsi qu'à Arnaud Derode pour avoir accepté d'examiner et juger mon travail.

Je tiens à remercier toute l'équipe de Theraclion pour leur sympathie prodiguée tout le long de ma thèse, leur présence et leur soutien unanimes lors de ma soutenance. À Quentin, pour m'avoir encadrée le premier à Theraclion avec grand professionnalisme et pour tous les fous rires partagés. Mes hommages à l'équipe très noble de production et service présente (Gaylord et Mathieu) et celle passée (Yasmine et Mickaël), avec qui j'ai toujours eu grand plaisir de discuter et plaisanter. A l'équipe de développement et test logiciel pour toutes leurs aides accordées. Une mention spéciale à Jérôme et Éric pour nos repas de midi partagés bien à quatorze heures.

Merci au trio de choc de l'équipe clinique, Michel, Dorothée et Carole pour leur travail d'arrache-pied pour les essais cliniques et leur gaieté (oui, toi aussi Carole...). A Vivien, l'auto-proclamé « King of QARA », pour sa bonne humeur contagieuse et ses anecdotes inépuisables. Merci à David Au. pour son intérêt porté à ma thèse. Enfin, j'exprime ma gratitude à la yogi de Theraclion, Sandrine, pour la gestion et les plis administratifs.

Je tiens également à remercier David Caumartin pour son énergie dépensée pour Theraclion et Mickaël Tanter pour m'avoir accueilli au sein du beau labo Physique pour la Médecine Paris.

À tous les membres du labo, qui même si je n'ai pas souvent été présente, m'ont toujours accueilli avec beaucoup de gentillesse et sympathie. Une attention particulière à Victor F., Daniel S., Guillaume M., Jérôme B., David A., Thomas B., Thomas T., Alexandre D., Momo et Hanna.

Merci à Benoît de l'École Nationale Vétérinaire de Maisons-Alfort pour son professionnalisme, son implication, ses lapins et ses brebis.

Je tiens finalement à adresser mes remerciements à toutes celles et ceux qui m'ont soutenu durant ces trois années et m'ont permis de me déloger de mes travaux. À mes amis intimes, Mathilde, Anaïs, Baptiste et Emna. A mon tonton, pour son intérêt et son affection. Merci à mes oncles, tantes, cousins, cousines et tous ceux qui sont venus à ma soutenance. A mon cousin et meilleur ami, l'hilare Youssef, pour toutes les bêtises passées et celles à venir et les rires qui n'ont jamais manqué.

Aux trois petits mousquetaires adorables et folichons de la famille, mes nièces, Lyna et Anna, et mon neveu Gabriel. J'ai enfin une pensée émue à ma grand-mère, mama Zohra, partie au début de ma thèse. Repose en paix Zouzou.

Je tiens finalement à remercier mon grand frère, Bady, pour m'avoir donné, le premier, goût aux sciences et pour ses nombreuses aides conférées. À ma grande sœur, Nouria, pour son oreille attentive et pour avoir fait preuve d'une grande et étonnante patience envers moi ces trois années. À ma petite sœur, Wided, pour avoir, la première, lu et apprécié mon introduction générale.

Pour terminer, je tiens à remercier de tout cœur mes parents, Mustapha et Latifa, pour leur confiance aveugle en mes capacités, leur soutien inépuisable, leur présence permanente et leur tendresse, qui m'est si chère. Ma thèse, c'est aussi la vôtre.

# Abstract

A novel thermal approach to treat non-invasively incompetent veins with high-intensity focused ultrasound (HIFU) is presented in this thesis.

The ability to occlude small veins was first investigated. Two different sonication procedures were evaluated by numerical simulations and tested *in vivo* on rabbit veins. The histologic examination of the treated veins demonstrated the efficacy of the treatments, especially when the vein was compressed during ultrasonic exposures.

A new procedure was then designed in order to coagulate larger veins, closer to human vein diameters. Experimental temperature measurements at the vein wall during HIFU pulses were used as inputs to determine numerically the optimum spacing between the pulses in order to induce a continuous coagulation along the vein. Acute animal trials on sheep veins were conducted to quantify tissue damages following such treatments. Finally, chronic studies up to 90 days were conducted on sheep in order to evaluate the long-term safety and efficacy of our treatment procedure. The histological findings validated the performance and safety of our HIFU thermal method, in a sheep model. From a pathology standpoint, the HIFU lesions are similar to those observed after radiofrequency ablation (an endovenous thermal modality used for the treatment of varicose veins).

The results presented in this thesis allowed Theraclion to get the authorization to conduct first-in-human clinical trials for varicose vein treatments. The results were very encouraging and led to the CE-marking of the HIFU system.

**Keywords:** HIFU, focused ultrasound, varicose veins, veins, thermal ablation, numerical simulations, preclinical trials, clinical trials.

# Résumé

Cette thèse avait pour objectif le développement d'une méthode d'ablation thermique non-invasive des veines par ultrasons focalisés de haute intensité (HIFU). Elle a pour but de démontrer la preuve de concepts et permettre à terme le traitement des varices des membres inférieurs avec le dispositif de Theraclion.

La possibilité d'occlure des vaisseaux de petits calibres a tout d'abord été investiguée. Deux procédures de traitement candidates ont été évaluées par simulations numériques puis *in vivo* sur des veines de lapin. L'analyse histologique a démontré l'efficacité des traitements, en particulier lorsque les vaisseaux étaient comprimés lors des tirs.

Une nouvelle procédure d'ablation thermique a ensuite été conçue pour coaguler des veines de plus gros calibres, de diamètre plus proche des varices humaines. Des mesures de températures *in vivo* sur des veines de brebis lors de tirs HIFU ont permis d'estimer le pas de tir permettant d'obtenir une coagulation continue le long de la veine. Des essais en aigu sur des veines saphènes de brebis ont permis de quantifier les dommages thermiques et de valider l'efficacité immédiate de notre méthode de traitement. Enfin, une étude avec suivis distants jusqu'à 90 jours a été conduite chez la brebis afin d'étudier l'efficacité et la sécurité à long terme de notre méthode de traitement. L'analyse histologique des dommages thermiques a validé sur la brebis la performance et la sécurité de notre méthode d'ablation thermique. D'un point de vue histopathologique, les dommages engendrés par nos traitements HIFU se sont également révélés similaires à ceux observés après traitement par radiofréquence, une technique endovasculaire d'ablation thermique des varices.

L'ensemble de ces travaux a permis à Theraclion d'obtenir l'autorisation de conduire un essai clinique sur 50 patients. Les résultats très positifs de cette étude ont

conduit à l'obtention du marquage CE du dispositif HIFU pour cette indication thérapeutique.

**Mots-clés :** HIFU, ultrasons focalisés, varices, veines, ablation thermique, simulations numériques, essais précliniques, essais cliniques.

# Contents

# List of Figures

# List of Tables

# List of Abbreviations

| | |
|---|---|
| AASV | Anterior Accessory Saphenous Vein |
| CFL | Courant-Friedrichs-Lewy |
| DF | Duty Factor |
| DVT | Deep Venous Thrombosis |
| EVLA | Endovenous Laser Ablation |
| FUS | Focused Ultrasound Surgery |
| GET | Gomori's Elastin Trichrome |
| GSV | Great Saphenous Vein |
| HE | Hematoxylin Eosin |
| HIFU | High-Intensity Focused Ultrasound |
| ITA | Temporal-Average Intensity |
| MRI | Magnetic Resonance Imaging |
| PASV | Posterior Accessory Saphenous Vein |
| PML | Perfectly Matched Layer |
| PRF | Pulse Repetition Frequency |
| PRP | Pulse Repetition Period |
| RF | Radiofrequency |
| RFA | Radiofrequency Ablation |
| rms | root mean square |
| SFJ | Sapheno-Femoral Junction |
| SSV | Small Saphenous Vein |
| US | Ultrasound |
| VTU | Visualization and Treatment Unit |

# 1

# Introduction

## 1.1 General introduction

Varicose veins of the lower limbs, referred to as pathologically enlarged superficial veins, are a common pathological condition known since the old ages [1], [2].

The earliest references to this affliction have been found in the Ebers papyrus written in the sixteenth century BC. Surgery for varicose veins is however clearly contraindicated in this medical papyrus [3]. The first description of a treatment for this disease can be found in the writings of Hippocrates in the fourth century BC: the treatment consisted in traumatizing varicose veins with a slender iron instrument in order to cause thrombosis [4].

Aulus Cornelus Celsus is attributed as one of the first operating on varicose veins [5]. He practiced avulsion of varicose veins with a hook [3]. The principle of this treatment is similar to the current technique of phlebectomy, except that at that time the patient experienced a terrible pain. Plutarch reported that the Roman general Gaius Marius, well-known to be extremely resistant to suffering, refused his second leg to be treated for varicose veins saying that: “the cure is not worth the pain [5]”.

The great boost to varicose vein surgery came from the Byzantine physician Oribasius of Pergamum [6]. He devoted three chapters of his surgery book to the treatment of varicose veins and some of his recommendations are still valid. Paul of Aegina, a Byzantine Greek physician of the seventh century, described the anatomy of varicose veins and identified the great saphenous vein (GSV) as the source of the problem. His approach consisted in combining phlebectomy and ligation for the treatment of an incompetent GSV [3].

The stripping method (that is still currently used) was first introduced by the Andalusian physician Abu Al-Qasim Khalaf Ibn Abbas Al-Zahrawi who was using an external stripper in a manner deemed remarkably precise [3]. More recently, in the latter part of the nineteenth century, the treatment of varicose veins took a new direction with the introduction of sclerotherapy [3].

The method of sclerotherapy, referring to the injection of a sclerosant agent into the vein lumen to obstruct it, was first applied to the treatment of varicose veins by the French surgeon Joseph Pierre Pétrequin [3]. The occurrence of adverse events following liquid sclerotherapy discredited this method and surgical removal of varicose veins remained the gold standard treatment for many years.

In the twenty-first century, the medical care for varicose vein disease has evolved and now varicose veins can be either surgically removed through small incisions or ablated with minimally invasive endovenous techniques like ultrasound-guided foam sclerotherapy (UGFS) or with endovenous thermal ablation therapies. In this latter case, ablation of varicose veins can be accomplished by either radiofrequency (RF) or laser. In both cases, a catheter is inserted into the targeted vein and the vein wall is heated via radiofrequency or laser irradiation. By thermally damaging vein walls, both methods aim at shrinking or occluding the varicose vein in the long-term.

These thermal-based ablation techniques have been proven to be safe and effective in treating varicose veins with even faster recovery and better cosmetic results than stripping [7]–[11]. However, these methods still involve cutaneous incisions as they require insertion of a laser or radiofrequency probes into the vein to deliver heat. In addition, catheter insertion and maneuver in a tortuous vein may be arduous [12] as well as the tumescent anesthesia usually performed before treatment to protect perivascular tissues, decrease diameter of the vein and provide a local anesthesia [13].

Similarly to endovenous thermal ablation, High-Intensity Focused Ultrasound (HIFU) can induce rapid temperature elevation deep within tissue. Moreover, HIFU has the major advantage over RF and laser thermal ablation methods of being completely non-invasive. When applied to tissue, a highly focused beam crosses the skin harmlessly and produces local temperature elevation within the focal volume only achieving a thermal energy deposition comparable to that reported with other thermal methods [14], [15]. This tissue ablation technique based on the use of high-intensity focused beams causes temperature elevation by absorption of ultrasound within tissues. An important feature of

this treatment modality is the ability of inducing a lesion non-invasively within the body, while leaving surrounding tissues unharmed.

The first suggestion of the use of HIFU for therapeutic purposes was in 1942 and the first report of application to humans was in 1960 [16]. The use of sharply focused beams to produce tissue ablation was initially investigated in the brain but was also explored for other purposes like in ophthalmology [17]. This technique did not gain much clinical acceptance before the mid-90s. Several reasons have been proposed to explain the initial lack of enthusiasm. One relates to the equipment that was cumbersome. Another reason of the restriction growth of HIFU application was attributed to the lack of imaging sophistication. Indeed, precise targeting is necessary to achieve accurate placement of HIFU lesions. Technological advances in diagnostic imaging within the past twenty years have contributed to the renewed interest of this technique in clinical medicine.

Today, HIFU is clinically used to treat a plurality of diseases ranging from ophthalmological treatments to solid tumors [16], [18]. In addition to these clinical applications, a number of other potential therapeutic purposes of HIFU are investigated. In particular, HIFU-induced vascular occlusion has been explored for the hemostasis of hemorrhaging vessels, to stop bleeding in trauma patients in the field, as well as for the occlusion of non-bleeding blood vessels for several applications ranging from the destruction of tumor vessels to fetal medicine [19]–[31]. The role of HIFU for the treatment of varicose veins has also been suggested. Indeed, the good absorption of the blood vessel walls [32] and the location (no bones neither air in the close proximity) of the majority of the varicose veins in the lower limbs make HIFU suitable for thermally ablating varicose veins.

The use of HIFU as a non-invasive alternative to endovenous treatments has already been investigated in a number of preclinical studies [33]–[36]. Different ultrasound exposure parameters and different types of sonication have been used. All achieved to occlude small blood vessels (less than 2 mm in diameter). However, no study has investigated the sustainability and safety of the treatments applied. Indeed, these animal studies were carried out for a short period, at most 4 weeks after treatment, which is not sufficient to observe vein fibrosis in its healed state. Amongst the few studies that investigated occlusion in a sub-acute setting, the majority of vessels initially occluded immediately after treatment tended to regain patency over time [34], [35]. Moreover, vascular occlusion (even transient) was achieved only on small blood vessels (< 2 mm) and was not always induced non-invasively [28], [34]–[36]. Some of the investigators injected

agents in synergy with HIFU, like circulating agents, fibrinogen or even pro-inflammatory agents, which are known to act as a vein sclerosant to produce durable occlusion [35], [36]. From an industrial point of view, the regulatory path to allow the use of such agents in synergy with HIFU is long and uncertain. Finally, in these studies, little attention to damage to surrounding structures during vascular targeting has been provided. No study comprehensively documented the effects of HIFU treatment on neighboring tissues in the short and long-term.

## 1.2 Thesis aim and content

To overcome the limitations of these studies, the aim of this thesis was to develop a non-invasive thermal alternative to existing endovenous thermotherapies using the HIFU system initially commercialized by Theraclion for treating benign thyroid nodules and breast fibroadenomas. In order to be readily translated to the clinic, the HIFU treatment method should induce therapeutic effects similar to those obtained with current endovenous thermal ablative therapies while being non-invasive, safe, stand-alone and easily integrable to clinical practice.

This thesis is divided into eight chapters. In the second chapter, HIFU ablation is introduced and its potential role in the treatment of varicose veins is discussed. The general principles of acoustics are overviewed and the pathology of varicose veins as well as the main varicose veins treatments are presented. This chapter also gives an overview of the HIFU effects on veins with an emphasis on the HIFU-induced vascular occlusion as it is believed to be the intended therapeutic aim in the long-term for treating varicose veins.

Chapter 3 describes the materials used in this thesis. The HIFU device used throughout this thesis is presented and an overview of the treatment procedure currently applied clinically for the treatment of breast fibroadenomas and thyroid nodules is given. A short introduction of a HIFU simulation package developed at Theraclion, called HIFU treatment simulator, is also provided as it was used in this thesis.

The main content of this thesis is described in Chapters 4, 5, 6 and 7.
Chapter 4 presents a feasibility study assessing the ability of occluding small veins (2 mm diameter) with 4 seconds long pulses generated by the HIFU device presented in Chapter 3. In this study, two pulse trajectories were studied and for each, the number of sonications and the spacing between pulses to continuously coagulate vein segments of 2-cm in length

and 2-mm in diameter were first numerically investigated and then evaluated in vivo on rabbit veins.

Chapter 5 investigates how to coagulate bigger vein diameters closer to humans veins. Longer pulses (8-s pulses) were used in vivo on sheep and the spacing between the pulses along the vein was adjusted to induce a continuous coagulation over the vein length. In this chapter, the temperature elevations induced to the vein during HIFU ablation were measured in-situ and were compared to the ones reported during endovenous thermal ablation.

Chapter 6 presents an *in vivo* sheep study evaluating the ability of the HIFU treatment protocol to achieve venous shrinkage, which is the therapeutic endpoint for immediate treatment success. The lesion size induced to venous and perivenous tissues after HIFU ablation are assessed with gross pathology.

In Chapter 7, a chronic study was performed to assess macroscopically and microscopically the thermal damages and the healing of the venous and perivenous tissues following HIFU ablation of veins.

Finally, Chapter 8 concludes the thesis and addresses perspectives for future work.

# 2

# Background

This chapter is divided as follows. Section 2.1 introduces HIFU ablation and provides an overview of basic acoustic notions. Section 2.2 presents a short summary of the pathology of varicose veins and discusses the main existing therapies. Finally, section 2.3 gives a state of the art of preclinical studies which investigated HIFU-induced vascular occlusion on non-bleeding blood vessels. In addition, therapeutic mechanisms for HIFU-mediated vascular occlusion are discussed.

## 2.1 HIFU ablation technique

### 2.1.1 Basics of HIFU

High-intensity focused ultrasound (HIFU), also known as focused ultrasound surgery (FUS) is one of the numerous therapeutic applications that uses ultrasound for therapeutic purposes. The technique employs high-intensity focused beams to concentrate acoustic energy into a small soft tissue volume with the aim of producing a localized biological effect [37]. The principle of this technique is shown in Figure 2-1. The frequencies commonly employed for tissue ablation range from 200 kHz to 10 MHz whereas acoustic intensities usually applied to the focal region are in the range of 1-10 $kW.cm^{-2}$.

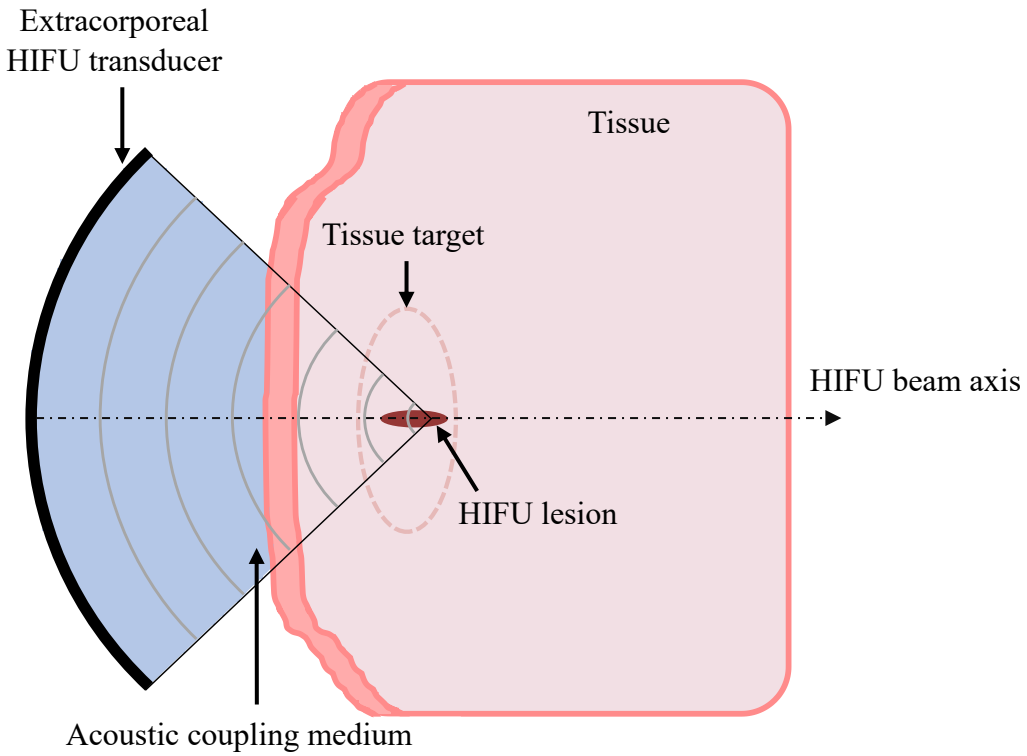


**Figure 2-1 – Illustration of the principle of HIFU.** In this diagram, HIFU waves are generated with an extracorporeal transducer and are focused deep onto a small volume of the tissue target. Intermediating tissues are undamaged.

The beam focusing enables to produce localized tissue destruction deep within the body without damaging intervening tissues. Focusing of the ultrasound can be achieved by several ways. Most often, it is produced by a spherical curved piezo-electric material [17] but focusing can also be achieved with multi-element phased-arrays allowing electronic beam steering. In the case of a single element transducer, the focus lies along the central axis of the transducer, near its center of curvature [17]. Figure 2-2 illustrates spherical focusing achieved with a single-element concave bowl transducer with an aperture diameter D, a radius of curvature R and a focal length F. The focal volume is cigar-shaped. The half width focal spot dimensions can be approximated to $l_{-6dB} \approx 1.41 \times \lambda \times \frac{F}{D}$ in the lateral dimension and to $L_{-6dB} \approx 9.7 \times \lambda \left(\frac{F}{D}\right)^2$ in the axial dimension (Figure 2-2). For example, at 3 MHz, and with a spherical transducer of 56 mm in diameter and a focal length of 38 mm, the focal spot is approximately an ellipsoid 1.6 mm long and 0.4 mm wide. As the frequency decreases, both the length and the width of the focal region increase.

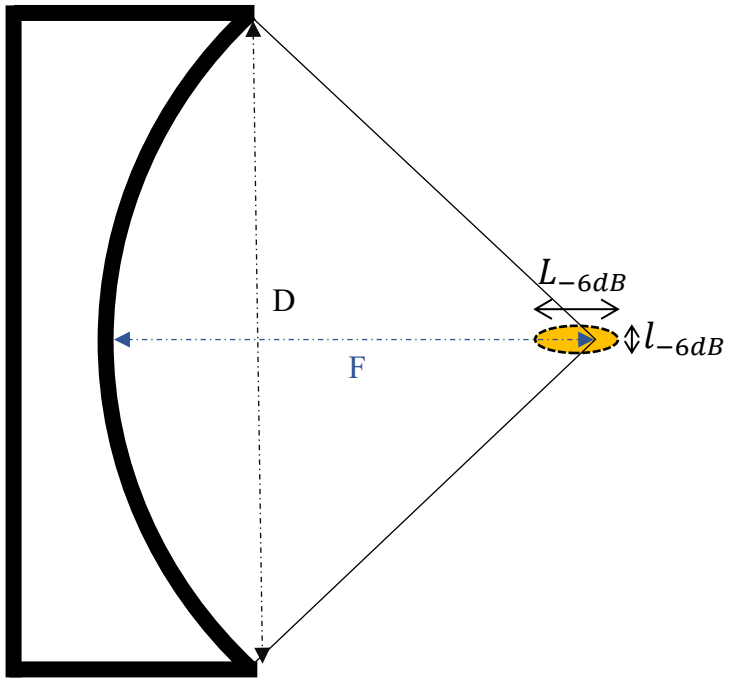


**Figure 2-2 – Schematic diagram of a spherical focusing with a single-element transducer.**

As for the size of the induced lesion following a single HIFU exposure, the precise shape and size depend on the ultrasound source characteristics but also on the properties of the tissue irradiated, the exposure power and the duration.

HIFU therapy is currently used throughout the world for many clinical applications like the treatment of benign and malignant solid tumors [18] and also for palliative care of bone metastasis [38] and neurologic applications [39]. Several other potential therapeutic applications are currently under investigation like for example gene therapy, thrombolysis, sonophoresis or vascular occlusion [40]–[43]. Depending on the clinical application, transducers can either be extracorporeal, transrectal or interstitial [16] and devices are commonly guided by ultrasound (US) imaging or magnetic resonance imaging (MRI) [44].

During tissue ablation, HIFU can be applied in continuous wave mode to maximize HIFU thermal effects or in pulsed wave mode to further use the HIFU mechanical effects. In

the case of pulsed wave mode operation, the duty factor (DF) is specified. It represents the ratio of the pulse duration to the pulse repetition period (PRP) [45]. It is given by:

$$DF = \frac{\tau}{PRP} = \tau \times PRF \tag{2.1}$$

with $\tau$ the pulse duration, defined for a number $N$ of cycles per pulse, as: $\tau = N \times T = \frac{N}{f}$.

As explained hereinabove, the basis of HIFU therapy is to induce a localized tissue bioeffect. The mechanisms by which HIFU induces tissue bioeffects are commonly classified into thermal and non-thermal mechanisms. Both mechanisms are reviewed in the next section.

## 2.1.2 Ultrasonic biophysics and bioeffects

### 2.1.2.1 Thermal mechanisms

As an acoustic wave propagates through a viscous medium, the energy transported by the ultrasound beam is attenuated due to absorption and scattering of the incident wave energy. Absorption represents the conversion of a portion of the energy carried by the wave into heat, whereas scattering corresponds to the re-direction of the wave energy out of the main beam direction. For a plane wave, if we consider $I_0$ the acoustic intensity at the point of origin $z_0$, the intensity of the wave $I$ following the ultrasound propagation through a distance $z$ from the origin is given by the expression:

$$I = I_0 \times e^{-2\alpha z} \tag{2.2}$$

with $\alpha$ the attenuation coefficient corresponding to the sum of the absorption $\alpha_a$ and scattering $\alpha_s$ coefficients.

For most tissues, the attenuation increases with the frequency via a power law of the form [46]:

$$\alpha(f) = \alpha_0 \left(\frac{f}{f_0}\right)^b = a f^b \tag{2.3}$$

where $\alpha_0$ corresponds to the value of tissue attenuation at a frequency $f_0$ [47] and $a = \frac{\alpha_0}{f_0^b}$. The power law exponent $b$ typically ranges between 1 and 2 [48]. Both $a$ and $b$ are tissue-specific constants and temperature dependant. The frequency dependence of acoustic attenuation implies that increasing the frequency results in higher heat deposition but also in a

lower depth penetration. The choice of the therapeutic ultrasound frequency represents therefore a trade-off between the tissue target depth and the desired rate of heating [16].

During HIFU exposure, if heat is deposited more rapidly than it is dissipated by vascular perfusion and conduction, a local temperature rise occurs. It can rise rapidly to reach temperatures at the focus above 80°C [18]. The rate of temperature rise depends on the tissue acoustic and thermal properties (absorption coefficient, density, perfusion rate…) and on the ultrasound parameters used during HIFU exposure. If the temperature is elevated above 56 °C for 1 s or longer, irreversible cell death occurs through coagulative necrosis [18]. The extent of the thermal tissue damage depends on the tissue temperature increase reached and on the duration of the temperature elevation. To estimate the thermal lesion following HIFU exposure, it is possible to use the empirical formula derived by Sapareto and Dewey relating the time $t$ (in minutes) required to produce a given bioeffect at a constant temperature $T$ to the time $t_{43}$ which would be required to produce the same effects at a reference temperature of 43 °C [49]. The formula is expressed as follows:

$$t_{43} = tR^{43-T} \tag{2.4}$$

with $T$ constant and the empirical thermal index $R$ equaling either to 0.5 if $T > 43°C$ or to 0.25 if $T < 43°C$. Depending on the tissue, different lethal thresholds exist. For example, for muscle tissue, the thermal dose required to induce a significant and chronic tissue damage is equivalent to the thermal dose of 80-240 min exposure at 43 °C [50].

#### 2.1.2.2 Non-thermal mechanisms

During HIFU exposures, non-thermal mechanisms such as cavitation, radiation force, or acoustic streaming can be induced and may also cause biological effects. A short review of all those non-thermal mechanisms is provided in the present section.

##### 2.1.2.2.1 Acoustic cavitation

Acoustic cavitation can be defined as the formation and activity of bubbles within a medium exposed to an ultrasound beam [17]. Two types of bubble activity are commonly distinguished: inertial (or transient) cavitation and non-inertial (or stable) cavitation. Inertial cavitation describes the phenomenon of the expansion of a gas-filled cavity during the negative part of

the acoustic cycle and then its rapid and violent collapse [17] during the positive part of the acoustic cycle. The bubble motion during collapse is dominated by inertia of the surrounding medium [17]. In contrast, non-inertial cavitation corresponds to the oscillation of an acoustically driven bubble around its equilibrium radius. The dynamics of the bubble motion are dominated by the compressibility of the gas and the characteristics of the acoustic wave (e.g. pressure) [51].

The occurrence of cavitation as well as the behavior of bubbles depend on several factors like e.g. the acoustic pressure, the focusing of the ultrasound beam, the mode of sonication (pulsed or continuous) and the nature and state of the medium [45]. It is generally difficult to generate cavitation *in vivo* (unless at low frequencies) as the pressures required are usually very high and tissue-specific [51]–[53]. To promote and incite bubble formation, nucleating agents like microbubbles can be used [51].

Cavitation can cause a biological effect by virtue of a temperature increase, mechanical stress and release of free radicals [45].

#### 2.1.2.2.2 Radiation force

The radiation force or the radiation pressure is defined as a steady time-averaged force exerted upon the propagating medium lying in the ultrasound field [17]. In the body, the radiation force induces local movements of tissues that tend to recover to their equilibrium position after the end of the exposure [37], [54], [55]. The magnitude of the radiation force is proportional to the intensity; the effects are thus concentrated within the focal zone. The radiation force is the underlying mechanism for the acoustic streaming phenomenon.

#### 2.1.2.2.3 Acoustic streaming

Acoustic streaming refers to the unidirectional fluid motion that may be set by an acoustic field in a fluid [17]. This is caused by the transfer of momentum to the fluid by acoustic energy absorption. The velocity gradients associated with fluid circulation may be high depending on several factors like e.g. the shear viscosity of the fluid and the shear stresses set-up may be sufficient to cause changes and/or damages [17].

The next section presents basic acoustic notions relevant to the HIFU ablation. Basic acoustic concepts and linear acoustic theory are first overviewed. Then, a short review of the non-linear phenomena is provided.

### 2.1.3 Basic acoustic notions

#### 2.1.3.1 Linear acoustics

The propagation of ultrasound waves in tissue follow the so-called wave equation. The equations used to derive the first-order wave equation are the equation of continuity, the Euler equation and an equation of state relating pressure to density and entropy. In linear acoustics, pressure $p$ and density $\rho$ variables are written in the form:

$$p = p_0 + p' \tag{2.5}$$

$$\rho = \rho_0 + \rho' \tag{2.6}$$

where $p_0$, $\rho_0$ are the constant equilibrium values of respectively the pressure and density of the fluid and $p'$, $\rho'$ their variations caused by the propagating sound wave. $p_0$ and $\rho_0$ are only functions of space while perturbations are functions both of space and time.

By introducing equation (2.6) in the equation of continuity and neglecting the second-order terms, we obtain the following continuity equation:

$$\frac{\partial \rho'}{\partial t} + \rho_0 \text{div } \mathbf{v} = 0 \tag{2.7}$$

Here $\mathbf{v}$ is the acoustic particle velocity and $t$ the time variable.
Likewise, with the same assumptions, the Euler equation becomes:

$$\frac{\partial \mathbf{v}}{\partial t} + \frac{1}{\rho_0} \nabla p' = 0 \tag{2.8}$$

To derive the wave equation, we use a pressure-density relation that can be written as [56]:

$$p' = c_0^2 \rho' \tag{2.9}$$

where $c_0$ is the isentropic sound speed.

The first-order linearized equations are then combined to yield to the wave equation:

$$\Delta p' - \frac{1}{c_0^2}\frac{\partial^2 p'}{\partial t^2} = 0, \Delta p' = \begin{pmatrix} \frac{\partial p'}{\partial x} \\ \frac{\partial p'}{\partial y} \\ \frac{\partial p'}{\partial z} \end{pmatrix} \tag{2.10}$$

From here forwards, $p = p'$.

For the acoustic pressure, the commonly used wave equation is expressed as:

$$\Delta p - \frac{1}{c_0^2}\frac{\partial^2 p}{\partial t^2} = 0 \tag{2.11}$$

The form of the D'Alembert solution of the wave equation can be expressed in one spatial dimension as:

$$p(z,t) = f_+\left(t - \frac{z}{c}\right) + g_-(t + \frac{z}{c}) \tag{2.12}$$

where $f_+$ and $g_-$ are any two functions respectively describing a wave traveling in the positive $z$ direction and a wave traveling in the negative $z$ direction. Both propagate at a speed $c$ and without any change in form or amplitude.

### 2.1.3.2 Energy conservation

In the context of HIFU ablation, the energy deposition caused by the sound wave drives the thermal rise. Considering a volume V, the total acoustic energy contained in that volume, $E_{\mathrm{V}}$, is given by the integral:

$$E_{\mathrm{V}} = \frac{1}{2}\int_{\mathrm{V}} (\rho_0 \|\mathbf{v}^2\| + \frac{p^2}{\rho_0 c_0^2})\, d\mathrm{V} \tag{2.13}$$

with the first term representing the acoustic kinetic energy density and the second the acoustic potential energy density.

Time derivative of (2.13) gives:

$$\frac{dE_{\mathrm{V}}}{dt} = \int_{\mathrm{V}} (\rho_0 \mathbf{v}\frac{\partial \mathbf{v}}{\partial t} + \frac{p}{\rho_0 c_0^2}\frac{\partial p}{\partial t})\, d\mathrm{V} \tag{2.14}$$

By using (2.7), (2.8) and (2.9), (2.14) becomes:

$$\frac{dE_{\mathrm{V}}}{dt} = \int_{\mathrm{V}} (-\mathbf{v}\nabla p - p div\, \mathbf{v})\, d\mathrm{V} \tag{2.15}$$

Finally:

$$\frac{dE_{\mathrm{V}}}{d\mathrm{t}} = \int_{\mathrm{V}} -\mathrm{div}\,(p\mathbf{v})\, d\mathrm{V} \tag{2.16}$$

The acoustic intensity vector is defined as:

$$\mathbf{I} = p\mathbf{v} \tag{2.17}$$

Its norm is expressed in W.m$^{-2}$ and it represents the acoustic power flux density.

The time-averaged acoustic power dissipated per unit volume is defined as:

$$Q = -\mathrm{div} < \mathbf{I} > \tag{2.18}$$

For a progressive plane wave, the velocity field can be regarded as a scalar and the time-averaged intensity of the wave is $I = \frac{P_{amp}^2}{2\rho_0 c_0} = \rho_0 c_0 v^2$, with $v$, the fluid particle velocity.

In that case, the expression (2.18) also simplifies into $Q = 2\alpha < I >$ with $\alpha$ expressed in $Np.m^{-1}$ and $< . >$ denoting the temporal average over one period.

In reality, the approximations made in linear acoustics are valid only for sound waves of small amplitudes. However, mechanical stresses like pressure perturbation imposed by HIFU waves can be of the order of tens of megapascals and are therefore high enough to induce non-linear response [46].

The next section presents a short overview of the non-linear phenomena. More details about non-linear acoustics can be found in Hamilton and Blackstock [57].

### 2.1.3.3 Nonlinear phenomena

When the accumulation of perturbations caused by sound wave propagation becomes large relative to the ambient values, non-linear phenomena become important. Therefore, the wave equation (2.11) does not apply anymore.

Several models have been developed for nonlinear acoustic wave propagation. These include the Westervelt equation, the Khokhlov-Zabolotskaya-Kuznetsov (KZK) equation (a parabolic approximation to the Westervelt equation) and Burger's equation (a simplified version of the Westervelt equation in a one-dimensional form). Burger's equation is the simplest equation that describes the effects of nonlinearity. It can be written as:

Burger's equation : $$(\frac{\partial}{\partial z} + \frac{1}{c_0 + \beta v})p = 0 \quad (2.19)$$

Nonlinearity can thus be simply modeled as a continuous variation of the celerity of the medium:

$$c(z,t) = c_0 + \beta v(z,t) = c_0 + \beta \frac{p(z,t)}{\rho_0 c_0} \quad (2.20)$$

with $\beta$ the non-linearity coefficient of the medium. $\beta$ is expressed as:

$$\beta = 1 + \frac{B}{2A} \quad (2.21)$$

with the values $A$ and $B$ corresponding to the coefficients of first and second order terms of the Taylor series expansion of the equation relating the pressure of the material to its density. $B/A$ and $\beta$ are material-specific properties and their values for different tissues are listed in Duck [58]. Tissues with higher fat content are generally more nonlinear [48].

The expression (2.20) physically means that the wave travels faster than $c_0$ during compression phases whilst it travels with a velocity smaller than $c_0$ during rarefaction phases. Consequently, when a large-amplitude acoustic wave propagates through a non-linear medium, the waveform gradually distorts and becomes progressively steeper. If unrestrained by attenuation, the waveform changes to a shocked-sawtooth shape. Distortion of an initial sinusoidal plane wave manifests in the frequency domain by the generation of harmonics. As the wave propagates, there is a decrease in the fundamental component and the wave energy is transferred to upper harmonics. Discontinuity in the shape of the wave appears for a given distance $\bar{z}_{shock}$usually known as the 'shock distance'. It can be expressed as:

$$\bar{z}_{shock} = \frac{c_0^3 \rho_0}{\beta p_0 2\pi f} \tag{2.22}$$

This expression implies that non-linearities will be observed earlier for acoustic waves of high frequency as well as for a medium with larger nonlinearity coefficient and lower speed of sound. Likewise, the larger is the initial pressure amplitude $p_0$, the shorter is $\bar{z}_{shock}$.

In the context of HIFU, the generation of harmonics is beneficial. As the wave propagates and approaches the focal spot, high harmonics are generated. High harmonics are more absorbed by tissues than the fundamental (2.3). The energy deposition at the focal spot is therefore greater than the linear theory would predict.

After this short overview of acoustical theory relevant to HIFU ablation, the next section is dedicated to the presentation of the pathology of varicose veins.

## 2.2 Varicose veins

The condition of varicose veins corresponds to a dilatation of superficial veins of lower extremities. It has a wide prevalence in industrialized countries: 25% of Western adults have varicose veins [59].

To understand the pathophysiology of varicose veins, a short summary of the anatomy and the physiology of the superficial venous system is presented. The pathogenesis of varicose veins as well as associated symptoms and clinical manifestations are then described. Finally, current interventional therapies for the treatment of varicose veins are overviewed.

### 2.2.1 Definition and symptoms

#### 2.2.1.1 Overview of the lower extremity venous system: anatomy and physiology

##### 2.2.1.1.1 Anatomy

The peripheral venous system has several physiological functions. The main ones consist in returning the blood to the heart and in storing the blood volume that is not immediately required. A short presentation of the venous return is provided in 2.2.1.1.2.

The veins of the lower limb are divided into three different systems. These include the superficial venous system, the deep venous system and the perforating vein network that connects the superficial and the deep venous systems (Figure 2-3).

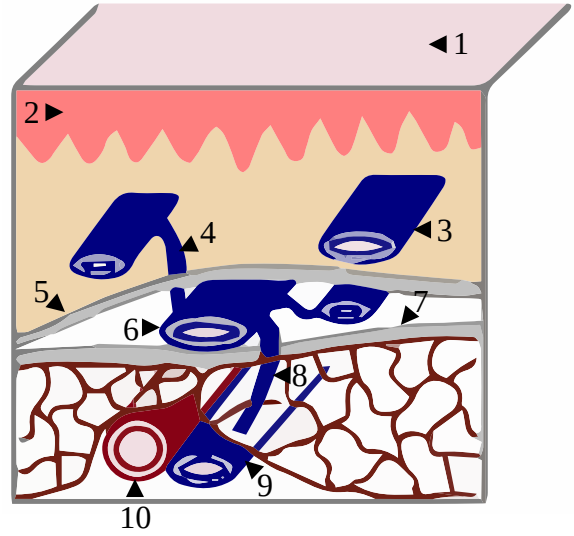


**Figure 2-3 – The three venous systems of the lower limb.** 1. Skin, 2. Epidermis, 3. Superficial vein, 4. Communicating vein, 5. Subcutaneous fascia, 6. Great saphenous vein (GSV), 7. Muscular fascia, 8. Perforating vein, 9. Deep vein, 10. Artery.

The superficial venous network transports 10 % of the venous blood whilst the deep venous network carries 90 % [60]. The superficial venous system is located in the superficial compartment comprised between the skin and the muscular fascia. It comprises an interconnecting network of veins that serves as the primary collecting system and numerous

truncal superficial veins that serve as conduits to return blood to the deep system [61] (Figure 2-4).

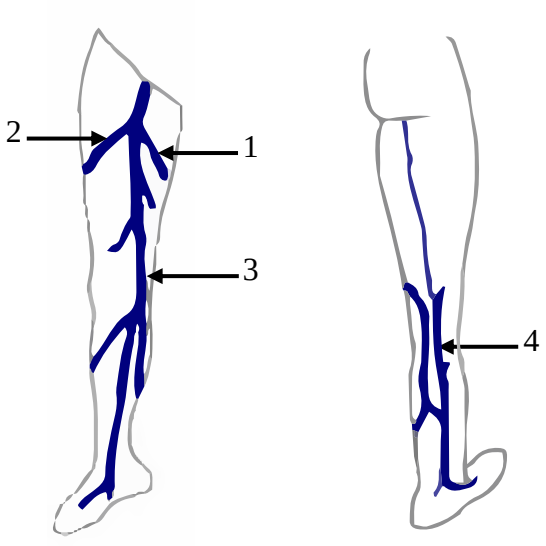


**Figure 2-4 – Main superficial veins of the lower limb.** 1. Posterior accessory saphenous vein, 2. Anterior accessory saphenous vein, 3. Great saphenous vein, 4. Small saphenous vein.

The main conducting superficial veins are the great saphenous vein (GSV) and the superficial saphenous vein (SSV). The GSV is the longest vein in the entire body conducting blood from the foot, leg and thigh to the deep femoral vein. It courses from the medial malleolus to join the deep femoral vein at the saphenofemoral junction (SFJ) located at the groin. Throughout its path, the GSV runs between the subcutaneous and the muscular fascia. The compartment delineated by these two fascias is commonly referred to as the 'Egyptian eye' [60] due to its shape. The GSV has two main tributaries draining into it. These are the anterior accessory saphenous vein (AASV) and the posterior accessory saphenous vein (PASV). Both run parallel to the GSV but in the first case (AASV) in front of it and in the second case (PASV) behind it. The second main conducting superficial vein, the SSV, runs from behind the lateral malleolus to the saphenopopliteal junction (SPJ) where it joins the deep popliteal vein. The GSV and the SSV are connected with intersaphenous veins. The most famous intersaphenous vein is the Giacomini vein.

The deep venous system is entirely located beneath the muscular fascia. It serves as a collecting reservoir and is responsible for the blood outflow from the limb into the central abdominal veins. It comprises intramuscular veins and axial veins that follow the course of the major arteries [61].

The perforating veins (also known as perforators) are the veins that perforate the muscular fascia and connect the superficial veins to the deep veins. There are numerous perforating veins that connect the GSV and SSV to the deep venous system (Figure 2-5).

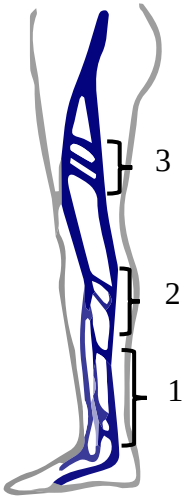


**Figure 2-5 – Perforators of the lower limb.** 1. Posterior tibial perforators, 2. Paratibial perforators, 3. Perforating veins of the femoral canal.

All the veins have the same venous wall structure, which is comprised of three concentric layers or tunics (Figure 2-6). These are the tunica intima, tunica media and tunica adventitia.

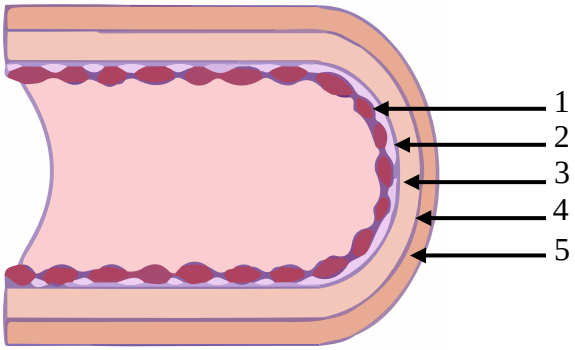


**Figure 2-6 – Structure of vein walls.** 1. Tunica intima, 2. Internal elastic lamina, 3. Tunica media, 4. External elastic lamina, 5. Tunica adventitia.

The tunica intima is the innermost layer of the vein. It contains the endothelium, a thin monolayer of cells in direct contact with the blood, connective tissue and a basal layer of elastic tissue called internal elastic lamina which separates the tunica intima from the tunica media. The tunica media is primarily composed of smooth muscle fibers, elastin and collagen. The

tunica media is separated from the tunica adventitia by the external elastic lamina. The tunica adventitia is the outer layer of the vein wall. It namely contains fibroblasts, collagen, lymphatics, nerve endings and also *vasa vasorum* which are the feeder vessels for the vein.

The leg veins have also bicuspid valves that are of great importance in the blood venous return. In standing position, the valves assist the unidirectional flow towards the heart preventing the blood to go toward the feet. However, they do not work alone to return blood to the heart but in concert with other components, which are detailed in the next section.

#### 2.2.1.1.2 Normal venous return in lower extremities

Regardless the posture and the physical activity, the blood that enters into the venous system of the lower extremities should return to the right heart. Several mechanisms are involved to ensure a proper venous return. A normal blood flow is directed from the superficial venous system towards the deep system and from the most distal part of the body towards the heart.

In standing position for example, blood should oppose gravity and thoracoabdominal pressures to return to the heart. The combination of the valvular system and muscle pumps, particularly the calf muscle pump, ensures mainly the venous return in standing and walking state. Contraction of the calf muscles compresses the intramuscular and the deep axial veins pushing the blood towards the heart. The unidirectional circulation of the venous blood is ensured by the competent valvular system. When the calf muscle relaxes, the blood cannot flow back because the valves close. This action results in a pressure drop in the deep veins which pump the blood from superficial veins throughout the competent valves of the perforators [62]. This enables to reduce the pressure in the superficial veins. The normal action of the calf muscle pump is illustrated in Figure 2-7. As said above, other mechanisms promote venous return particularly when the subject is lying. These include for example respiration, cardiac aspiration etc. More details about the return circulation can be found in Ramelet [60].

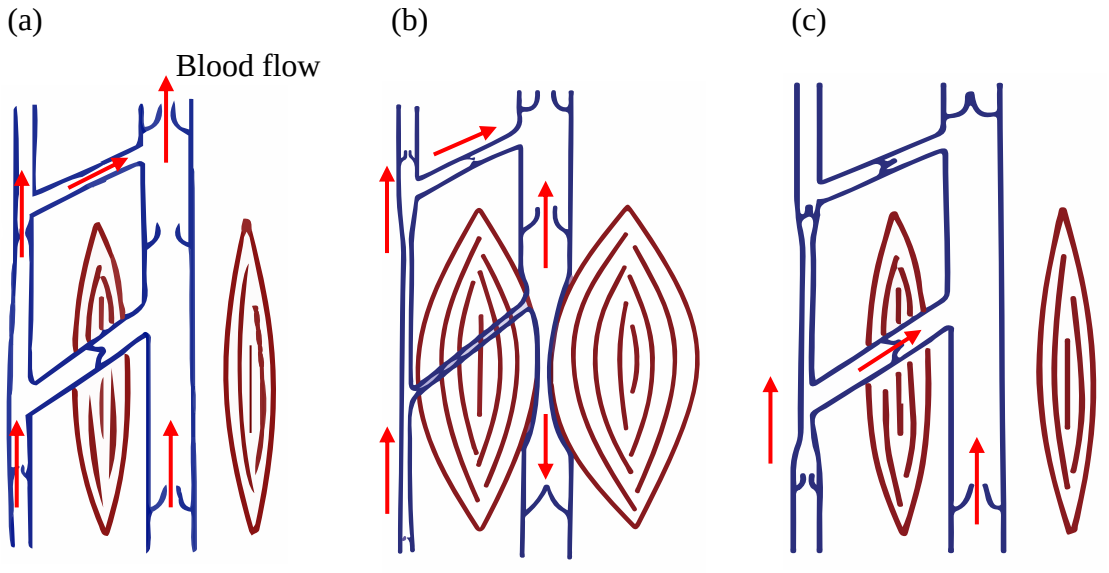


**Figure 2-7 – Normal venous hemodynamics in the lower limb before (a), during (b) and after (c) the action of the muscle pump (Adapted from Ramelet [60]).**

A failure in the mechanisms involved in venous return can cause or worsen chronic venous disease. Varicose veins are one of the manifestations of such failure.

### 2.2.1.2 Development of varicose veins

Varicose veins are defined as pathological enlarged subcutaneous veins of a diameter superior or equal to 3 mm in the upright position [63]. They can involve the main axial superficial veins, *i.e.* the GSV or the SSV, or any other superficial vein tributaries of the lower limbs.

The development of varicose veins is thought to result mainly from venous reflux (reversal of blood flow), venous obstruction or a combination of both [64]. Other pathophysiological mechanisms like for example the deficiency of the muscle pump or vein wall damage can also lead to venous disease. Only venous reflux and obstruction will be considered.

Venous reflux is caused by valvular dysfunction. This can occur within any superficial, deep or perforating veins of the lower limbs [64], [65]. It can be the consequence of either a primary event due to a defective structure of cuspids [61], or it can be secondary vein wall dilatation. Reflux enhances further distal vein wall dilatation, valvular incompetency, retrograde flow and venous hypertension within pathological veins. Figure 2-8 illustrates the development of varicose veins due to valvular insufficiency.

Venous obstruction of deep or superficial veins may impede the blood outflow causing venous reflux distal to the obstruction and resulting in further damage of the vein valves. According to Tafur *et al.* [66], approximatively eight in ten individuals with varicose veins have primary valvular insufficiency.

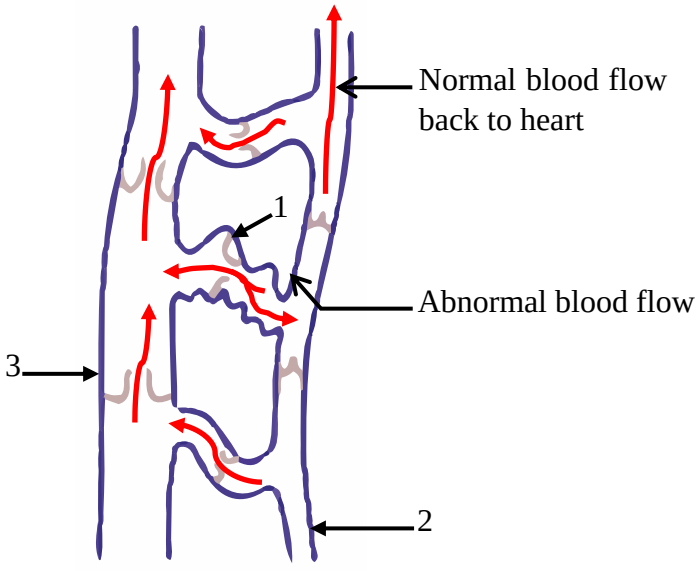


**Figure 2-8 – Failure of perforating valves (1) allows high pressure from deep veins (3) to extend to superficial veins (2).** Under high pressure veins dilate and varicose veins form.

#### 2.2.1.3 Symptoms and clinical manifestations

Patients with varicose veins suffer from various uncomfortable sensations like aching, itching, heaviness, pain or night cramp in the affected lower extremity. These symptoms usually worsen with prolonged standing and improve with leg elevation or walking [64]. Varicose veins may progress and lead to more severe complications. Patients with varicose veins may develop eczema, ulcers and other pathological skin changes. Finally, varicose veins may also be subjected to rupture and provoke spontaneous bleeding. Several treatment options exist to treat varicose veins. These are detailed in the next section.

### 2.2.2 Main existing treatments

Treatment options for superficial venous reflux are commonly divided into conservative and invasive or minimally invasive methods.

Conservative treatments mainly include lifestyle changes, for example return to physical activity, optimization of body weight, pharmacology and compression therapy. The use of compressive stockings improves venous hemodynamics and may alleviate venous symptoms. However, compressive therapy has little influence on the cause and evolution of varicose veins.

Depending on the size of varicose veins and on associated complications, other therapeutic options may be recommended. These mainly include surgery, radiofrequency ablation (RFA), endovenous laser ablation (EVLA) and sclerotherapy. These techniques primarily aim at eliminating the refluxing vein from the venous circulation. Once venous reflux is abolished, symptoms attributed to superficial venous insufficiency should be relieved and complications prevented [67]. As venous return is mostly achieved by deep veins, removing a diseased superficial vein does not compromise the venous return provided that the deep vein network remains patent.

#### 2.2.2.1 Surgery

The conventional treatment option for varicose veins is surgery. Surgical options include ligation, with or without stripping. Since the majority of patients with varicose veins have incompetent sapheno-femoral junction (SFJ) and reflexive GSV [65], the classical treatment consists in ligating the SFJ and all saphenous tributaries then removing the refluxing GSV with the help of a stripping tool. This widely used surgical approach involves significant scars and a long and painful recovery period [67] [68]. It is common to observe hematoma along the stripping tract [69]. In addition, vein surgery potentially carries serious complications risks like nerve injury or deep venous thrombosis (DVT) for the most serious ones [60], [68], [69].

Treatment of superficial venous reflux can be accomplished with less invasive methods divided into chemical (sclerotherapy) or thermal (RFA and EVLA) methods.

#### 2.2.2.2 Sclerotherapy

Sclerotherapy was first described by Chassaignac in 1855 [67]. It consists in injecting a chemical agent into a varicose vein to damage its endothelium in order to induce thrombosis and subsequently vein wall fibrosis and obliteration of the lumen. It is usually performed under ultrasound guidance. This technique is frequently used but limited to benign varicosities or as

a complement after stripping or endovenous ablations since high recurrence rates and recanalizations have been reported [67].

Endovenous thermal procedures are competing minimally-invasive therapeutic modalities for the treatment of varicose veins. These mainly include radiofrequency and laser ablation.

#### 2.2.2.3 Radiofrequency

Endovenous radiofrequency ablation is a catheter-based technique. It consists of introducing a catheter into the incompetent vein and delivering RF energy over the length of the vein to be treated. The Closure® technique is the most used in clinics. With this technique, the RF energy is adjusted to raise the temperature of the vein to 85 to 120 °C [60]. The thermal energy delivered leads to the destruction of the intima and the contraction of the collagen in the vein wall. It induces fibrous changes that lead to occlusion of the venous lumen [60]. The effectiveness of this method depends on the control of the heating: it needs to be sufficient to denature the vein wall collagen to an extent that will cause maximal lumen contraction, but without affecting the integrity of the vein [70].

The procedure is performed under ultrasound guidance and requires local tumescent anesthesia [71]. Tumescent anesthesia consists in injecting a local anesthetic around the vein in order to prevent pain, protect surrounding tissues from thermal energy and also mechanically compress the vein, which increases the contact between the catheter and the vein wall tissue.

RF ablation has been demonstrated to be as successful as classic surgical vein removal with the advantages of a shorter convalescence time and a better post-operative quality of life.

#### 2.2.2.4 Laser

Endovenous laser ablation (EVLA) is also a catheter-based thermoablation technique. The energy is produced by monochromatic light radiation emitted by a laser diode generator.

Like RFA, EVLA is usually performed under local tumescent anesthesia. Laser fibers emit a single wavelength between 810 and 1500 nm [72]. The laser beam causes thermal energy via absorption of the light by chromophores, each absorbing light in a specific part of the electromagnetic spectrum. At the shortest wavelengths, the major chromophore is hemoglobin whilst longer wavelengths may be preferentially absorbed by water and collagen [73].

Vein wall damage with EVLA is thought to result from steam bubbles generation. Boiling blood transmits thermal energy to the vein wall via high temperature gradient, which induces vein thrombosis and vein wall lesions [60].

Endovenous thermal ablations have been proven to be safe and as effective as surgery [8], [9]. However, they are preferentially dedicated to veins having a rectilinear section sufficient for the insertion of the catheter or the optic fiber. Moreover, inserting and navigating a catheter into a tortuous vein can be very challenging and risky since vein wall perforation can occur.

For all the reasons already listed in the Introduction, HIFU is an appealing therapeutic alternative for varicose veins ablation.

In the next section, a review of relevant studies that demonstrated vascular occlusion of non-bleeding blood vessels of diameters larger than 0.5 mm is presented. The mechanisms of HIFU-induced vascular occlusion are discussed.

## 2.3 HIFU on veins

### 2.3.1 State of the art of vascular occlusion in non-bleeding veins

The use of HIFU to occlude intact veins of diameters superior to 0.5 mm has been proven in several biological studies.

Delon-Martin *et al.* [34] occluded rat femoral veins with a transducer operated at 7.31 MHz. Veins were surgically exposed and pulses were distributed along the vein at an intensity of 167 $W.cm^{-2}$ for 3 s. Treated veins were examined 2 days after sonications except one that was re-evaluated 4 weeks after treatment. Vascular occlusion was assessed by Doppler, histology and light microscopy evaluations. The treatment protocol used in this study produced thermal damage to the vein walls and venous thrombosis but occlusion was not maintained at 4 weeks post-treatment. The authors concluded that the ultrasound parameters used were insufficient to induce long-term occlusion.

Hynynen *et al.* [19] induced persistent occlusion up to 7 days post-treatment. Rabbit renal arteries (0.6 mm in diameter) were sonicated percutaneously with a 1.5 MHz transducer

and under MRI-guidance. Renal arteries were exposed first to short pulses (1s) at high intensity (6500 $W.cm^{-2}$) with the intention to induce transient cavitation in order to interrupt blood flow. Once the blood flow reduced or stopped, the artery was then thermally coagulated with 10-s pulses at 2800 $W.cm^{-2}$ distributed around the target artery. This treatment protocol successfully occluded renal arteries. However, the authors reported vein rupture and animal death because of involuntary exposures of bowels during treatment.

Rivens *et al.* [27] reported occlusions in rat femoral arteries and veins (0.5-1.5 mm in diameter) using a 1.69 MHz transducer. Femoral vessels were surgically revealed and were exposed to multiple pulses distributed in rows transecting the vessels at 4660 $W.cm^{-2}$ for 2 s. Magnetic resonance angiogram (MRA) and polylysine-Gd-DTPA contrast agents were used to assess vascular patency immediately following treatment. This study was aimed at investigating the role of HIFU as a method for vascular occlusion in the treatment of fetal medical disorders. Successful occlusion was demonstrated but a high incidence of hemorrhages was reported. According to the authors, this sonication technique needs refinement and survival studies need to be conducted before being applied to humans.

Denbow *et al.* [28] also demonstrated a reproducible vascular occlusion in rat femoral vessels with a 1.7 MHz transducer. The vessels were surgically externalized and were exposed to intensities in the range of 1000 to 4660 $W.cm^{-2}$ with a linear tracking method in which each pulse was delivered for 5 s while the transducer was moved at 1 $mm.s^{-1}$ orthogonal to the target vessels. Like Rivens *et al.* [27], MRA and contrast agents were used to evaluate vascular occlusion. All the veins treated at an intensity superior or equal to 1690 $W.cm^{-2}$ showed vascular occlusion but 4660 $W.cm^{-2}$ exposures always caused vascular rupture. The authors concluded that the longevity of the occlusion needs to be further investigated and that microscopic changes induced to vessels need to be evaluated before clinical use.

Contrary to previous studies, Mahoney *et al.* [74] exposed rabbit auricular vessels to pulsed-HIFU at two different frequencies (0.68 MHz and 2.02 MHz). HIFU was applied up to 180 s per sonication at peak pressures varying from 4 to 17 MPa at 0.68 MHz and 9 to 37 MPa at 2.02 MHz. The authors reported vascular occlusion at 0.68 MHz but also a high incidence of vessel rupture. On the other hand, most of the vessels treated at 2.02 MHz were constricted or occluded without vessel wall rupture. The authors hypothesized that the higher rate of vascular rupture at 0.68 MHz was due to the size of the induced cavitation bubbles, which were

supposed to be bigger and to collapse more violently at 0.68 MHz. In addition, the stiffening of the surrounding tissues observed at 2.02 MHz as a result of thermal coagulation was deemed to have prevented vessels from rupturing.

Fujiwara *et al.* [29] were able to occlude rat femoral arteries of 0.5 mm in diameter when applying 3 MHz pulses at 10 000 $W.cm^{-2}$ for 5 or 10 s. They reported no occlusion when applying 1 MHz pulses at 800 $W.cm^{-2}$. In this study, femoral arteries were sonicated through the skin and occlusion was assessed by color Doppler. Animals were followed up 24 hours, 48 hours or 12 days after sonication for those treated at 1 MHz. According to histological analysis, vascular occlusion at 3 MHz resulted from thermal effects.

Ishikawa *et al.* [31] also demonstrated the ability to occlude rat femoral arteries (0.5 mm in diameter). The arteries were exposed through the skin under US-guidance with a 3.2 MHz transducer. Pulses were applied along a line transecting the target vessel at different intensities ranging from 530 to 4300 $W.cm^{-2}$ for 5 s. Occlusion was achieved with either a single exposure at 4300 $W.cm^{-2}$ or after 3 to 5 rounds of 5-s pulses at 2750 $W.cm^{-2}$. Histological analysis of the vessels treated at 4300 $W.cm^{-2}$ and harvested 3 days post-treatment revealed venous thrombosis attributed by the authors to thermal effects.

In a study aiming at investigating the role of HIFU for non-invasively occluding feeding tumor arteries, Ichihara *et al.* [22] sonicated rabbit renal arteries with a transducer operating at 2.2 MHz using an ultrasound imaging probe for guidance. Renal arteries were occluded after several 5-s pulses delivered at one location at an intensity of 4000 $W.cm^{-2}$. This treatment produced necrotic changes in arterial wall and surrounding tissues at 2 days and 7 days post-treatment. Vein hemorrhages as well as minor skin burns were also reported.

In a study investigating the role of HIFU for fetal umbilical artery blood flow occlusion, Ichizuka *et al.*[21] demonstrated the ability to occlude rabbit umbilical arteries of a diameter of 0.6 mm. Using a US-guided 2.26 MHz transducer, fetal arteries received several single exposures at different intensities (1400, 2750 or 5500 $W.cm^{-2}$). Each exposure was 5 s long. After treatments, animals were euthanatized, fetuses delivered and umbilical arteries extracted and sent for histological analysis. Occlusion of the arteries was reported only within 3 to 15 courses of sonications at 5500 $W.cm^{-2}$. Histological evaluation revealed thrombus inside the vessel and vacuolar degeneration in the tunica media. Coagulative necrotic changes of surrounding tissues were also observed on histological examination. No vascular rupture was

observed but mild skin burns in maternal and fetal rabbits were reported. The authors concluded that long-term effects and potential adverse events had to be further investigated before clinical translation.

Finally, HIFU was used to induce vascular occlusion in non-bleeding blood vessels by Hwang *et al.* [35]. In this study, acute occlusion was successful for rabbit auricular vessels that were exposed to pulsed HIFU at 1.17 MHz in the presence of circulating microbubbles and followed by fibrinogen injection. They used very high peak pressures (+27 MPa and -9 MPa) with a low duty cycle (0,43 % duty factor, 5000-cycle pulse, 1 Hz PRF), resulting in a low time average intensity (23 $W.cm^{-2}$). However vascular occlusion was not durable over 14 days post-treatment. The authors hypothesized that the fibrinolytic system was the cause of vascular recanalization. Recognizing that successful long-term vascular occlusion involved intense inflammation, they suggested to refine the treatment protocol and boost inflammation by adding an additional agent, such as alcohol.

In a subsequent study Zhou *et al.*[36] reproduced the protocol introduced by Hwang *et al.* [35] and applied it on rabbit auricular veins and injected a pro-inflammatory agent after ultrasound exposure. Vessels were exposed to 1 MHz pulsed HIFU (9 MPa peak rarefaction pressure, 10-ms pulse, 1-Hz pulse repetition frequency and 45 pulses per site) in synergy with an ultrasound contrast agent, followed by a local injection of fibrinogen and a pro-inflammatory agent used as a vein sclerosant. Vascular thrombosis was successfully observed 14 days after treatment.

Table **2-1** and Table **2-2** provide a summary of the experimental conditions and results of the identified in vivo animal studies examining vascular occlusion in non-bleeding vessels respectively. Studies are in chronological order.

**Table 2-1 – Summary of exposure conditions used in animal studies investigating the role of HIFU for vascular occlusion.** Key: NR, not reported; NA, not applied.

| Study | Animal Model | Vessel type | Vessel diameter (mm) | Vessel depth (mm) | Non-invasive? | Sonication guidance | Frequency (MHz) | Intensity ($W.cm^{-2}$) | Duration (s) | Cavitation? Pulsing regime | Sonication Layout | Step-size (mm) | Injection? | Follow-up length (days) |
|---|---|---|---|---|---|---|---|---|---|---|---|---|---|---|
| Delon-M (1995) [34] | Rat | Femoral vein | < 2 | NR | No | A-mode | 7.31 | 167 | 3 | No | 4 - 7 × 1 | 1 | No | 2<br>28 |
| Hynynen (1996) [19] | Rabbit | Renal artery | 0.6 | NR | Yes | MRI | 1.5 | 6500-2800 | 1<br>10 | Yes | 1 (repeated)<br>3 - 4 × 3 - 4 | 0.7 | No | 0<br>2<br>7 |
| Rivens (1999) [27] | Rat | Femoral artery<br>Femoral vein | 0.5<br>1.5 | NR | No | Visual | 1.7 | 4660 | 2 | NR | 2 × 4 | 2 | No | 0 |
| Denbow (2000) [28] | Rat | Femoral artery<br>Femoral vein | 0.5<br>1.5 | NR | No | Visual | 1.7 | 1690-4660 | 5 | NR | Linear tracking | NR | No | None |
| Mahoney (2000) [74] | Rabbit | Auricular vessels | NR | NR | Yes | Visual | 0.68<br>2.02 | NR | 10, 60, 180 | Yes<br>4-37 MPa<br>5-20 PRF<br>10 ms burst | NR | NR | Yes<br>contrast agent | 0 |
| Fujiwara (2002) [29] | Rat | Femoral artery | 0.5 | NR | NR | NR | 1<br>3 | 800<br>10 000 | 5-10 | NR | NR | NR | No | 0-1-2-12<br>0-1-2 |
| Ishikawa (2003) [31] | Rat | Femoral artery | 0.5 | 5-8 | Yes | Color Doppler | 3.3 | 2750<br>4300 | 5 | NR | 1 × 5 | 1 | No | 0<br>3 |
| Ichihara (2007) [22] | Rabbit | Renal artery | 0.5 | 15-20 | Yes | Color Doppler | 2.2 | 4000 | 5 | NR | 1 (repeated) | NA | No | 0<br>2<br>7 |
| Ichizuka (2007) [21] | Rabbit fetuses | Umbilical artery | 0.6 | 20-30 | Yes | Color Doppler | 2.26 | 1400<br>5500 | 5 | NR | 1 (repeated) | NA | No | 0 |
| Hwang (2010) [35] | Rabbit | Auricular vessels | NR | NR | Yes | Visual | 1.17 | 23 | 60 | Yes<br>+27/ -9 MPa<br>1 Hz PRF | 2 × 1 | 4 | Yes<br>UCA+fibrinogen | 0<br>14 |
| Zhou (2011) [36] | Rabbit | Auricular vessels | NR | NR | Yes | B-mode Color Doppler | 1 | NR | 45 | Yes<br>9 MPa<br>1 Hz PRF | 3 × 1 | 3 | Yes<br>UCA+fibrinogen+ pro-inflammatory agent | 0<br>14 |

**Table 2-2 – Summary of reported occlusion results and vascular changes in the animal studies.** Key: NR, not reported.

| Study | Vessel type | Intensity ($W.cm^{-2}$) | Method of assessment | Follow-up length (days) | Occlusion | Thrombus | Endothelium damage | Vascular wall damage | Vascular shrinkage | Vascular spasm | Vascular rupture | Collateral damage |
|---|---|---|---|---|---|---|---|---|---|---|---|---|
| Delon-M (1995) [34] | Femoral vein | 167 | Doppler<br>Histology microscopy | 2<br>28 | Yes | Yes | Yes | No | NR | NR | NR | No |
| Hynynen (1996) [19] | Renal artery | 6500-2800 | MRI<br>X-Ray | 0<br>2<br>7 | Yes | NR | NR | Yes<br>Necrosis | NR | Yes | Yes | Bowels |
| Rivens (1999) [27] | Femoral artery<br>Femoral vein | 4660 | MRA | 0 | Yes | NR | NR | NR | NR | Reduced blood flow | Yes | Whitening Surrounding tissues |
| Denbow (2000) [28] | Femoral artery<br>Femoral vein | 1690-4660 | MRA | None | Yes | NR | NR | NR | NR | NR | Yes at 4660 W/cm2 | NR |
| Mahoney (2000) [74] | Auricular vessels | NR | Visual | 0 | Yes | NR | NR | Yes | NR | Yes | Yes | Surrounding tissue |
| Fujiwara (2002) [29] | Femoral artery | 800<br>10 000 | Color Doppler<br>HE | 0-1-2-12<br>0-1-2 | No<br>Yes | NR<br>NR | NR<br>NR | Vacuolar degeneration<br>Yes | NR<br>NR | NR<br>NR | NR<br>NR | Necrotic muscle |
| Ishikawa (2003) [31] | Femoral artery | 2750<br>4300 | Visual<br>Color Doppler<br>Histology | 0<br>3 | Yes<br>Yes | Yes | NR | Yes<br>Vacuolar degeneration | Yes | Yes | No | Firm muscle |
| Ichihara (2007) [22] | Renal artery | 4000 | Color Doppler<br>Histology | 0<br>2<br>7 | Yes | NR | NR | Yes<br>Vacuolar degeneration | NR | Yes | Yes | Minor skin burns<br>Necrosis surrounding tissue |
| Ichizuka (2007) [21] | Umbilical artery | 1400<br>5500 | Histology | 0 | Yes | Yes | NR | Vacuolar degeneration | NR | NR | No | Mild skin burns |
| Hwang (2010) [35] | Auricular vessels | 23 | Doppler<br>Angiography<br>Histology | 0<br>14 | Yes | Yes | Yes | NR | NR | NR | No | NR |
| Zhou (2011) [36] | Auricular vessels | NR | Visual<br>Angiography<br>Doppler<br>Histology | 0<br>14 | Yes | Yes | NR | NR | NR | NR | NR | NR |

Figure 2-9 presents a summary of the HIFU-induced effects on blood vessels for sonication intensity versus time of exposure for the exposure conditions listed in Table 2-1 and . Only continuous HIFU exposures are considered in Figure 2-9.

All animal studies that attempted to produce *in vivo* vascular occlusion with HIFU demonstrated the potential of HIFU to occlude vessels, at least temporarily. Ultrasound exposure parameters were different in each study. Vessels were exposed at frequencies extending from 0.68 MHz to 7.3 MHz and to intensities ranging from 23 $W.cm^{-2}$ to 10 000 $W.cm^{-2}$ (reported as spatial average or spatial peak). In most cases, the duration of the pulses was inferior or equal to 10 seconds. The spatial pulse distribution and sonication method also varied amongst studies. Generally, one of the following characteristics were reported: (1) pulses were repeatedly applied at the same position at the vessel location until cessation of blood flow, (2) numerous pulses were delivered along or across the vessel, (3) pulses were distributed in a close-packed array around the blood vessel or (4) sonications were applied along a linear track by moving the transducer along a line transecting the vessel while the pulse was emitted continuously. Finally, to achieve occlusion, some investigators have used HIFU treatments in synergy with additional products ranging from contrast agent injection, to injection of proteins or pro-inflammatory agents.

Independently from the sonication method, immediate vascular occlusion of small diameter vessels (0.5-1.5) following HIFU was always reported. However, results provided by these studies are either insufficient or not acceptable for the clinical application of HIFU to varicose veins treatment. Indeed, vascular occlusion was been demonstrated for small vessels only, whilst varicose veins have, by definition, diameters superior or equal to 3 mm. In addition, HIFU as a stand-alone method for occlusion has only been proven to occlude vessels in acute, whereas a viable treatment of varicose veins requires long-term occlusion. Moreover, protocols consisting in applying multiple pulses (as much as 15 times) until the blood flow has stopped are too long to be implemented in clinics. The use of additional agents comprising contrast agents or pro-inflammatory agents in synergy with sonications should be prohibited as HIFU would lose the advantage of being non-invasive. Moreover, the effects of HIFU on the vasculature and on surrounding tissues have not always been microscopically documented. For the treatment of varicose veins, it is essential to assess histologically the nature and the progression of the damage induced to both vessels and to the surrounding tissues, for efficacy

and safety reasons. Doppler or MR Angiography are not sufficient to assess the efficacy. Finally, several studies have reported major complications like vascular rupture, which are to be avoided.

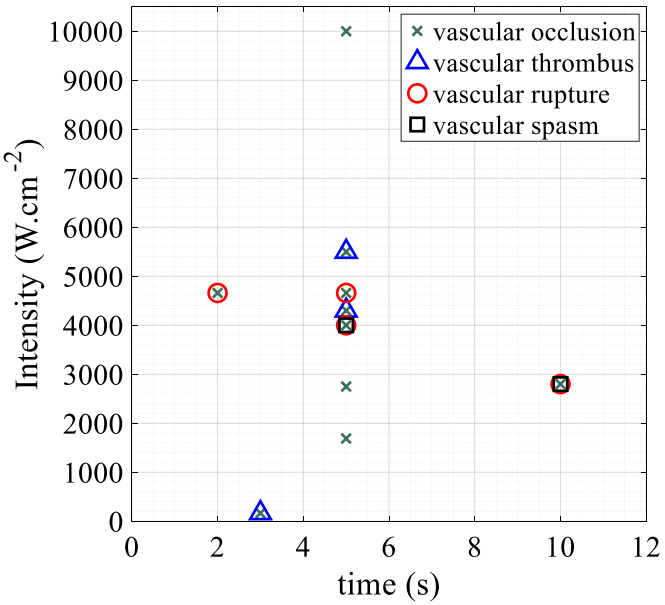


**Figure 2-9 – Summary of effects of HIFU on blood vessels for intensity vs. pulse duration for 10 exposure conditions listed in Table 2-1 and .** Data include stationary and scanned pulses applied continuously to a target vessel between 0.5 and 1.5 mm in diameter with exposure duration between 1 and 10 seconds and a reported intensity (spatial peak or spatial intensity). Vascular bioeffects observed are coded with four symbols: green crosses referred as to occlusion, red circles to vascular ruptures, blue triangles to thrombus and black squares to vascular spasm.

As observed in Table 2-1, and Figure 2-9, when HIFU is applied to blood vessels, several bioeffects can be elicited. These include vascular occlusion, rupture, spasm and shrinkage.

For the treatment of varicose veins, HIFU-mediated vascular occlusion is the most important effect. By analyzing the ultrasound exposure parameters used in previous studies and comparing the occlusion outcomes, it is difficult to infer the mechanisms that led to the occlusion of the blood vessels. The delivered power is not predictive of the vascular outcome. Some investigators have achieved vascular occlusion at low power whilst others reported vascular wall damage without occlusion at higher power.

The mechanisms through which HIFU produces vascular occlusion have been hypothesized by Shaw *et al.*[43], Serrone *et al.*[75] and Goertz *et al.*[37] are discussed in the next section.

### 2.3.2 Effects of HIFU on veins – Mechanisms of vascular occlusion

The majority of preclinical studies that demonstrated the ability of HIFU to occlude intact blood vessels of diameters between 0.5-1.5 mm, used devices initially designed for ablative purposes. Thermal effects of HIFU have predominantly been exploited. Two dominant effects giving rise to vascular occlusion have been outlined. These include vessel wall thermal coagulation and HIFU-induced thrombogenesis [37], [43], [75].

Collagen is a prominent tissue component of the vascular walls. It has been demonstrated to play a pivotal role in the processes governing thermal vessel occlusion [75], [76]. During vessel heating, coagulated collagen fibers can form bridging bonds outside the laminar structure and fuse vascular wall layers together [43], [76]. Such a vascular closure occurs more easily when vessel edges are physically close or mechanically apposed.

Collagen coagulation may also contribute to vascular occlusion in a different way. If collagen is heated beyond its denaturation threshold, ranging between 62 to 67 °C, its structure fractures and collagen fibers undergo isovolumetric shrinkage [43]. Thermal shrinkage of the collagen fibers circumferentially arranged in the vascular wall induces radial compression and thickening of the vascular wall, which leads to luminal narrowing and occlusion.

Vascular occlusion via collagen coagulation has been indirectly suggested in several HIFU studies. For example, Fujiwara *et al.* [29] measured the peak temperatures induced at the vascular wall during sonications. They reported arterial occlusion at peak temperature reaching 97 °C (above collagen denaturation) and not at temperatures between 46 °C and 48 °C. Moreover, they reported vacuolar degeneration in occluded arteries, which suggests indirect collagen denaturation. By shrinking, collagen fibers create spaces within the vascular wall, which is considered to correspond to the vacuolization observed within the tunica media [43]. Ishikawa *et al.*[31] reported vascular occlusion when the temperature reached 98 °C, accompanied with strong vacuolar degeneration and lumen narrowing, as evidenced in the microscopic section of the vessels where high temperature elevation was recorded. Lumen narrowing is thus a good indicator of successful treatment. Vacuolar degeneration associated with vascular occlusion was also reported in other studies [21], [22].

Low temperature elevation yields very different results. Non-occlusive vascular damages have thus been reported for peak temperatures in the range of 43 to 69 °C. This is

consistent with theoretical modelling of vascular thermal damage which suggests that the first tissue changes in the vessels are associated with the denaturation of collagen [77].

The main challenge to coagulate the collagen of the vein wall is to reach high enough temperatures in the vascular walls. This is difficult in the presence of blood flow, since it acts as an energy sink. Non-thermal effects induced by HIFU have been shown to produce bio-effects that could improve heat deposition: Hynynen *et al* induced vascular spasm prior to coagulation [19], which was shown to reduce blood flow and allow faster tissue heating. According to the reviews of Shaw *et al.*[43], Serrone *et al.*[75] and Goertz *et al.*[37], ultrasound radiation force may induce vascular spasm. Acoustic cavitation is also known to enhance heating and could allow more rapid tissue heating [51], [78].

In addition to vascular wall thermocoagulation, thrombogenesis induced by HIFU can also play a role in vascular occlusion [37], [43], [75]. Thrombus formation has been observed in several studies with vascular occlusion (Table 2-1). Intraluminal thrombus formation following HIFU exposures is thought to occur as a result of numerous contributing factors. According to Virchow's triad, three predisposing factors may result in thrombus formation *in vivo:* (i) endothelial damage, (ii) hypercoagulability and (iii) blood flow stasis. All these three have been suggested to occur following HIFU:

i. Endothelial damage can be due to mechanical or thermal phenomena [37].
ii. Blood hypercoagulability describes the activation and aggregation of platelets in the absence of triggers from endothelial damage. It may occur in response to acoustic cavitation and acoustic streaming [75]. In studies conducted by Poliachik *et al*. [79], [80], platelet activation and aggregation after HIFU have been observed at intensities causing cavitation. Authors have attributed this mechanism of platelet activation to shear stress at the surface of platelets arising from acoustic cavitation or acoustic streaming. Indeed, it is well known that platelets can be activated by shear stress on their surface without tissue damage [81].
iii. HIFU was hypothesized to contribute to blood flow stasis in several ways. One is lumen narrowing which may result from denaturation and shrinkage of collagen fibers or as a temporary result from mechanical effects induced by

acoustic radiation forces [43]. The presence of a partial thrombus may also disturb blood flow and contribute to further thrombogenesis.

Based on the reviews from Shaw *et al.*[43], Serrone *et al.*[75] and Goertz *et al.*[37], a schematic of possible mechanisms of vascular occlusion with HIFU is provided in Figure 2-10.

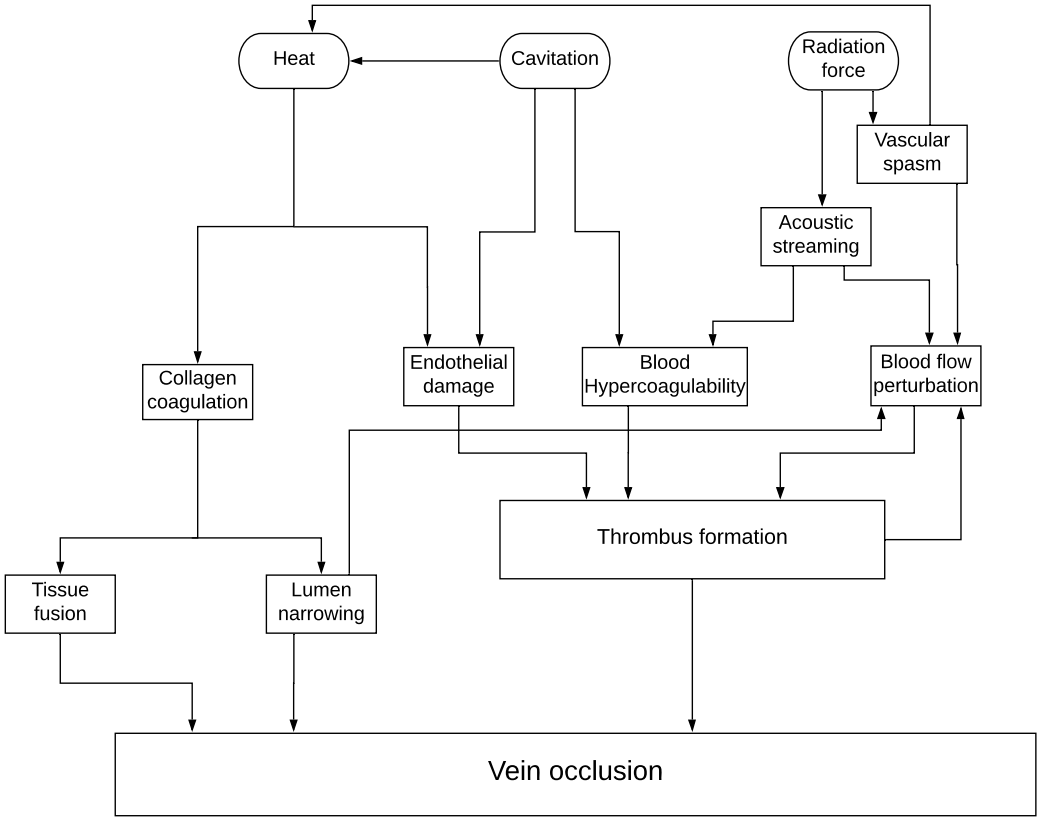


**Figure 2-10 – Suggested mechanisms of vascular occlusion with HIFU.**

.

# 3

# Materials

The purpose of this chapter is to present the materials and methods that were used during this thesis, unless specified otherwise. This chapter is divided into two sections. Section 3.1 introduces the device employed to generate, deliver and monitor HIFU. A general description of the different components of the HIFU device is provided with particular emphasis on the HIFU transducer. The relevant elements of the current ultrasound clinical therapy procedure applied for the treatment of benign tumors are overviewed. Finally, section 3.2 presents the numerical model used to simulate the treatments.

## 3.1 The ultrasound therapy equipment: the Echopulse®

### 3.1.1 General apparatus description

All experiments conducted in this thesis were carried out with an Echopulse device manufactured by Theraclion. This medical device is CE-marked for the treatment of breast fibroadenomas and benign thyroid nodules. The Echopulse is composed of several subsystems (Figure 3-1), including a mobile console, a touchscreen user interface and a treatment head on which is mounted a visualization and treatment unit (VTU). The complete system is shown in Figure 3-1.

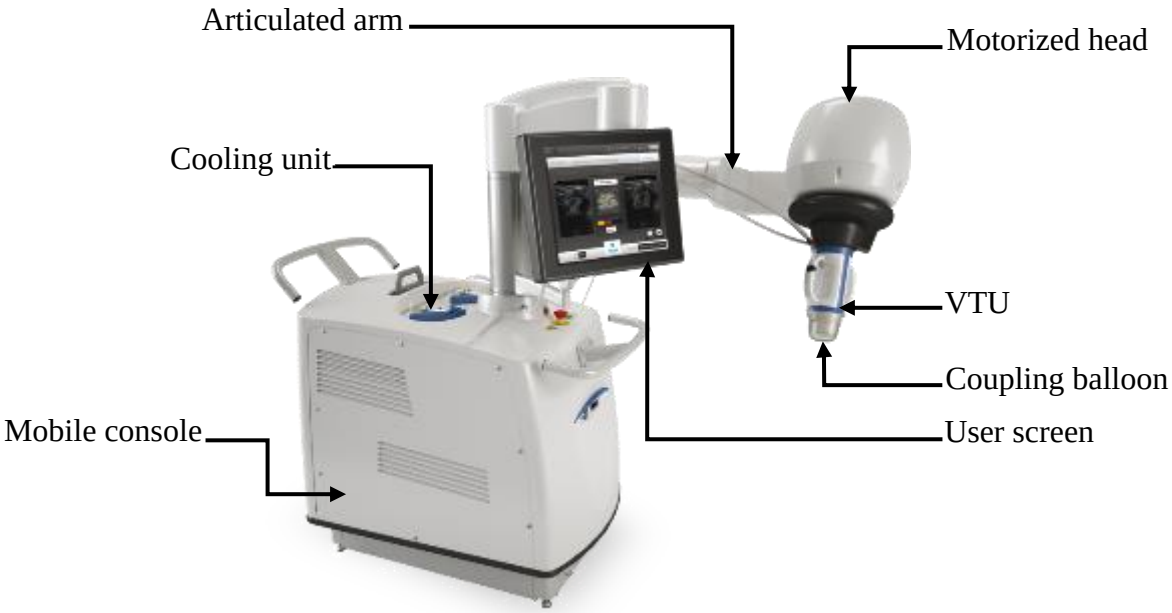


**Figure 3-1 – Echopulse system.**

The Echopulse system contains a motorized visualization and treatment unit (VTU) mounted on an articulated arm to facilitate the positioning. The VTU is a removable part that incorporates both imaging and therapy transducers (Figure 3-2).

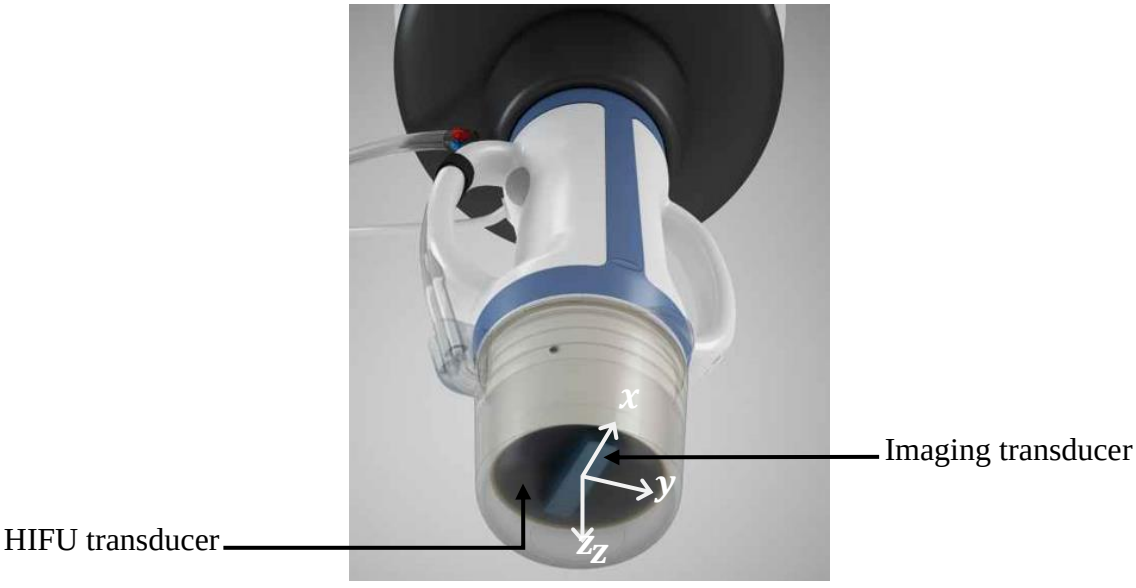


**Figure 3-2 – Visualization and Treatment Unit.** The HIFU transducer appears in black and the imaging transducer in blue.

The diagnostic transducer is placed at the center of the HIFU transducer to provide real-time imaging and monitoring during sonications. The imaging probe is a linear array operating at 6.2 MHz and offering both B-mode and color Doppler imaging. A motorized head permits micro-movements of the VTU in $(x, y, z)$ so that the VTU can be accurately moved to the desired location. It also allows a rotation around the propagation axis of the therapeutic ultrasound beam to allow a transition between longitudinal and transverse imaging. The HIFU source is described further in the next section.

The system operates in conjunction with a single-use disposable kit called EPack. The EPack comprises a prefilled pouch with a degassed fluid, a balloon and tubes to connect the balloon to the pouch. The pouch is placed in a dedicated bracket and incorporated into the cooling unit where the fluid is cooled by Peltier modules. The balloon is mounted on the VTU, in front of the therapeutic transducer. Pumps circulate the fluid in a closed loop from the pouch to the balloon, and back. The fluid serves as an acoustic interface coupling the ultrasound energy between the VTU and the skin. Acoustic gel is applied between the balloon and the skin to optimize transmission. The temperature of the circulating fluid is continuously evaluated with thermal sensors included in the VTU and is maintained during treatment between 8 °C and 14 °C. The cooling liquid protects the transducer from overheating. More importantly the cooling liquid removes excess heat from the patient's skin preventing skin burns during treatment.

The hardware that drives the VTU as well as the electrical and software components for treatment delivery and monitoring is housed into the system console. It comprises the HIFU beam generator, a personal computer (PC), control and data acquisition electronics and an ultrasound scanner. The PC communicates with the hardware and the ultrasound scanner for both control and data acquisitions. The operator controls the system hardware components with a touchscreen. The touchscreen also displays the user interface for treatment delivery and real-time monitoring. The current interface offers a number of key features. It guides the operator through the clinical procedure, such as the installation of the kit (Figure 3-3 (a)), the visualization and pre-determined treatment steps. During treatment steps, the user outlines the target on the ultrasound image and treatment sites within the target are proposed by the software (Figure 3-3 (b)). The user interface additionally allows the operator to define and

execute the treatment plan and adjust the energy level and the sonication duration during the course of the treatment (Figure 3-3 (c)).

(a) (b)

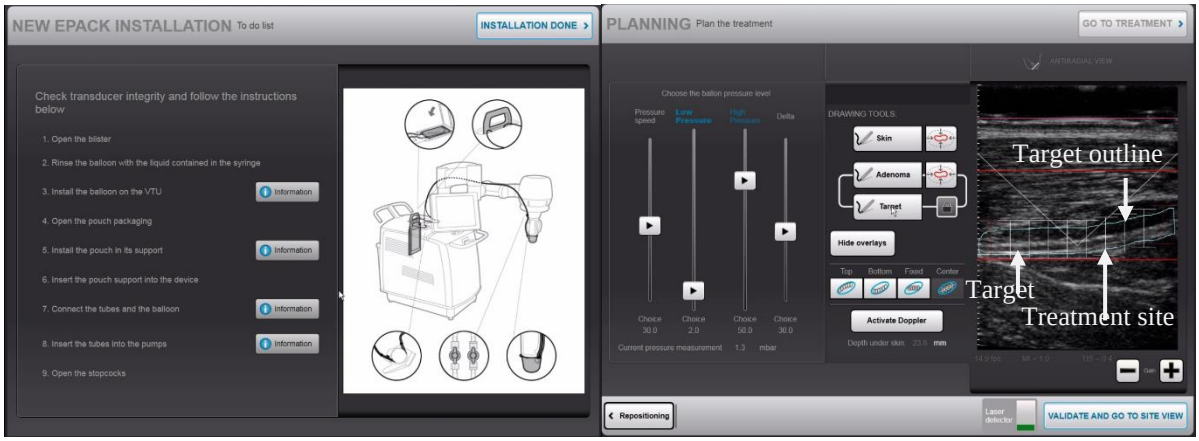


(c)

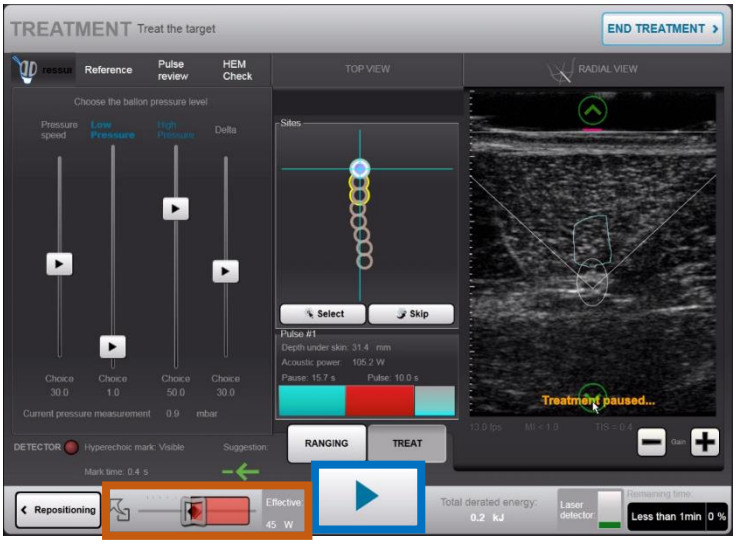


**Figure 3-3 – User Interface.** (a) Instruction for the EPack installation. (b) Planning step: The user outlines the target (blue line). Treatment sites (white lines) are automatically generated. (c) Treatment step: The user can start/pause the treatment (blue rectangle), refine the focus position (green arrowheads) and adjust the power (orange rectangle).

### 3.1.2 The HIFU source

The therapy transducer is a single element concave transducer made of piezo-composite materials. It operates at 3 MHz and has a curvature radius of 38 mm and an outer diameter of 56 mm. The f-number of this transducer is 0.7, which makes the transducer strongly focused.

All experiments conducted during this thesis used equivalent transducers, but not exactly the same. Before the experiments, the acoustic power of the VTU transducer was

calibrated and the efficiency was determined. In addition, the acoustic intensity distribution on the focal plane was characterized, as described below.

To calibrate the acoustic power output of the VTU transducer, a radiation force balance (RFB-2000, ONDA Corporation, Sunnyvale, CA, USA) was used. The RFB consists of a recipient filled with degassed water (water tank) inside which is deposited at the bottom a weight sensor holding an absorbing target (an absorbing brush). The transducer is immersed in the water tank and is aligned towards the brush. The transducer is then excited at 3 MHz and at various electrical powers. The electrical power delivered effectively is recorded and the acoustic power is measured. All the transducers used during our experiments had an efficiency superior or equal to 70 %.

Additionally, the acoustic field was also characterized in terms of free field measurements conducted in water with a three-dimensional scanning tank (AIMS III scanning tank, ONDA, Sunnyvale, CA, USA) comprising a 75-µm needle type hydrophone. The beam profile was measured at low power level (0.25 W). The transducer was driven at 3 MHz by an arbitrary function generator (Agilent 33220A, Agilent, Santa Clara, CA, USA) and at an amplitude of 10 V peak to peak. Once the position of the focus was determined, the root mean square (rms) pressure field was measured within the three orthogonal planes containing the focus. Figure 3-4 shows an example of a measured rms pressure field in the $xy$ plane. Intensity was then derived from acoustic pressure measurements and the temporal-average intensity (ITA) along the propagation axis $z$ was calculated. An example of a typical beam scan is given in Figure 3-5. From pressure measurements, the extent of the focal spot is determined by the -6 dB level and is equal to 2.20 mm in the axial direction and 0.5 mm in the transverse direction.

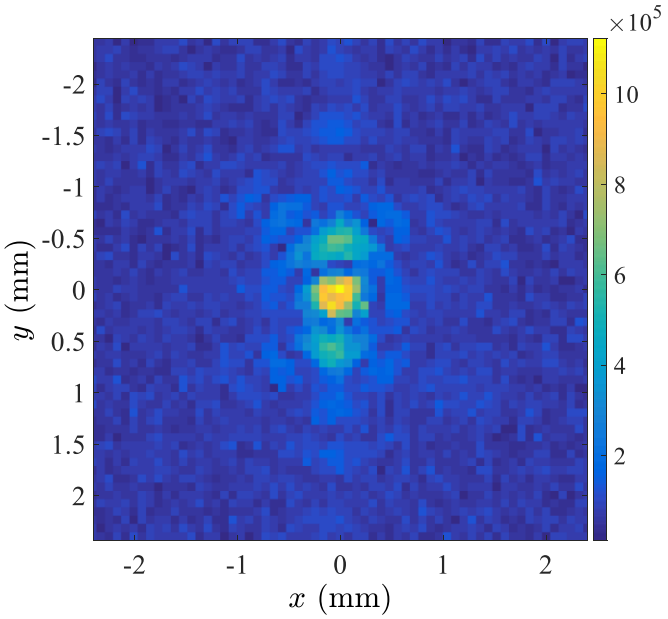


**Figure 3-4 – rms pressure field in the focal *xy* plane.** Pressure is expressed in Pascals.

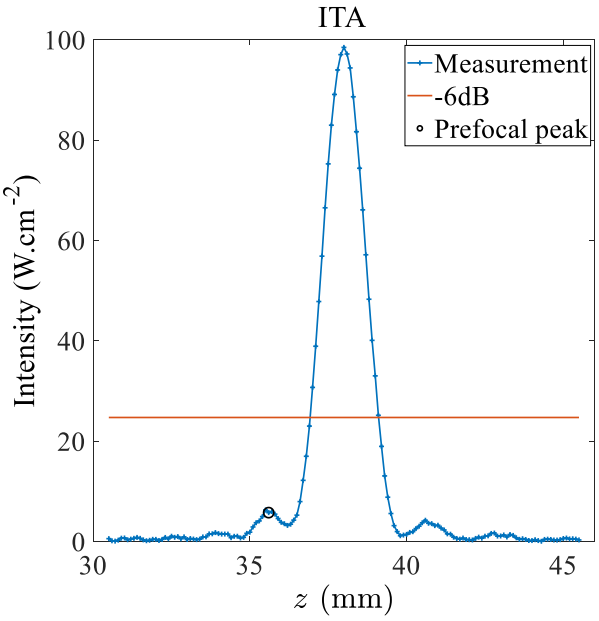


**Figure 3-5 – Typical intensity distribution of the acoustic field along *z* axis.**

### 3.1.3 Current ultrasound therapy procedure

Pulses currently used in clinics for the CE-marked Echopulse® are either 4 s or 8 s long. The acoustic power to be delivered is adjusted during treatment according to the appearance of

hyperechoic regions on the ultrasound image. The acoustic powers range typically from 60 to 85 W. This procedure was validated to induce reproducible lesions. When the target volume is larger than the unitary lesion size, the HIFU transducer is moved from site to site and one pulse is delivered at each site. Pauses are automatically set following each exposure to allow skin cooling. The minimal required pause time is calculated depending on the depth under skin and on the acoustic power delivered.

For the application of HIFU to veins, the sonication method was refined. In particular, simulations were performed to adapt the treatment parameters. The next section gives an overview of the HIFU treatment simulator that was used for this purpose.

## 3.2 The HIFU treatment simulator

The numerical modeling of an ultrasound thermal treatment is divided into two main steps. First, the propagation of the ultrasound wave in tissue is computed and the acoustic field in the tissue is determined. Second, the temperature evolution in the tissue is modeled. The HIFU therapy simulator of Theraclion developed by Grisey [82] and utilized throughout this thesis is thus composed of two modules: an acoustic simulator and a thermal simulator. These modules are summarized in the following sections.

### 3.2.1 Acoustic simulator

The modeling of the ultrasound propagation in tissue is based on the use of the k-Wave library1 [83]–[85], which is based on a k-space pseudospectral method. The open source k-Wave software, developed by Bradley Treeby, Ben Cox and Jiri Jaros, was chosen for several reasons. First, the pseudo-spectral method enables the modeling of a nonlinear ultrasound propagation in heterogenous media with power law absorption. Second, the ultrasound model enables to simulate the ultrasound propagation for non-axisymmetric transducers, like the one used in this work and it is not limited to parabolic approximation, which is only valid for f-numbers above 1.5. Furthermore, the k-space pseudospectral method efficiently allows small

[1] http://www.k-wave.org/

grid steps, which enables large HIFU fields to be simulated. The k-Wave software was validated previously for high acoustic intensities [86] as well as for the modeling of HIFU treatments with Theraclion's transducer [82], [87]. Last, it is well documented and maintained.

Instead of solving the wave equation, k-Wave solves the coupled first-order system of equations comprising the conservation equations and a pressure-density relation that incorporates non-linear effects and power law absorption [88], [89]. The set of governing equations is the following:

Momentum conservation $$\frac{\partial \mathbf{v}}{\partial t} = -\frac{1}{\rho_0}\nabla p$$

Mass conservation $$\frac{\partial \rho}{\partial t} = -(2\rho + \rho_0)\nabla \cdot \mathbf{v} - \mathbf{v} \cdot \nabla \rho_0$$

Pressure-density relation $$p = c_0^2(\rho + \mathbf{d} \cdot \nabla \rho_0 + \frac{B}{2A}\frac{\rho^2}{\rho_0} - L\rho) \quad (3.1)$$

Here, $\mathbf{v}$, $p$ and $\rho$ refer respectively to the acoustic particle velocity, the pressure and the density, $\rho_0$ corresponds to the equilibrium density of the medium, $c_0$ is the isentropic sound speed, $\mathbf{d}$ is the acoustic particle displacement, $\frac{B}{A}$ is the nonlinearity parameter and $L$ is the power law absorption operator. $L$ is given by the following expression:

$$L = \tau \frac{\partial}{\partial t}(-\nabla^2)^{\frac{y}{2}-1} + \eta(-\nabla^2)^{\frac{y+1}{2}-1} \quad (3.2)$$

where $y$ is the power law exponent and $\tau$ and $\eta$ respectively the absorption and dispersion coefficients. These are given by: $\tau = -2\alpha_0 {c_0}^{y-1}$ and $\eta = 2\alpha_0 {c_0}^{y}\tan(\pi y/2)$, $\alpha_0$ representing attenuation prefactor in units of Np.(rad/s)$^{-y}$.m$^{-1}$.

Solving this coupled first-order system gives the advantage to compute the particle pressure and velocity, which allows direct calculation of the acoustic intensity. Further details on the method are provided in the k-Wave user manual [85] and in the related publications [83]–[85], [90].

In spite of the efficiency of the mathematical approach used in k-Wave, the 3D nonlinear simulation of the HIFU field at 3 MHz over the required computational domain remains too costly in terms of memory. To overcome limits associated to the computational burden, Grisey *et al.* developed a 'layer-by-layer' approach [82], [87]. This approach takes advantage of the beam convergence, which becomes smaller as harmonics are generated. The

principle consists in splitting the computational domain along the main propagation axis and successively simulating the ultrasound propagation from the upper simulation domains to the focus and beyond with finer grid steps. The principle is illustrated in Figure 3-6.

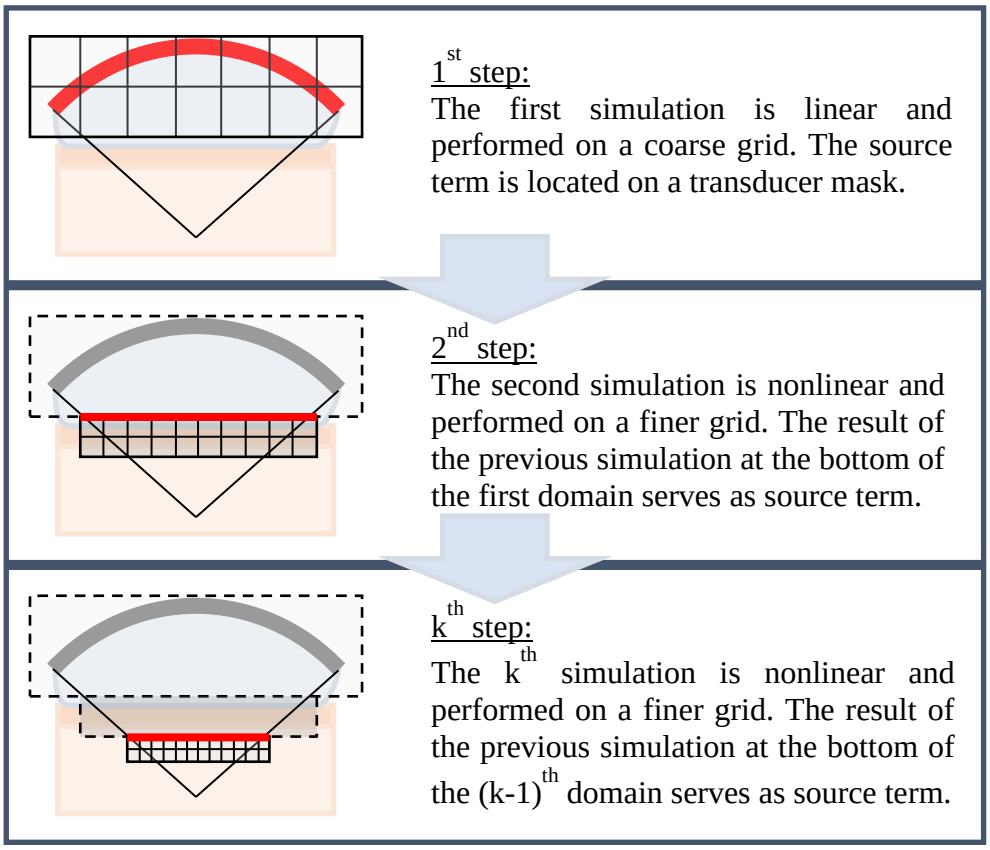


**Figure 3-6 – Illustration of the layer-by-layer approach (taken from Grisey *et al* [82], [87]).** The source term is set at the position of the red line.

In this model, acoustic parameters are treated as temperature independent. As k-Wave allows for direct calculation of the velocity field, the temporal-averaged intensity is calculated as: $\mathbf{I} = < p\mathbf{v} >$ with $p$ the pressure field, $\mathbf{v}$ the vector velocity field and $< . >$ referring to the temporal average over one period.

The acoustic energy lost by the wave between two consecutives $xy$ planes is first computed based on the intensity field. It is then distributed in each plane according to $\frac{2\,\alpha\,\langle p^2 \rangle}{\rho c}$. Further details about the computation of the acoustic heat source can be found in [82], [87].

It is then utilized as source term in the thermal simulator which computes the temperature field within tissue. The next section presents the thermal module.

### 3.2.2 Thermal simulator

The temperature evolution in tissues is modeled with the Pennes' bioheat equation [91]:

$$\rho_t C_t \frac{\partial T_t}{\partial t} = k_t \nabla^2 T_t + \omega_b \rho_b C_b (T_b - T_t) + Q \tag{3.3}$$

Here, $\rho, C$ and $T$ refer to density, specific heat and temperature respectively, $k_t$ is the tissue heat conductivity, $\omega_b$ represents the perfusion rate and the subscripts $t$ and $b$ refer to tissue and blood respectively. Finally, $Q$ is the heat source term.

The equation is solved in 3D using a first-order explicit finite-difference scheme with Matlab (Mathwork, Natick, USA). Further details can be found in [82], [87].

In the next chapter, the ability of occluding small veins non-invasively with the Echopulse HIFU device is investigated.

# 4

# Identification and validation of sonication parameters to occlude veins of 2 mm in diameter

## 4.1 Introduction

The success of endovenous thermal techniques for the treatment of varicose veins is usually defined in clinical studies as the achievement of vein occlusion [13]. To create venous obliteration, these treatment modalities require contact with the target vein, which is accomplished through transcutaneous insertion of catheters into the vein. In contrast to endovenous thermal modalities, HIFU can reach subcutaneous tissues without the necessity of skin incisions. The ability of HIFU to occlude non-invasively intact blood vessels *in vivo* and within deep tissue has been demonstrated in several animal models [19], [21], [22], [29], [31].

However, durable occlusion was either not demonstrated in previous studies or only achieved in small diameter vessels (0.5 – 0.6 mm) [19], [31]. Furthermore, these studies were limited to gross assessments of the presence or absence of blood flow, with the exception of the study conducted by Ishikawa *et al.* [31] who provided histological evidence of occlusion in the days following sonications.

In this chapter, we investigate the feasibility of inducing non-invasively and with 3-MHz ultrasound reproducible and sustained occlusion of veins larger than those investigated in the literature ($\geq$ 2 mm in diameter). The model selected for this feasibility study is the rabbit saphenous vein because it provides a cost- and size-efficient model for the study of venous occlusion. Moreover, the saphenous vein is part of the superficial venous system, which allows chronic studies to be performed without the risk of limb necrosis. The exposure parameters

(pulse duration and acoustic power) routinely used in clinics with the Echopulse device were used here.

Prior to the *in vivo* investigation, the number of sonications and the spacing between pulses were first investigated numerically with the k-Wave toolbox [83]–[85]. The objective was to continuously coagulate vein segments of 2-cm in length. Finally, experimental studies were performed to occlude rabbit saphenous veins *in vivo* in a sub-acute setting, based on the sonication strategies identified during the numerical study. The acute and sub-acute venous tissue damages were evaluated by color Doppler and histology.

The results in this chapter have been previously presented (*International Symposium on Therapeutic Ultrasound 2018 , Focused Ultrasound Symposium 2018*) and published [92].

## 4.2 Methods

### 4.2.1 Numerical study

We assumed that the vein would need to be continuously coagulated in order to induce an effective and long lasting occlusion. Simulations were therefore performed to adjust the sonication layout to ensure continuous coagulation of a vein of 2-cm in length and 2-mm in diameter. In this numerical study two types of pulses were considered: (1) fixed pulses and (2) moving pulses at constant speed (0.75 $mm.s^{-1}$). In both cases, we used 4-s long continuous pulses at an acoustic power of 85 W. These exposure parameters were chosen because they have been successfully used in clinics to coagulate soft tissues (fibroadenomas [93] and Thyroid [94]), with an averaged lesion width of 2.6 mm [87]).

The corresponding acoustic pressure field, temperature rise and vascular thermal damages were successively simulated. The therapy transducer described in Chapter 3 was modelled. Because of the rectangular hole in the transducer for the imaging probe, the generated beam is not axisymmetric, and three-dimensional simulations were therefore necessary.

Hereinafter, $z$ denotes the main ultrasound propagation axis, pointing from the transducer to the focus towards the subject anatomy, $x$ is the axis of the imaging transducer and oriented along the left-to-right direction of the generated images, and $y$ results from the

cross product of $z$ and $x$, for the frame $(x, y, z)$ to be orthonormal and right-handed. The frequency used for the treatments was 3 MHz.

We modeled a particular configuration in which the blood flow was stopped by compressing the vein upstream. In the simulations, the vein was thus considered as collapsed and the blood flow abolished. The geometrical focal point was considered to be located at 15 mm under the skin. We assumed that the ultrasound beam propagates through three layers, from top to bottom: (1) the coupling liquid located in front of the transducer; (2) the skin and (3) the muscles. Skin was modelled as a 2-mm thick layer. For illustration purposes, a 2D view of the geometrical model is shown in Figure 4-1.

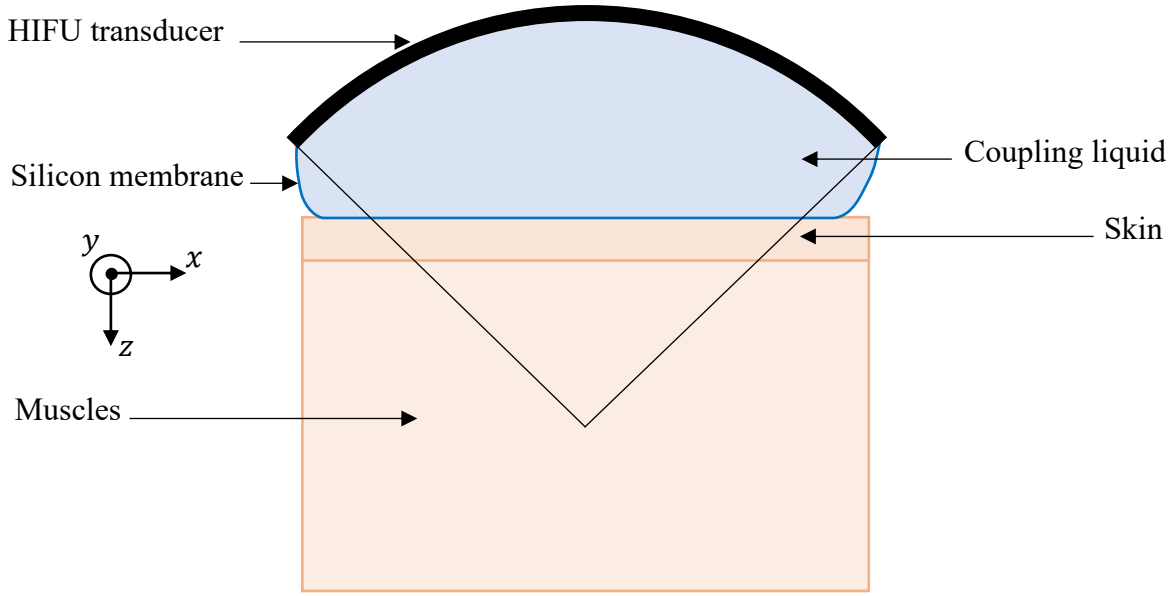


**Figure 4-1 – Model used in the simulations.**

The acoustic propagation of the focused ultrasound beam was first simulated. The corresponding thermal rise was then simulated by solving the Pennes' bioheat equation. A thermal damage function was finally used to calculate the extent of the thermal damage based on the temperature profile.

#### 4.2.1.1 Acoustic simulations

The wave field was computed using a k-space pseudo-spectral method with the k-Wave toolbox 1.2 [83]–[85] as described in Chapter 3.

Nonlinear effects were taken into account in the simulations with the 'layer-by-layer' approach [87]. Without the layer approach, the simulation of the nonlinear propagation up to the fifth harmonic with the minimum of two points per wavelength would have required a grid of $1.37 \times 10^9$ points, with our of $60 \times 60 \times 46$ mm grid and at a 3 MHz central frequency.

We used one layer for the cooling liquid, one layer for the skin and five layers for muscle tissue. Nonlinearities were modeled up to the fifth harmonic in the widest layer. The size of the smallest layer was $4 \times 4 \times 4$ mm with a spatial grid step of 49.8 µm. A perfectly matched layer was used to avoid reflections at the boundaries of the domain. The Courant-Friedrichs–Lewy (CFL) number was set to 0.5 resulting in a smallest time step of 14.8 ns. The acoustic source term was computed as:

$$p^2 = \frac{2 \times P_{ac} \times \rho \times c_s}{S_{transducer}} \tag{4.1}$$

where $p$ is the pressure amplitude, $P_{ac}$ is the acoustic power, $\rho$ the density, $c_s$ the speed of sound and $S_{transducer}$ the area of the active surface of the transducer, which is equal to $2.07 \times 10^{-3}$ m$^2$. $P_{ac}$ was set to $P_{ac} = 85$ W. The cooling liquid, skin, fat and muscle tissue were modeled as homogenous media with the acoustic properties listed in Table 4-1.

Tissue properties were assumed to remain constant during the full procedure. Variability of parameters with temperature was neglected for all simulations.

**Table 4-1 – Acoustic properties of tissues used for simulations.**

| | Cooling liquid [95] | Superficial tissue (skin…) [87] | Muscle [48] |
|---|---|---|---|
| Sound speed (m.s$^{-1}$) | 1495 | 1547 | 1587 |
| Density (kg.m$^{-3}$) | 1000 | 1214 | 1041 |
| Attenuation (dB.cm$^{-1}$) | 0 | 2.2 | 3.0 |
| Acoustic non-linearity parameter | 4.9 | 9.0 | 7.8 |

#### 4.2.1.2 Thermal simulation

Tissue heating was modeled using the Pennes's bioheat equation [91]:

$$\rho C \frac{\partial T(\mathbf{x},t)}{\partial t} = k\nabla^2 T(\mathbf{x},t) + Q(\mathbf{x},t) + \omega_b \rho_b C_b (T_b - T(\mathbf{x},t)) \quad (4.2)$$

where $\rho, C, T, k$ and $Q$ are the density, special heat, thermal conductivity, tissue temperature and heat source respectively. The last term corresponds to the blood perfusion with $\omega_{b,}\ \rho_b, C_b$ and $T_b$ corresponding to the blood perfusion rate, blood density, blood specific heat and blood ambient temperature respectively. **x** corresponds to the spatial coordinates (*x*,y,z) and $t$ is the temporal variable. The equation is solved in 3D by using a first-order Euler explicit scheme in time and a centered difference scheme in space. The time step was 50 ms and the spatial step was 200 µm. The grid size was 38 × 38 × 29 mm. The heat source term was computed as described in Grisey *et al.* [87].

The tissue initial temperature was set to $T_0 = 39.5$ °C, which is the mean body temperature for rabbits [96]. Dirichlet boundary conditions were used with $T = T_0$ on the boundaries. The cooling time between subsequent sonications was set to 15 s.

The tissue properties used in the thermal simulations are listed in Table 4-2. They were assumed invariant with temperature in simulations.

**Table 4-2 – Thermal properties of media used in thermal simulation.**

| | Muscle [48] |
|---|---|
| Specific heat capacity ($J.kg^{-1}.K^{-1}$) | 3600 |
| Thermal conductivity ($W.m^{-1}.K^{-1}$) | 0.47 |
| Perfusion ($s^{-1}$) | 0.018 |

#### 4.2.1.3 Thermal damage

Modelling of vascular thermal damage [77] suggests that vessel thermal damage correlates with the denaturation of collagen fibrils, which begins at 62 °C [97]. In this study the extent of thermal damage to vessels was evaluated based on the dedicated thermal damage model derived by Agah *et al.* [77]. By considering denaturation of collagen as a first-order reaction, damage was modelled using a general Arrhenius equation:

$$\Omega(\mathbf{x},t) = \ln\left(\frac{c(\mathbf{x},0)}{c(\mathbf{x},t)}\right) = A_f \int_0^{\tau} \exp\left(\frac{-E_a}{RT(\mathbf{x},t)}\right) dt \quad (4.3)$$

where **x** denotes the spatial coordinates $(x, y, z)$, $t$ the temporal variable and $\Omega(\mathbf{x},t)$ the damage parameter. $c(\mathbf{x},0)$ and $c(\mathbf{x},t)$ are the concentrations of the undamaged molecules at the beginning and at time $t$ respectively. $A_f$ is the frequency factor, $E_a$ the activation energy, $R$ the universal gas constant and $T(\mathbf{x},t)$ the temperature. According to Agah *et al.* [77], $E_a$ and $A_f$ were set to $E_a = 430$ kJ.mol$^{-1}$ and $A_f = 5.6 \times 10^{63}$s$^{-1}$.

The degree of vessel damage is appraised by $\Omega(\mathbf{x},t)$ where $\Omega(\mathbf{x},t) = 1$ defines the first noticeable irreversible damage and formally corresponds to the denaturation of 63 % of the native proteins [77]. For an effective occlusion, we assume that the whole vein wall needs to be extensively damaged. Therefore, the threshold for thermal damage was set to $\Omega(\mathbf{x},t) = 5$, which formally corresponds to the denaturation of 99 % of the collagen.

Based on the results of the simulations, the ultrasound treatment parameters were then experimentally tested *in vivo* on rabbit saphenous veins. One has to note here that the rabbit thigh has a collateral circulation which enables the limb to remain viable even after occlusion of its saphenous veins. This allows the conduction of chronic studies without the risk of phlebitis.

### 4.2.2 Animal experiments

All animal work was approved by the institutional ethics committee for animal experiments under the agreement number CE16/2016082512126208. Experiments were carried out according to the guidelines of the French National Comity for animal trials C.N.R.E.E.A (Comité national de réflexion éthique sur l'expérimentation animale). Fifteen New-Zealand white rabbits, five males and ten females were used for the experiments (2 to 4 months old and 2.7 to 4.5 kg weight). HIFU exposures were applied on medial saphenous veins. Prior to sonications, the animals were anesthetized intramuscularly with a mixture of Ketamine (0.33 mg.kg$^{-1}$, Virbac, France), Domitor (0.5 mg.kg$^{-1}$, Vetoquinol, France) and Valium (0.17 mg.kg$^{-1}$, Roche, Switzerland). They were then intubated with an endotracheal tube and ventilated with Isoflurane (2-2.5 %, Virbac, France) to be maintained under anesthesia throughout the procedure. The fur of their hind limbs was shaved with a hair trimmer and then

carefully depilated with a depilatory cream (Klorane, Laboratoires Klorane , France) to ensure good acoustic coupling and prevent skin burns.

Before the procedure, the rabbit was placed on the table in supine position to access the targeted vein. Ultrasonic gel (Polysonic®, Parker Laboratories, USA) was applied to the area to be treated to ensure appropriate coupling. B-mode ultrasound and color Doppler imaging were used to position the focus on the vein. Ultrasound imaging was performed before and after sonication to assess the HIFU-induced effects on the vein. Twenty-seven medial saphenous veins with an average diameter of 2 mm were exposed to HIFU. HIFU sonications were applied for 4 s and at an acoustic power of 83 $\pm$ 10 W. This latter was determined by multiplying the electric power by the efficiency of the transducer (previously measured to be equal to 70 %). The corresponding spatial-peak intensity estimated from linear extrapolation from low power hydrophone measurement in water is 28 $kW.cm^{-2}$.

Blood flow is known to hamper thermal therapies by cooling down the vein wall [98]–[102]. Therefore, several configurations based on previous simulations were tested during the HIFU treatments: (1) 5 veins were treated with multiple pulses (median 1.5 mm spacing) distributed along the target vein (Figure 4-2 (a)); (2) 14 veins underwent the same treatment protocol than the one used in configuration (1) but the hind limb was elevated to about 25° from the horizontal to diminish blood flow (Figure 4-2 (b)); and (3) 8 veins were sonicated with moving pulses ($0.75\ mm.s^{-1}$ along a 3 mm line transecting the vein) and were mechanically compressed by pressing a finger on the groin during exposures to stop blood flow and minimize its heat sink effect (Figure 4-2 (c)). Rear limb elevation drains the intraluminal blood from the veins and reduces the lumen diameter (illustrated in Figure 4-2 for configurations (2) and (3)). For configuration (3), according to the simulations, the spacing between moving pulses was reduced to 0.5 mm to account for the smaller lesion size in the longitudinal direction (Figure 4-2 (c)). The number of sonications was thus increased to sonicate the same length of 2 cm. A minimum waiting time period of 15 s was set between two sonications to allow the skin to cool down. Experimental protocols are summarized in Table 4-3.

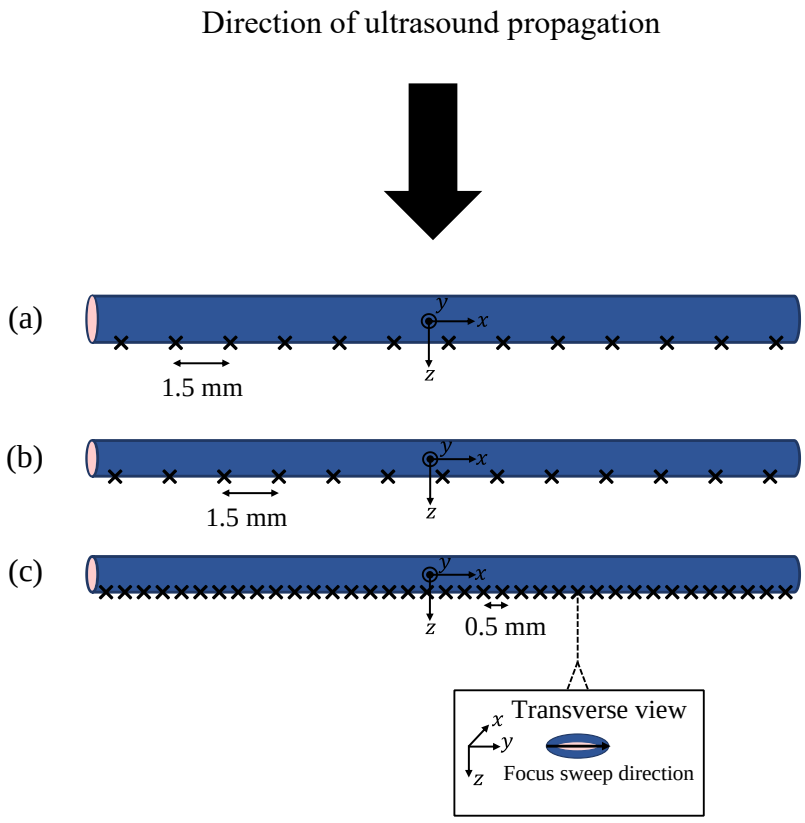


**Figure 4-2 – Schema illustrating dispositions of HIFU exposures.** (a), (b) and (c) stand for configurations (1), (2) and (3) respectively. Sonication sites are represented by black crosses.

**Table 4-3 – Experimental conditions.**

| Protocol ID | 1 | 2 | 3 |
|---|---|---|---|
| Number of veins | 5 | 14 | 8 |
| Sonication types | Fixed pulses 1.5 mm apart | Fixed pulses 1.5 mm apart<br>Hind limb elevated | Linear track with sites 0.5 mm apart<br>Hind limb elevated<br>Vein compressed |

After the experiments, the rabbits were woken up and were monitored for a mean period of 15 days after the treatment to assess the sustainability of the effects of HIFU exposures on the veins. Animals were then euthanized by intravenous injection of Pentobarbital (1 $mL.kg^{-1}$, Med'Vet, France).

The day of euthanasia, the animals underwent a *postmortem* dissection and the targeted vessel was harvested. A venous sample was also extracted from untreated region and served as a control. In some cases, the perivenous conjunctive tissue was adhering to the vein and

could not be separated. In such cases, the vein was sent for analysis with the attached perivenous tissue.

The proximal tip of each venous section was sutured, preserved in labelled cassettes, fixed in 4 % formalin and sent for histologic examination. Samples were then cross-sectioned into three subsections and included in paraffin. 4 µm slices were cut and stained with hematoxylin-eosin (HE) for evaluation. Each section was evaluated by a pathologist, blinded to the experiment.

Excision of the proper vein segment was difficult since other veins branch in the vicinity of the target. Therefore, samples were taken into account only when a vein was present on the slide and was located within the HIFU lesion. Changes were graded as described in Table 4-4.

**Table 4-4 – Histological grades.**

| Grade | Histological features |
|---|---|
| 0 | Normal vein |
| 1 | Reactive endothelium |
| 2 | Myoendothelial proliferation |
| 3 | Acute fibrinous thrombi |
| 4 | Thrombus organization |

## 4.3 Results

### 4.3.1 Simulations

Figure 4-3 shows the distribution of peak positive and peak negative acoustic pressures in the *yz* plane simulated with the ‘layer by layer’ approach. Simulations were run at 3 MHz and at an acoustic power of 85 W. Maximum peak positive and peak negative pressures are 40.3 and -13.2 MPa respectively.

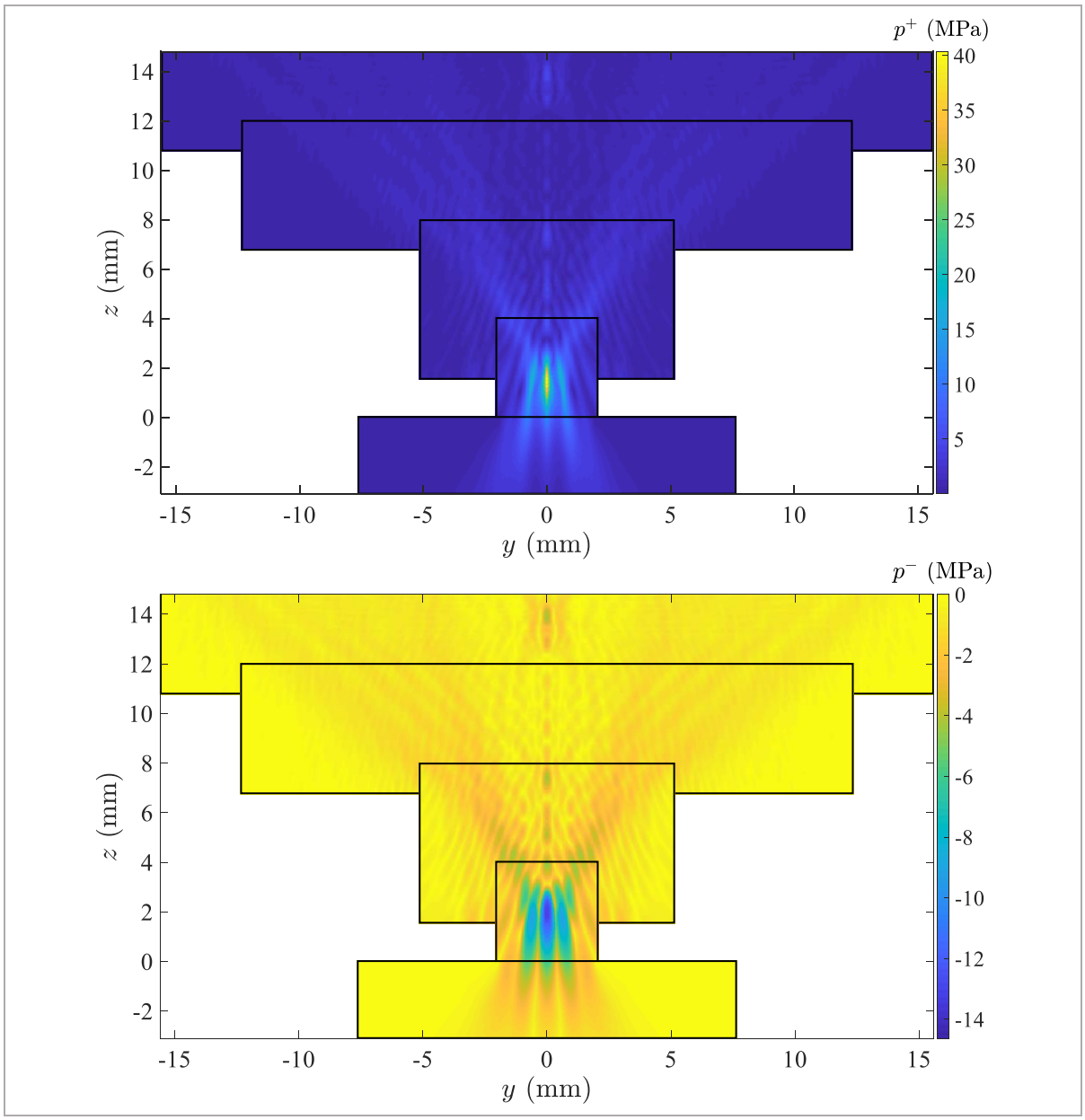


**Figure 4-3 – Peak positive and peak negative pressure fields at 3 MHz in the *yz* plane.** Pressure is expressed in MPa and black rectangles represent the limits of the successive simulation layers.

Temperature elevation at the expected location of the upper vein wall, i.e. 2 mm above the focal point centered on the lower vein wall, is plotted on Figure 4-4 for configurations (2) and (3).

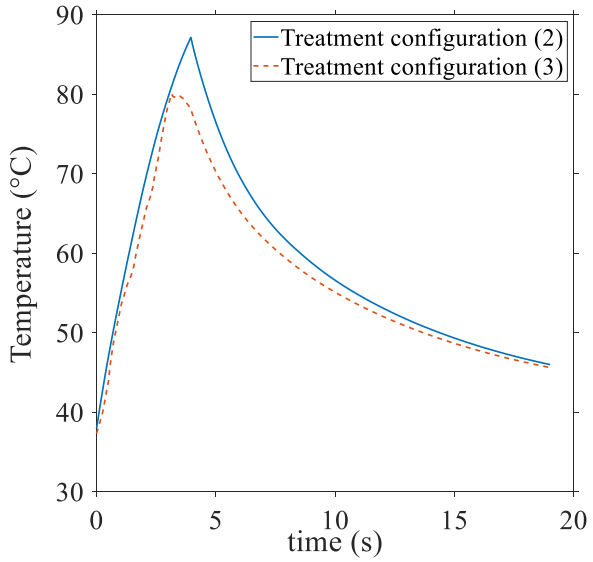


**Figure 4-4 – Estimated temperature rise at the location of the upper vein wall during 4 s sonication followed by 15 s cooling for unitary fixed pulse (solid line) and moving pulse (dash line).**

For unitary fixed and moving pulse, the extent of the coagulated zone calculated with the thermal damage model was 1.2 mm and 0.6 mm respectively along the vein, and 1.8 mm and 2.7 mm respectively in the direction orthogonal to the vein.

To induce homogeneous and extensive heating of a 2-cm vein segment, we introduced a series of pulses distributed along the vein. 13 fixed pulses were first modeled, with a spacing of 1.5 mm.

Figure 4-5 shows the results of thermal damage distribution for such treatments. An iso-contour representing the area corresponding to denaturation of 99 % of native proteins is displayed. The simulated distribution of thermal damage is displayed using maximum intensity projections. To quantify the impact of the trajectory, attention has been given to the extent of the region corresponding to protein denaturation.

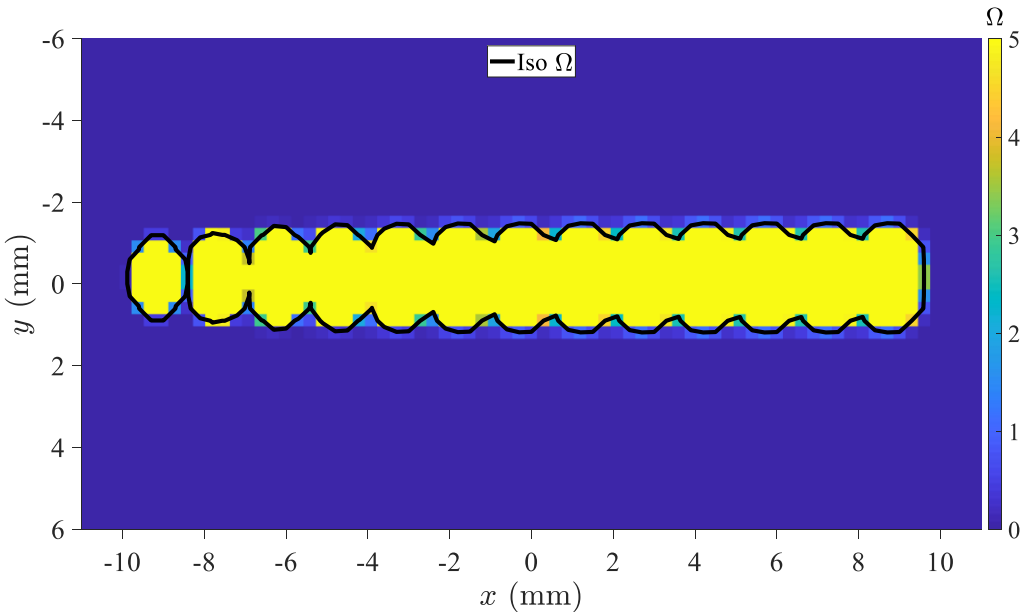


**Figure 4-5 – Maximum intensity projected damage map at the end of a treatment comprising thirteen 4 s fixed pulses delivered 1.5 mm apart at an acoustic power of 85 W and with the focus located at 15 mm under skin.** Iso-contour corresponding to the thermal damage where 99 % of native proteins denature is displayed in black.

As can be seen on Figure 4-5, the lesion size hardly covers the 2 mm diameter of the vein. We thus proposed to simulate 37 pulses moving along the cross-sectional axis with a spacing of 0.5 mm and distributed along the longitudinal axis of the vein, for the treatment of veins with larger diameters. Figure 4-6 shows the results of thermal damage distribution for such treatments with 37 moving pulses, with the same display as in Figure 4-5.

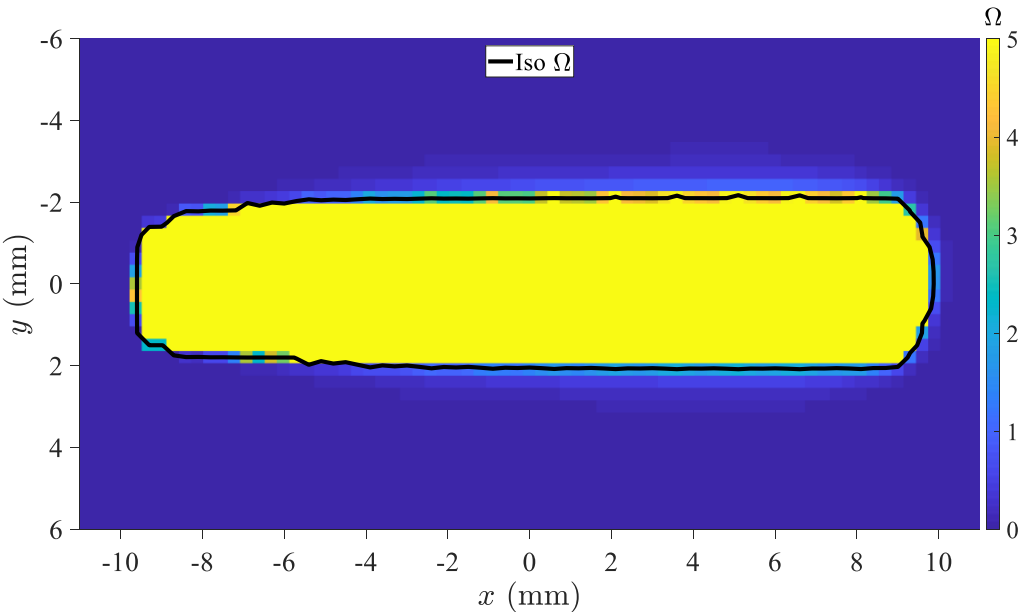


**Figure 4-6 – Projected damage map at the end of a treatment comprising thirty-seven 4 s pulses during which the focus was moved at 0.75 mm.s$^{-1}$.** Sonications were delivered at an acoustic power of 85 W, with a spacing of 0.5 mm and with the focus located at 15 mm under skin. Iso-contour corresponding thermal damage where 99 % of native proteins denature is displayed in black.

Damaged zones in the $xy$ plane of the vein are summarized in Table 4-5 for treatment layouts (1) and (2).

**Table 4-5 – Simulated results in terms of damaged areas for treatment plannings (1) and (2).**

| Treatments ID | Damaged zone | Lesion area |
|---|---|---|
| 1 | 19.2 × 2.4 mm$^2$ | 42.8 mm$^2$ |
| 2 | 19.2 × 4.2 mm$^2$ | 72.0 mm$^2$ |

### 4.3.2 Animal experiments

Ultrasound imaging was performed before and after HIFU exposures. Following HIFU treatment, it was possible to observe HIFU-induced vessel damage, as assessed by vein shrinkage (Figure 4-7).

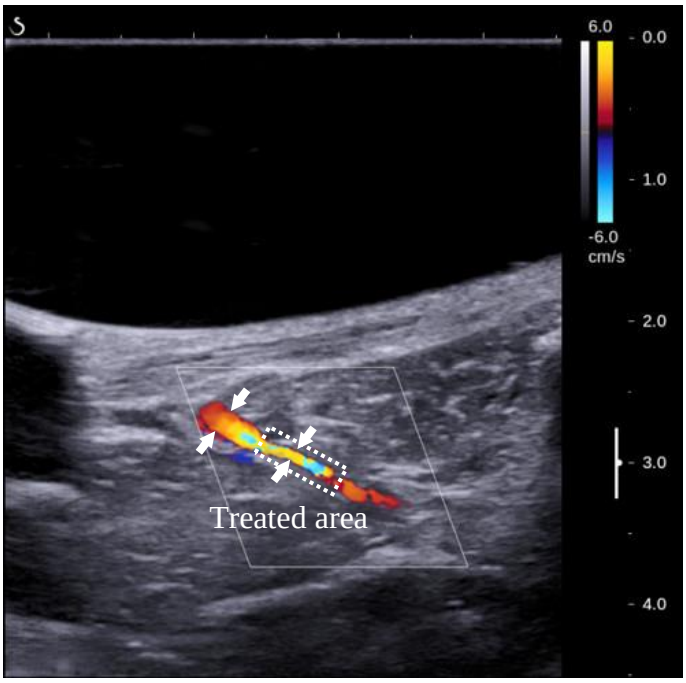


**Figure 4-7 – Acute vascular shrinkage following HIFU pulses.**

Clinical follow-up of the animals showed that recovery after HIFU treatments is well tolerated. All animals survived until the day of euthanasia and no abnormal behavior was noted postoperatively. All animals continued their normal pattern of feeding. As mentioned in the Methods, only samples satisfying acceptance criterion were considered in the study. In total and excluding the control sample, 17 samples (63 %) were taken into account in this study. Histological results are reported Table 4-6.

**Table 4-6 – Results of vessel occlusion for each batch.**

| Protocol ID | 1 | 2 | 3 |
|---|---|---|---|
| Number of accepted samples | 1 | 10 | 6 |
| Sonication types | Fixed pulses 1.5 mm apart | Fixed pulses 1.5 mm apart<br>Hind limb elevated | Linear track with sites 0.5 mm apart<br>Hind limb elevated<br>Vein compressed |
| Follow-up duration | 15 days | 15 days | 13 days |
| Histological score | **0**: 1/1 | **0**: 2/10<br>**3**: 1/10<br>**4**: 7/10 | **3**: 3/6<br>**4**: 3/6 |

The follow-up duration indicated in Table 4-6 corresponds to the median value. Follow-up duration extended from 7 days for the shortest one to 19 days for the longest one, due to the availability of the animal facility.

For all samples treated with fixed pulses and with a score superior or equal to 3, histological findings revealed a thrombo-vasculitis of the saphenous vein characterized by a transmural thickening and collapse of the lumen. Fibrinous thrombi were also present. These lesions are irreversible by nature or expected to be irreversible for the samples with a follow-up duration inferior to 13 days, as assessed by our pathologist. Lesions were expected to evolve towards the formation of large fibrotic scars incorporating saphenous veins. Figure 4-8 shows illustrative HE stained cross sections. Two different types of vascular occlusion were observed: a complete collapse and sealing of the vein (Figure 4-8 (a)) or an occlusive fibrinous thrombus in the lumen (Figure 4-8 (b)).

(a)

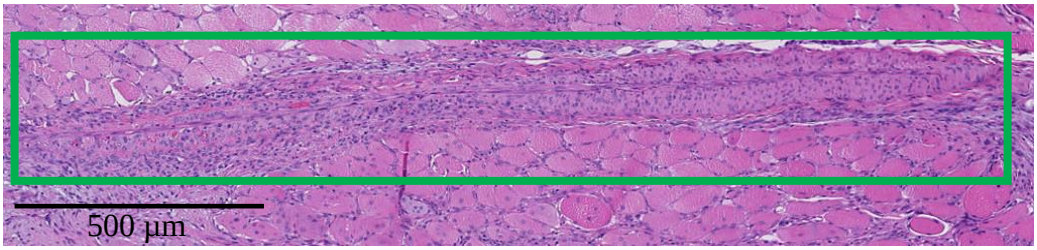


(b)

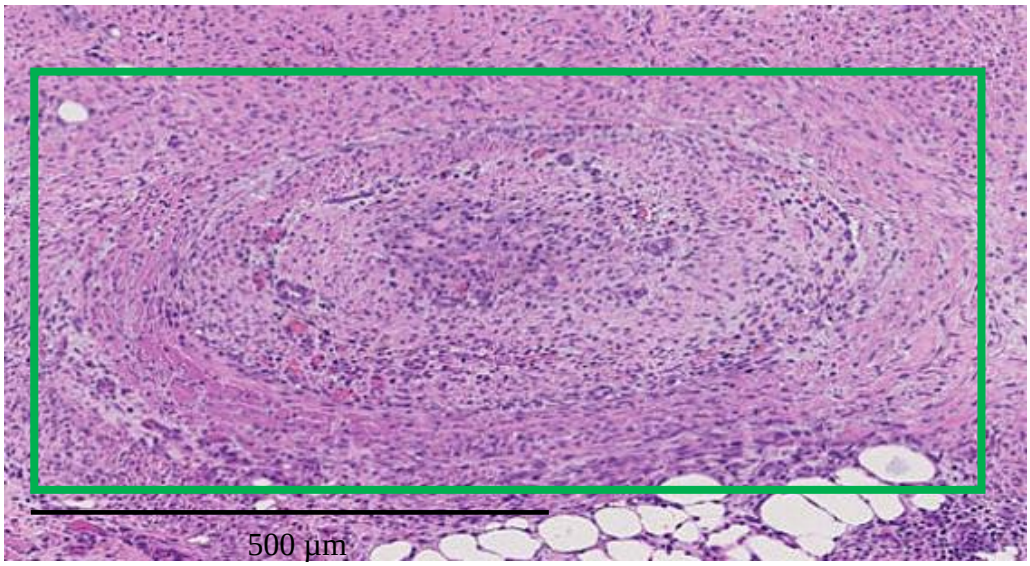


(c)

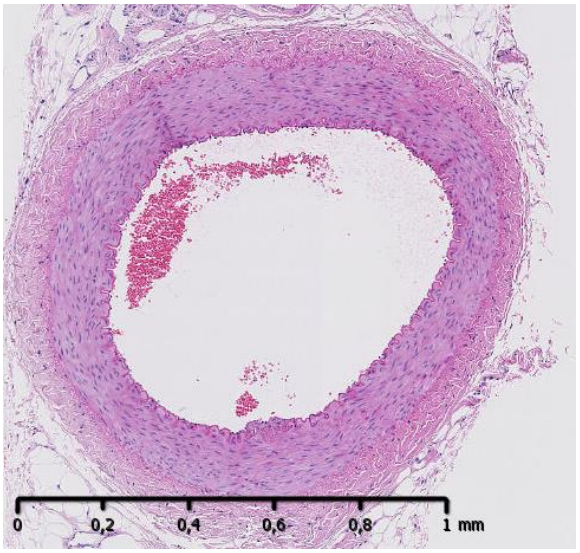


**Figure 4-8 – HE sections of representative saphenous veins (green rectangles) showing a transmural thickening and collapse of their lumen.** The sections (a) and (b) correspond to veins treated according to protocols (2) and (3) respectively and (c) represents a vein section of a sham.

The lesions observed on the samples sonicated with moving pulses were histologically identical to those treated with fixed pulses. However, variability in the severity of the lesions was observed between samples. The majority of samples (73 %) treated with fixed pulses

showed a severe thrombo-vasculitis while lesions were evenly distributed between severe and moderate for samples sonicated with moving pulses.

## 4.4 Discussion

The feasibility of inducing sustainable vascular occlusion with HIFU thermal effects at 3 MHz was demonstrated. Histology reported 82 % of vascular occlusion. Occlusion was successful in all cases where compression was applied.

Histological analysis systematically showed severe lesions for samples which underwent fixed point-by-point sonications and moderate lesions for half of the ones that were treated with moving pulses. With moving pulses, the energy delivered is spread more and results in less severe lesions.

However, all vein samples that showed no occlusion were treated with fixed pulses. According to the simulations, the extent of the coagulated zone after fixed pulses treatments is barely large enough to cover the entire vein (Figure 4-5). More precisely, for fixed pulses, the coagulated zone is 2.4 mm in diameter. It does not cover the whole circumference for all the veins targeted experimentally (the diameter ranges between 1.1 and 3.7 mm). Fixed pulses are effective when the vein wall is completely encompassed in the lesion.

Conversely, moving pulses cover an area 1.8 times wider than with fixed pulses, which reliably damages the whole circumference of all the veins. However, the treatments with moving pulses required nearly three times more sonications than the treatments with fixed pulses to treat the same vein length.

The lack of symmetry observed in the Figure 4-5 results from heat accumulation effect. As sonications are delivered, the thermal energy deposited during previous pulse is added to the energy deposition of the current pulse. There is therefore an overlap in heat accumulation between two successive pulses.

Considering the good correlation between simulations and histologic findings, the model used to assess thermal damage in the vein, based on the denaturation of collagen, appears to be consistent. This is supported by the study conducted by Fujiwara *et al.* [29] where vessel occlusion was observed when peak temperature of the sonicated sample hit 98 °C, but not at 47 °C or 54 °C. Area corresponding to denaturation of 99 % of native proteins correlates

with the region where temperature reached 85 °C. The same temperature threshold is recommended for radiofrequency closure ablation to seal veins. Total coagulation of the vein wall is expected to occur when the intima is heated homogeneously to 85 °C.

In our study, the three occlusion-free samples correspond to treatments without compression. We hypothesize that blood flow could have acted as a heat sink which prevented the temperature elevation of the vein wall from reaching sufficient levels. Compression should be considered for future clinical treatments as it helps to abolish blood flow and to decrease lumen area. The high temperature elevations obtained in the simulations indicate that thermal effects of HIFU are expected to play a major role in our venous occlusions. Thermal mechanism compares favorably to the use of purely mechanical occlusion effects as reported by Hwang *et al.* [35], which lead to a recanalization of the veins after the treatment. Hwang *et al.* [35] used pulsed HIFU exposures with a low duty cycle in synergy with ultrasound contrast agent. The treatment was effective but could not maintain rabbit auricular vein occlusion over 14 days. With similar pulsing regime (9 MPa peak rarefaction pressure, 1 Hz pulse repetition frequency), Zhou *et al.* [36] demonstrated a sustainable occlusion with mechanical effects of HIFU but only by injecting proinflammatory agents corresponding to the detergents found in sclerosing agents [103].

Groups who used ultrasound alone reported a temporary occlusion that did not exceed one week after treatments [19], [29], [104]. Notwithstanding that they have demonstrated occlusion in small veins (<1.5 mm), no long-term occlusion was proved.

Our exposure ultrasound parameters without additives were sufficient to induce venous closure. To date and to the best of our knowledge, no other study reported noninvasive occlusion in a subacute setting on veins of similar size with the use of HIFU induced thermal effects.

## 4.5 Conclusion

In this study, two sonication strategies were identified and evaluated in a rabbit model. Histologic changes in the targeted veins show that all sonications methods resulted in thrombotic lesions within a few weeks. Vein compression was identified as a key factor contributing to successful vascular occlusion. *In vivo* experiments have demonstrated that

thermal ablation with the Echopulse® HIFU device can induce a sealing of small veins (1.1-3.7 mm diameter) in the subacute setting.

However according to simulations, a large number of sonications would be required to coagulate bigger vein diameters, closer to the size of human varicose veins (> 3 mm). This treatment approach would result in long treatment times, which would present an obstacle to clinical practice. To make a HIFU treatment clinically viable for the coagulation of large veins, the ultrasound parameters should be further adjusted.

In the next chapter, the spacing between pulses to ensure complete treatment along the vein length is investigated with 8-s pulses, in order to be able to treat veins with a diameter larger than 3 mm. Furthermore, the temperatures induced to vein walls during HIFU ablation are measured and compared to the ones usually reported during endovenous thermal ablation.

# 5

# Characterization of the thermal heating induced during the sonication of a large vein diameter ( ≥ 4 mm)

## 5.1 Introduction

In the previous chapter, the feasibility of achieving vascular occlusion *in vivo* with 3-MHz ultrasound was demonstrated. The treatment parameters used in the preceding study were able to occlude small veins.

To coagulate bigger vein diameters closer to human varicose veins, new ultrasound exposure parameters including both duration and trajectory are investigated in this chapter. Longer pulses 8-s pulses are selected for this purpose.

To define a relevant HIFU thermal ablation technique with these HIFU pulses, current endovenous thermal treatment protocols were first examined, in order to propose an equivalent treatment effect with ultrasound and thus to ease regulatory approval.

Endovenous thermal techniques aim at heating the pathologic vein continuously over its entire length [73], [105], [106] to coagulate veins effectively. During radiofrequency ablation for instance, veins are heated between 70 °C and 120 °C, depending on the RF device [14], [15], [107]. These temperatures are targeted to induce vein wall coagulation and cause collagen contraction which stimulates vein wall thickening, lumen shrinkage and ultimately occlusion [106].

In this chapter, the objective was to identify the maximal spacing between 8-s pulses along the vein to ensure a continuous coagulation.

For this purpose, the temperature profile induced along the vein wall with a single ultrasound exposure (8-s at 85 W acoustic) was first estimated through *in vivo* experiments on sheep veins (5 mm in diameter). Similarly to the methods introduced in Chapter 4, the spatiotemporal temperature profile was simulated and coupled with the vascular thermal damage model developed by Agah *et al.* [77], in order to estimate the theoretical extent of the thermal damage along the vein. In addition, the peak temperatures induced to the vein wall during sonication were compared to the peak temperatures induced by current RF devices.

## 5.2 Methods

### 5.2.1 *In vivo* experiments

Preclinical trials were conducted in accordance with the guidelines of the Comité national de réflexion éthique sur l'expérimentation animale (CNREEA). The study was validated by the ethic committee n°16 under the reference: 9028-2017022116542356.

One sheep, 17 months old and 55 kg weight, was used for the experiments. The sheep was initially anesthetized with an intramuscular injection of a mixture of ketamine (5 mg/kg, Ketamine 1000, Virbac, France) and Diazepam (0.5-1 mg/kg, Diazepam TVM5, TVM Lab, France). The animal was then installed on the table, intubated and ventilated with Isoflurane (2-2.5 %, Vetflurane, Virbac, France) to be kept under anesthesia throughout the experiments. HIFU exposures were applied on the lateral saphenous veins of each hind limb, but treatments were delivered one day apart. The second day after the experiments, the animal was sacrificed with an intravenous injection of 25 mL of Pentobarbital (Dolethal, Vetoquinol, France).

The sheep lateral saphenous vein was chosen to be targeted for several reasons. First, this vein is easily accessible with the device's transducer. Second, the sheep saphenous vein shares similarities with the human saphenous vein: it is located under superficial tissues, surrounded by a *fascia* and has several tributaries.

The day of the treatment and before sonications, the hind limb of interest was first shaved with a hair trimmer and then with a commercial hair-removing cream (Klorane, Laboratoires Klorane, France), in order to improve ultrasound transmission through the skin.

Prior to HIFU exposure, a small skin incision was performed on the lower rear limb to introduce thermocouples in the saphenous vein. The vein (mean diameter of 5 mm) was then catheterized with a 14G catheter (BD Angiocath™, BD, USA ), inferior to the treatment site (Figure 5-1), and two K-type thermocouples (outer diameters of 0.2 mm and 0.075 mm / Accuracy of 1.5 $\pm$ 0.25 %) (identified as TC1 and TC2) were introduced into the catheter. The distance between the tips of the thermocouples was 2.5 mm.

**Figure 5-1 – Catheterization of the vein.**

The same transducer as the one described in Chapter 3 (central frequency: 3 MHz, curvature radius: 38 mm, aperture diameter: 56 mm) was used. The transducer was positioned in the region of interest to target the lateral saphenous veins. Thermocouples were visualized under ultrasound guidance. Once everything was in place, standard HIFU procedures were delivered. In total, five HIFU procedures were delivered in each hind limb. Each procedure comprises a sequence of 8-s pulses distributed in a row of 5 spots placed every 3.5 mm along the vein. Thermocouples were positioned within the vein in such a way as to have the tip of TC1 in the middle of the targeted venous segment, at spot #3 (Figure 5-2).

Pulses were applied at 85 W and a minimal pause time of 40 s was observed between subsequent sonications. Before shooting, the fluid pressure within the balloon mounted on the transducer was increased to mechanically compress the vein to ensure a good contact between

the thermocouple and the tunica intima. Temperature recording during sonications was achieved by an acquisition board (TC-08, Pico Technology, Cambridgeshire, UK) connected to a computer.

As mentioned in the Introduction, these *in vivo* experiments were conducted in order to estimate the temperature profile induced along the vein wall with a single 8-s HIFU pulse delivered at 85 W acoustic. The data processing performed for this purpose is described in the next section.

### 5.2.2 Data processing

#### 5.2.2.1 Spatiotemporal registration

For feasibility reasons, inserting more than two thermocouples in the targeted veins was impossible. Therefore, thermocouples were kept at a fixed location and the HIFU pulses were delivered at five different positions along the vein (Figure 5-2). We assumed each pulse to be independent from each other, so that the temperature profile obtained for five pulses is equivalent to the one that would be obtained with five temperature measurements at different spatial locations for one single pulse (Figure 5-3).

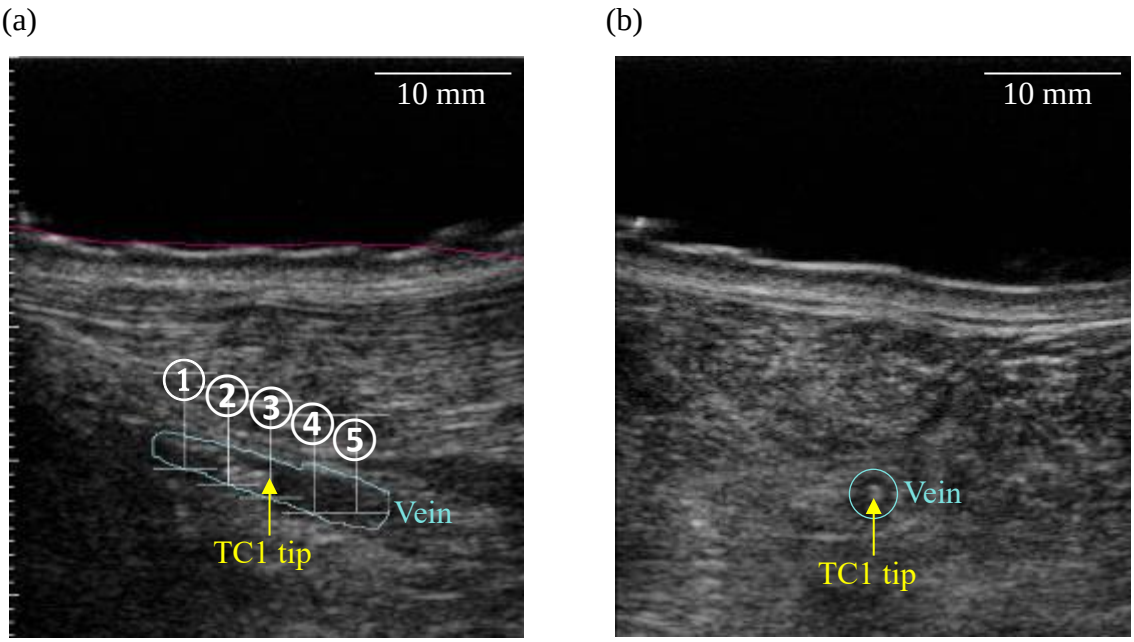


**Figure 5-2 – Longitudinal (a) and transverse (b) views of the positioning of the thermocouple TC1 in the vein.** Spots are referred by their numbers.

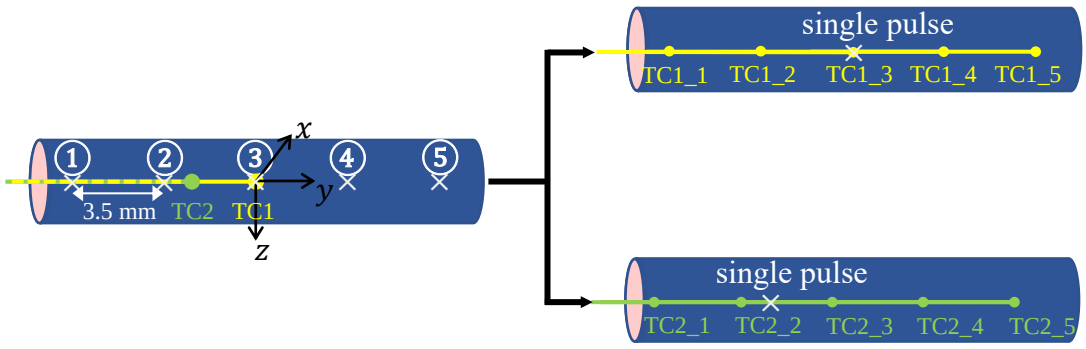


**Figure 5-3 – Illustration of the change of frame of reference.** Delivering five pulses at given positions (symbolized by crosses) and measuring the temperature with two thermocouples into the vein at fixed locations is considered equivalent to virtual situations where one pulse would be delivered and five thermocouples would acquire temperatures at the same positions. TCX_Y represents a virtual thermocouple TCX that measures the temperature rise during pulse Y.

Since the distance between the two thermocouples was subject to small variations during insertion into the catheter, the two sets of temperature profiles were considered independently. For each treatment, the temperature measured with the thermocouples was synchronized with HIFU pulse delivery. Then, for each pulse, a temperature curve was extracted from the beginning of the pulse to 15 seconds after the end of the pulse. Since five

pulses were delivered for each treatment and five treatments per vein were performed with temperature acquisitions by two thermocouples, the whole dataset was considered equivalent to having delivered one pulse with 100 recording thermocouples.

To correct the spatial errors in the positions of the thermocouples relatively to the focal spot, the curves were spatially registered. The spacing between two adjacent sites did not vary and was set to 3.5 mm. Each set of five curves corresponding to the data acquired during the five pulses of a given treatment by a given thermocouple was fitted with a spatial gaussian function at every time step. For the gaussian curves to be spatially consistent, a series of optimizations (see Appendix A) was performed for all subsets of five curves.

Once the 20 sets of 5 curves were spatially registered, the same process of gaussian fit was applied on the resulting set of 100 temperature curves. This resulted in the final estimated spatiotemporal temperature distribution induced by a HIFU pulse along the vein.

#### 5.2.2.2 Data aggregation and thermal damage estimation

To estimate the extent of thermal damage along the vein, the spatiotemporal temperature distribution was coupled to the metric of vascular thermal damage described by Agah *et al.* [77]. Theoretical modeling of vascular thermal damage suggests that vessel damages correlate with thermal denaturation of collagen fibers which begins between 62 °C and 67 °C [97], [108].

By considering the denaturation of collagen as a first-order reaction, vascular damage was modelled using a general Arrhenius equation and is appraised by the parameter $\Omega(y,t)$:

$$\Omega(y,t) = \ln\left(\frac{c(y,0)}{c(y,t)}\right) = A_f \int_0^t \exp\left(-\frac{E_a}{R \times T(y,t)}\right) dt \tag{5.1}$$

with $\Omega(y,t)$ the degree of vessel damage along the axis of the vein $y$, $c(y,0) = c_0$ and $c(y,t)$ are the concentrations in undamaged collagen molecules respectively before sonications and at a time $t$. The final time $t_f$ was set to 23 s i.e. 15 s after the end of the 8-s pulse.

In (5.1) $A_f$ is the frequency factor, $E_a$ is the activation energy, $R$ is the universal gas constant and $T(y,t)$ is the temperature. $A_f$ and $E_a$ were set to $A_f = 5.6 \times 10^{63}$ s$^{-1}$ and $E_a = 430$ kJ mol$^{-1}$

according to Agah *et al.* [77]. $\Omega(y,t) = 1$ defines the first noticeable irreversible damage and corresponds to the denaturation of 63 % of the collagen [77].

As discussed in Chapter 4, to achieve successful vascular coagulation, we assumed that the vein would need to be extensively damaged. The threshold of vessel damage was therefore set to $\Omega(y,t) = 5$, which formally corresponds to denaturation of 99 % of the native collagen fibers.

## 5.3 Results

The maximum temperature rise recorded by each thermocouple for each treatment is reported in Table 5-1.

**Table 5-1 – Maximum temperatures recorded by each thermocouple during each treatment performed in both left and right hind limb.**

| Laterality | Treatment ID | Thermocouple ID | Maximum Temperature (°C) |
|---|---|---|---|
| Left | 1 | TC1 | 88 |
| | | TC2 | 78 |
| | 2 | TC1 | 92 |
| | | TC2 | 84 |
| | 3 | TC1 | 88 |
| | | TC2 | 90 |
| | 4 | TC1 | 88 |
| | | TC2 | 82 |
| | 5 | TC1 | 91 |
| | | TC2 | 92 |
| Right | 1 | TC1 | 95 |
| | | TC2 | 83 |
| | 2 | TC1 | 100 |
| | | TC2 | 92 |
| | 3 | TC1 | 96 |
| | | TC2 | 89 |
| | 4 | TC1 | 103 |
| | | TC2 | 86 |
| | 5 | TC1 | 101 |
| | | TC2 | 87 |

The mean temperature rise recorded during all sonications was $90.3 \pm 6.5$ °C.

Figure 5-4 displays an example of temporal registration of the thermocouples measurements with respect to the delivered pulses.

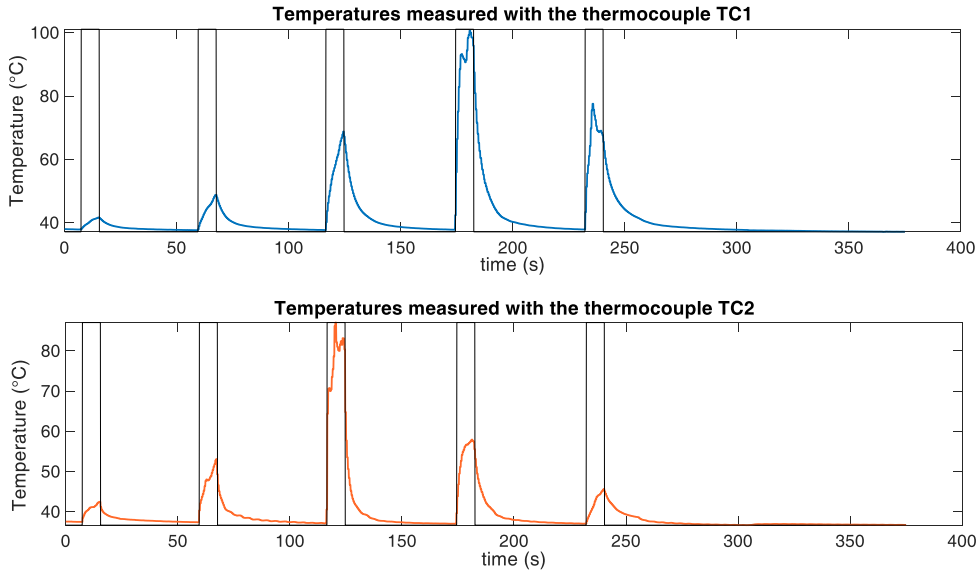


**Figure 5-4 – Temporal registration of the thermocouples measurements with respect to the delivered pulses.** The pulses delivery times are represented by the black rectangular signal of arbitrary amplitude.

Figure **5-5** represents the aggregated temperature profiles for the right treated vein.

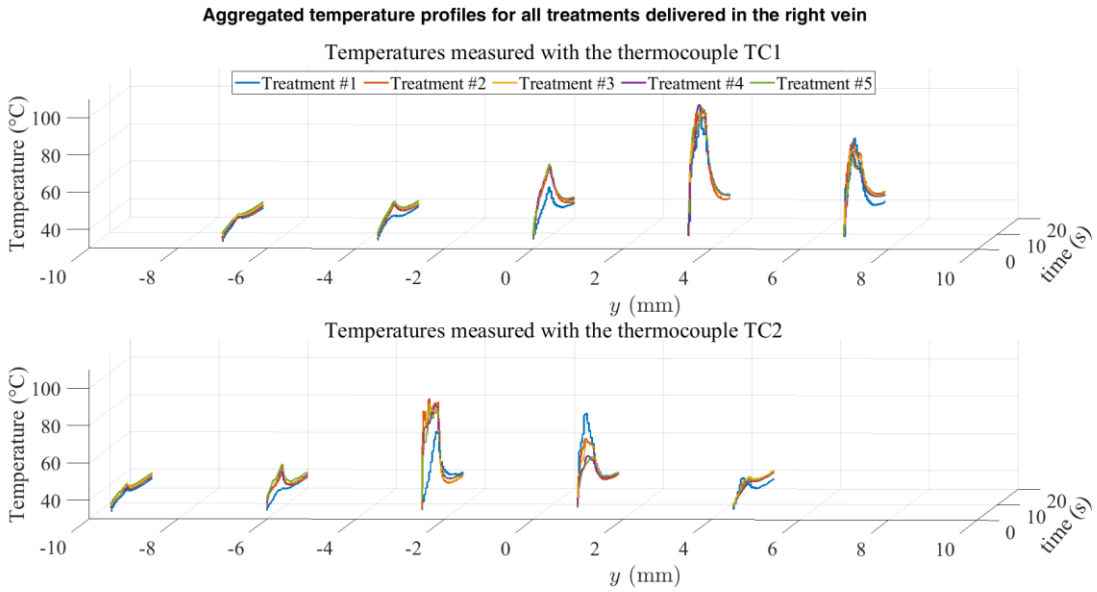


**Figure 5-5 – Aggregated temperature profiles before spatial registration.** The colors represent the five different treatments delivered in the right hind limb. The two sets of five curves of each color refer to the temperatures recorded by the two thermocouples TC1 and TC2 during the delivery of the five pulses.

Figure 5-6 shows an example of a gaussian fit of the temperatures acquired by the thermocouple TC1 during the treatment #3 delivered in the right saphenous vein.

The mean spatial correction over the 20 sets of 5 curves was 1.8 ± 1.6 mm.

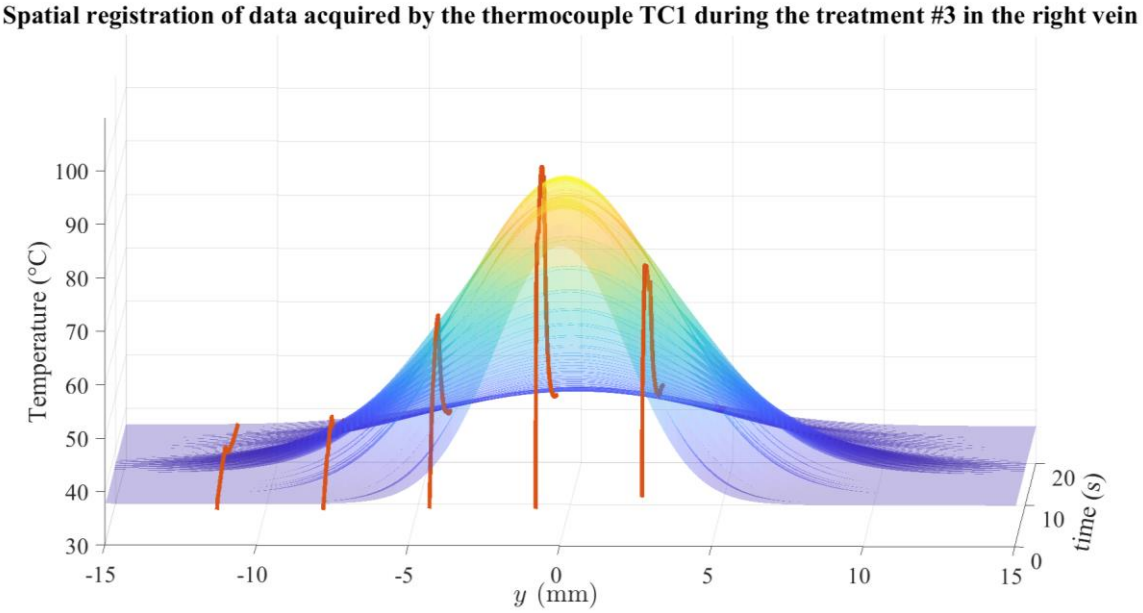


**Figure 5-6 – Spatial registration of the data acquired by the thermocouple TC1 during the treatment #3 delivered in the right vein.**

The 100 temperature curves spatially registered are represented in Figure 5-7.

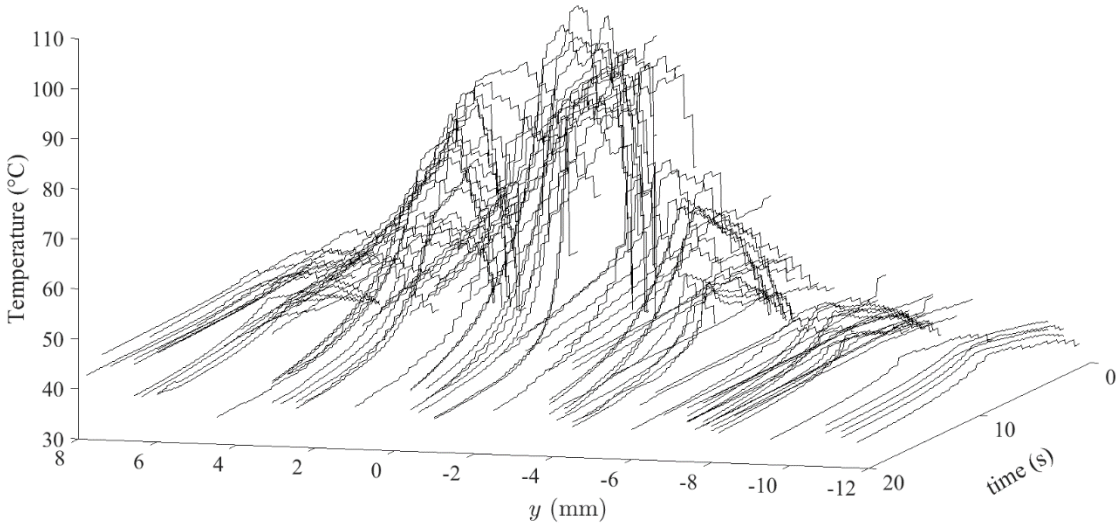


**Figure 5-7 – Representation of the 100 temperature curves spatially registered.**

The final estimated spatiotemporal distribution is represented in Figure 5-8.

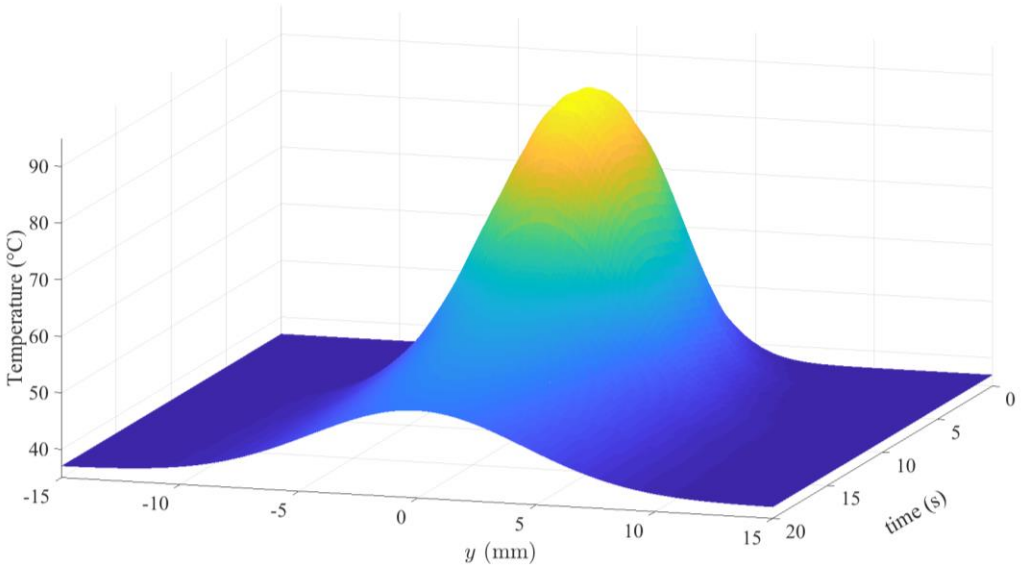


**Figure 5-8 – Estimated spatiotemporal temperature distribution for one pulse.**

Based on the estimated spatiotemporal temperature distribution represented in Figure 5-8, the spatial profile of thermal damages $\Omega(y, t_f)$ was computed. It is displayed in Figure 5-9. The result demonstrates that the collagen is expected to be denatured over a length of 3.6 mm along the vein.

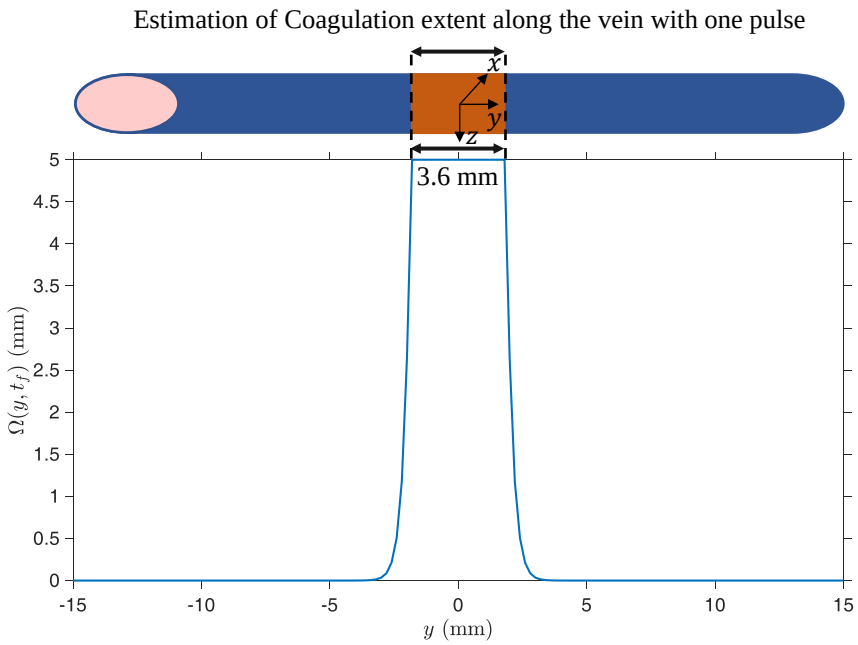


**Figure 5-9 – Spatial profile of $\Omega(y, t_f)$ along the vein after one pulse**. $\Omega(y, t_f)$ is capped to 5 since it formally corresponds to 99 % of collagen denaturation.

## 5.4 Discussion and conclusion

In this *in vivo* study, the temperatures generated at the vein wall during sheep veins HIFU ablation were measured for 8-s sonications at 85 W acoustic. Based on the temperatures recorded by the thermocouples, the mean peak temperature achieved at the intima was $90 \pm 7$ °C. Using the metric of vascular thermal damage developed by Agah *et al.* [77], the veins were estimated to have been heated sufficiently to cause irreversible thermal damage of the vein wall.

Furthermore, the temperatures induced at the vein wall are within the range of the working temperature of the most commonly used RF devices (Figure 5-10): Closure (Medtronic, Ireland), Venclose (Venclose, USA), CElon (Olympus, Japan).

The presence of thermocouples under ultrasound exposures introduces different types of errors which can be associated to thermocouple self-heating or viscous heating artifact. Regarding the errors caused by thermocouple self-heating, a previous study conducted by Hynynen *et al.*[109] evaluated it and found that errors were small when the diameter of the probes is 1/2 of the square root of the wavelength or less. Given the diameters of the thermocouples used in this study (0.2 mm and 0.075 mm ), the artifact due to thermocouple

self-heating was deemed negligible. On the other hand, the viscous heating artifact had certainly introduced more significant measurement errors in our study. However, preceding studies have demonstrated that the magnitude of this artifact decreases with the distance to the focal spot [110]–[112] and given the small focal spot of the transducer used in the experiments (-6 dB focal width and length of 0.5 mm and 2.2 mm respectively), the probability to have had the tip of the thermocouple exactly at the focus is very low. Moreover, our thermocouples were aligned normal to the beam axis and this configuration was also found to minimize the proportion of viscous heating artifact [110], [111]. If not because of lack of time, a simulation approach, of a similar design to the one proposed by Tiennot *et al.* [112], could have been implemented to determine the contribution of the viscous heating in the measurements.

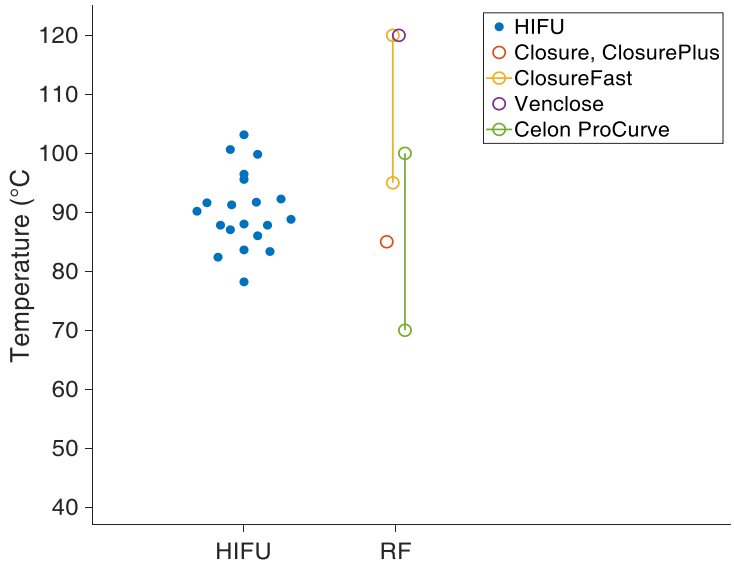


**Figure 5-10 – Comparison between HIFU and RF treatment temperatures.**

Other studies have measured the temperature during thermal ablation of veins and have correlated vascular effects with the temperature elevation. In a laser study, Martinot *et al.* [113] reported the vascular changes observed for different peak temperatures generated at the vein during irradiation. No effects were observed when the measured temperature was below 54 °C. However, successful vascular welding was reported when temperatures reached 77 °C on average, during 3-4 s irradiation. The accumulated thermal damage (Ω) was calculated for these exposure parameters. For the irradiations where a peak temperature of 54 °C was measured, the estimated accumulated damage value was below the threshold reported for first noticeable irreversible damage. On the contrary, the predicted accumulated thermal damage for the

exposures where the reported temperatures reached 77 °C was above the threshold for an irreversible thermal damage. Observations agree with the theoretical modeling of vascular thermal damage suggested by Agah *et al.* [77].

In the published literature, the response of blood vessels to the HIFU-induced temperature rise was also investigated [19], [29], [31]. Amongst these studies, Fujiwara *et al.* [29] measured the local temperature induced for different sonication exposure parameters [29]. Investigators reported a successful vascular occlusion at peak temperatures reaching 97 °C during the delivery of a 5-s pulse but not when the temperature achieved 46 °C at the end of the pulse. No occlusion was reported for a measured peak temperature of 48 °C during a longer sonication (10 s). Again, by translating the exposure parameters into Ω values (Table 5-2), the observations agree with theoretical modeling of vascular thermal damage.

**Table 5-2 – Vascular damage computed for the exposure parameters reported in studies [29] and** [113]**.**

| Study | Fujiwara *et al* [29] | | | Martinot *et al* [113] | |
|---|---|---|---|---|---|
| Duration (s) | 5 | 5 | 10 | [3-4] | [3-4] |
| Peak temperature (°C) | 46 | 97 | 48 | 54 | 77 |
| Accumulated thermal damage Ω | $1.2 \times 10^{-6}$ | $\mathbf{5.8 \times 10^{3}}$ | $6.4 \times 10^{-6}$ | $[3.7 \times 10^{-5} - 4.9 \times 10^{-5}]$ | [**1.2-1.6**] |

In the formulation of the vascular thermal damage, the accumulated damage Ω is exponentially related to the temperature and linearly related to heating time. The temperature reached during heating is therefore a key factor for generating thermal injury to the vein wall almost immediately.

As mentioned in the Introduction, this study was primarily conducted in order to evaluate the thermal coagulation induced by a single HIFU exposure (85 W, 8-s) along the vein. For this purpose, the spatiotemporal temperature distribution was first estimated and then coupled with the thermal vascular damage metric developed by Agah *et al.* [77]. The theoretical modeling of thermal damage along the vein demonstrated that delivering a single 8-s pulse at 85 W acoustic would induce a continuous vein wall coagulation over a length of 3.6 mm along the vein. Thus, to ensure a continuous coagulation along a vein segment, pulses shall be aligned along the vein axis with a spacing inferior or equal to 3.6 mm.

In this study, the thermal damage to the vein was not experimentally evaluated following sonication. The next chapter will focus on macroscopic damages induced by the HIFU exposures. Both thermal injury to the vein and to perivenous tissues are assessed.

# 6

# Immediate tissue changes associated with HIFU thermal ablation of veins

## 6.1 Introduction

In the previous chapter (Chapter 5), the vein wall heating during HIFU exposure of sheep veins was experimentally investigated and the corresponding vascular thermal damage was numerically estimated.

Regardless of the thermal modality, heating veins was previously demonstrated to induce vein wall contraction [76]. Reduction of vein lumen diameter is therefore expected following HIFU thermal ablation of veins. In addition to being a marker of vein coagulation, shrinkage is also part of the sequence of actions leading to vascular occlusion with all current endovenous thermal modalities [61], [114]–[116]. Shrinkage was even proposed as a predictor of success for thermal ablation [76], [116]–[122]. To ensure long-term durability of the venous ablation and to reduce the likelihood of an early recanalization, it is generally recommended to induce significant shrinkage [116]–[118], [123]–[125]. This can be done by adequately adjusting the treatment parameters [118], [124], [125]. For example, Proebstle *et al.* [125] increased the laser energy delivered to the vein wall in order to achieve an immediate shrinkage of 50 %.

Based on the experience of endovenous thermal ablation for the management of varicose veins, the reduction of vein wall shrinkage after HIFU treatments was thus investigated and is reported in this chapter. The relevance of the HIFU parameters used for

vein ablation was assessed depending on the amount of vein shrinkage achieved following sonications.

The veins to treat, such as the great saphenous vein, are mainly surrounded by muscle and adipose tissues. Given the high absorptive properties of these surrounding structures [32], thermal lesions in the perivenous tissues are expected to be induced by HIFU treatments. Therefore, the extent of the thermal lesions induced by the treatments was also evaluated here.

In this study, six sheep veins of medium diameters ($3.4 \pm 1.1$ mm) were treated with HIFU and changes induced to venous and perivenous tissues were analyzed. The vein shrinkage was first assessed immediately post-treatment on living animals with B-mode imaging. After sacrifice, the animals were deep-frozen and the extent of the lesions was then measured using macroscopic slicing and segmentation.

The experimental data regarding the post-treatment reduction of the vein lumen diameter were additionally used to validate a numerical model, developed by Anthony Grisey, to predict the shrinkage induced by HIFU treatments.

## 6.2 Quantitative analysis of the thermal alterations induced following HIFU ablation of veins

### 6.2.1 Animal experiments

#### 6.2.1.1 HIFU treatments and examination of the thermally induced vein shrinkage

Six sheep (22-29 months old, 51-65 kg, female) were enrolled in this study. The protocol was approved by the ethical committee for animal experiments ANSES/ENVA/UPEC under the agreement number of CE16/2017022116542356. Experiments were performed according to the 2010/63 European directive. Each animal had its left lateral saphenous vein treated with the Echopulse® device (Theraclion, Malakoff, France).

As mentioned previously, the sheep saphenous vein was chosen because of its similarities with human saphenous veins. The transducer utilized throughout these experiments had identical geometry and features as the one described in Chapter 3 (3 MHz central frequency, 38 mm curvature radius, 56 mm outer diameter).

Prior to the treatments, the sheep were anesthetized with intravenous injection of ketamine (5 mg/kg, Ketamine 1000, Virbac, France) and Diazepam (0.5 – 1 mg/kg, Diazepam TVM5, TVM Lab, France). Anesthesia was maintained by endotracheal intubation: oxygen (100%) and Isoflurane (2-2.5%, Vetflurane, Virbac, France). Intravenous Morphine (0.1-0.2 mg/kg, Chlorhydrate de Morphine, Renaudin, France) was injected five minutes before sonications to prevent pain. Electrocardiography, blood pressure, body core temperature, end-tidal $CO_2$, $O_2$ saturation, respiratory rate and pattern were steadily monitored during the procedure.

Animals were in lateral decubitus position to access the lateral saphenous vein and the left hind limb was slightly elevated. The sheep were installed on a rigid assembly, specially built for maintaining the left hind limb position after treatment during the transportation to the cold room and freezing (Figure **6-3**). Hind limbs were shaved with a hair trimmer (Aesculap® Favorita II, B-Braun, Germany) and thighs were then depilated with a hair-removing cream (Klorane, France) in order to limit the presence of air bubbles and improve the ultrasound transmission through the skin.

Ultrasound examination included both B-mode and Duplex imaging were performed with an Aixplorer® ultrasound system (SuperSonic Imagine, Aix-en-Provence, France) to map and identify the portion of the vein to be sonicated. The diameter of the target vein segment was measured before treatment with the hind leg elevated.

The HIFU transducer was first manually positioned on top of the lateral saphenous vein and then robotically adjusted to position the focus on the targeted spots. Six veins in total, one in each sheep, with a mean pre-treatment diameter of $3.4 \pm 1.1$ mm (mean ± SD) were exposed at nine sites along the longitudinal vein with a spacing of 3.5 mm between subsequent sites, according to the results of Chapter 5 for inducing a continuous coagulation along the vein.

Heating homogeneously the whole circumference of the vein wall is thought to lead to a more successful treatment outcome [28], [126]. Therefore, to ensure that the whole vein circumference would be sonicated, two symmetrical pulses across the transversal axis of the vein in each slice were delivered for 8 s and at an acoustic power of $61 \pm 15$ W (mean $\pm$ SD) (Figure 6-1).

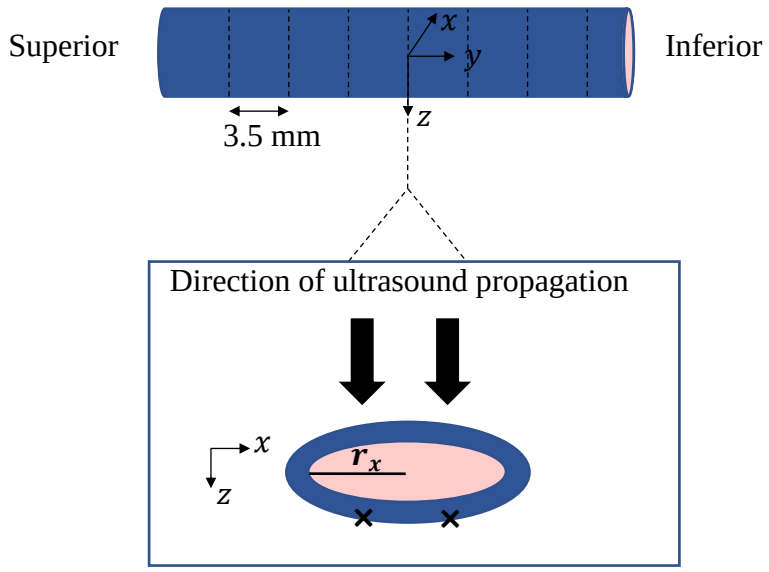


**Figure 6-1 – Illustration of the HIFU exposures (black cross) on a site and definition of the frame of reference with respect to the anatomy.**

Between two sonications, an average cooling time of 30 s was added to allow the skin to cool down. During sonications, blood flow was stopped by mechanical compression, induced by increasing the pressure inside the coupling balloon.

Immediately following the HIFU procedure, ultrasound images were acquired to measure the vein diameter of the treated segment. Vein diameter contraction was quantified as follows:

$$diameter\ contraction = \left(1 - \frac{diameter\ after\ treatment}{diameter\ before\ treatment}\right) \times 100 \qquad (6.1)$$

Where the $diameter\ after\ treatment$ is the diameter of the treated vein segment and the $diameter\ before\ treatment$ the diameter of the same vein segment before the HIFU exposures.

### 6.2.1.2 Investigation of the thermal lesion sizes

#### 6.2.1.2.1 Skin marking of the lesion location

At the end of the HIFU treatment, the therapy transducer was robotically moved along the longitudinal vein axis to a position located proximally to the treated area. Always robotically, the transducer was then moved away from the skin to allow for mounting a dedicated cap on

the transducer. The cap, illustrated in Figure 6-2, comprised two orthogonal lines representing the transverse and the longitudinal orientation with respect to the treated vein segment. A laser level was then utilized to materialize the transverse and longitudinal planes all along the thigh. The laser level was positioned in such a way the projected line simultaneously overlaid the appropriate line on the transducer's cap and the landmarks directly on the transducer denoting the vertical axis.

**Figure 6-2 – Transducer's cap.**

As illustrated in Figure **6-3**, the handles and the blue strips located on the transducer materialize the transverse and longitudinal planes of the targeted vein, respectively. The laser was maintained with an arm system with friction joint (Manfrotto 244, Manfrotto, Italy) and the skin was marked accordingly with a dedicated skin marker (Devon skin marker, Covidien, Ireland). Once the four branches of the cross were marked on the skin, the transducer was removed, and the branches were interpolated to complete the cross. The laser level positioning and the skin marking are illustrated in Figure 6-3.

Animals were then euthanized by an intravenous injection of Pentobarbital (25 mL, Dolethal, Vetoquinol, France) and were immediately transported to a cold room and stored at -17 °C for at least 48 hours.

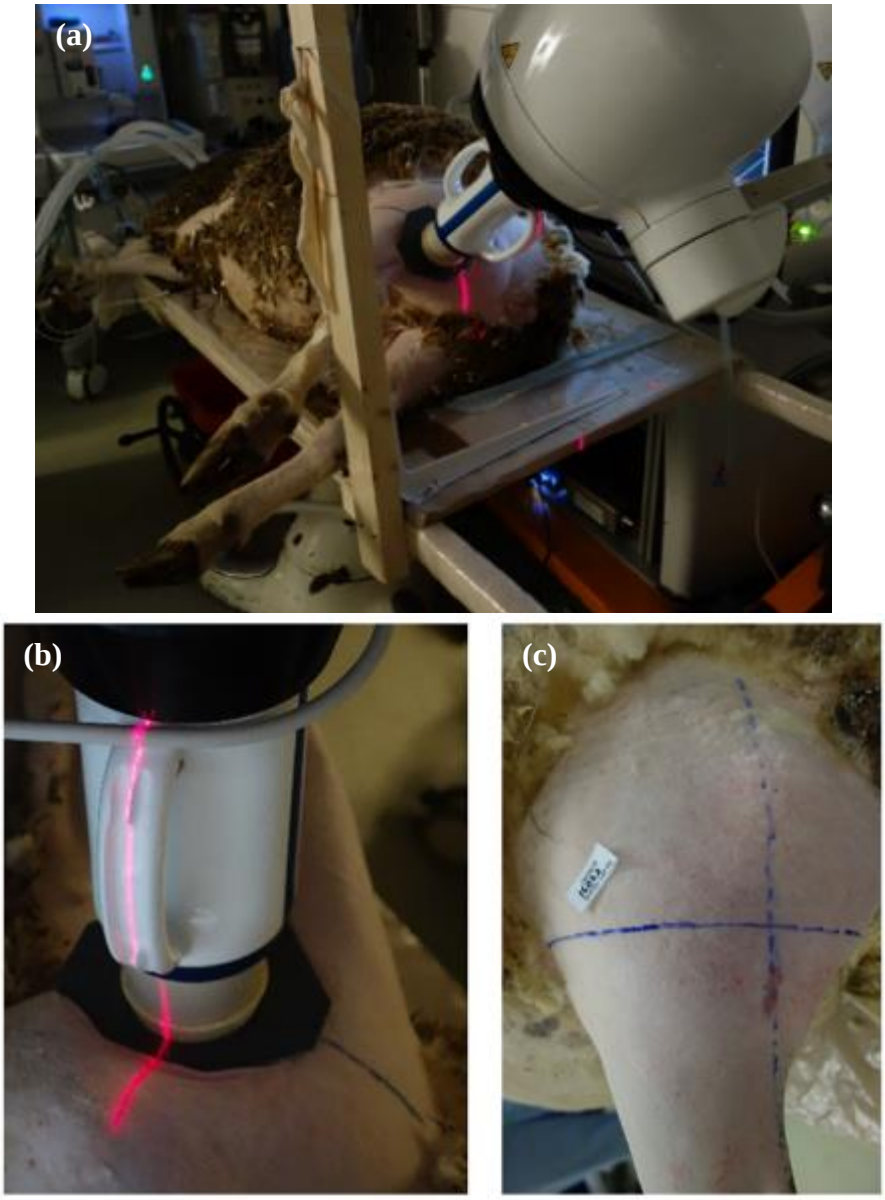


**Figure 6-3 – Skin Marking process.** (a) represents the setup at the end of the treatment. A cap is positioned on the vein and the projected laser line was aligned with the middle of the transducer's handles and with the line drawn on the cap (b). Once crosses marked, the transducer was removed, and branches were interpolated to complete the cross (c).

#### 6.2.1.2.2 Slicing and 3D reconstruction of the thermal lesion

The left leg of the frozen sheep was first detached from the rest of the body. The region of interest was then extracted by removing the proximal part of the leg. The region of interest was

sliced orthogonally to the *z* axis (Figure 6-1), i.e. perpendicular to the direction of propagation of the beam.

Parallel slices were cut using a band saw. Slices were 3-mm thick and about 1 mm of tissue was lost per slice due to the cutting operation. Block-faces of each slice was subsequently photographed with a constant lighting. A picture of a typical slice is shown in Figure 6-4.

The block-face pictures were then stacked using a Matlab interface (MathWorks, Natick, USA) in order to obtain a gross pathology volume. The drill holes illustrated in Figure 6-4 were performed on the region of interest to serve for slices registration during the stacking. For each sonicated vein, the resulting 3D volume was cropped and saved into a NifTI file. The mark on the skin, which is visible at the bottom of the slice (Figure 6-4), served to retrieve the *z* axis in the 3D volume.

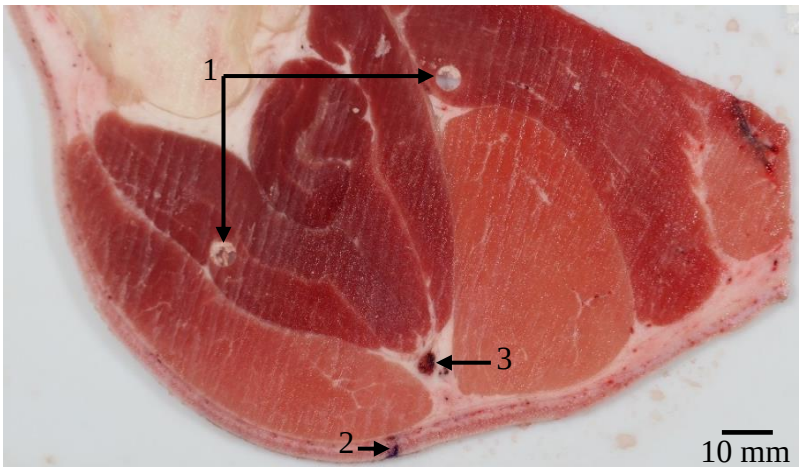


**Figure 6-4 – Example of a slide picture.** 1: Drill holes for slice registration. 2: Mark on the skin for orientation. 3: Vein.

For each volume, the vein lumen, the vein wall and the lesion were manually segmented in each slice using the 3D Slicer software (Slicer 4.10). Figure 6-5 shows an example of segmentation.

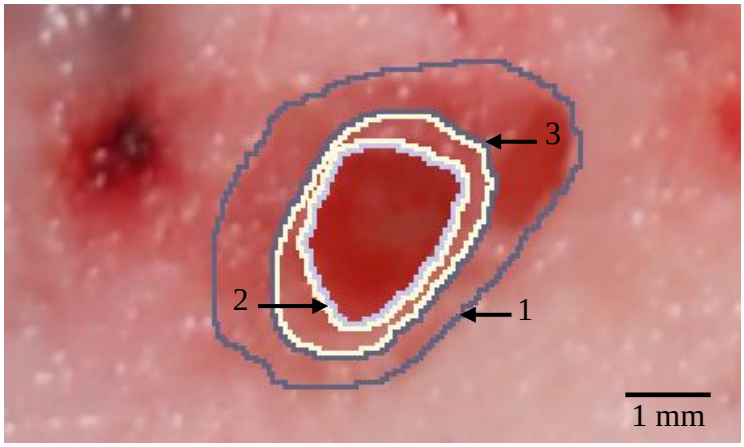


**Figure 6-5 – Example of a segmented slice.** 1: Lesion outline. 2: Vein lumen outline. 3: Outer wall outline.

Gross lesion sizes were computed along the $x$ and $z$ axis. In all slices where a gross lesion was visible in the surrounding tissues, the lesion masks were projected on the $x$ and $z$ axis and outliers were removed with a mathematical morphological approach by eroding 10 % on each side of the histograms. These points correspond to local irregularities observed on the lesion surface, due to stacking and segmentation imprecisions. The sizes of the lesion along $x$ and $z$ were then computed in each slice.

The areas of the lumen were also measured in each slice. In the slices where the vein was completely collapsed and the lumen was invisible, the lumen area was considered to be null.

The population of the measured lumen areas was split into two groups based on the position of each slice with respect to the distal border of the slices where a lesion was visible in the surrounding tissue. The "distal" group corresponded to the slices located distally to the border of the lesion while the "proximal" group assembled the slices located proximally to it.

## 6.2.2 Results

### 6.2.2.1 Vein wall shrinkage analysis

During sonications, the blood flow was not completely stopped by external compression for all the veins (Table 6-1). All treated veins showed sonographically visible diameter reduction. Measurements of pre-treatment and post-treatment vein diameters as well as diameter

contraction are reported in Table 6-1.

Compared to pre-treatment diameters, the mean diameter reduction was 53 ± 14 %.

**Table 6-1 – Vein diameter reduction measurements.**

| Sheep ID | Blood flow visible during sonications? | Vein diameter before treatment (mm) | Vein diameter post treatment (mm) | Diameter constriction (%) |
|---|---|---|---|---|
| #01 | No | 2.3 | 0.7 | 68 |
| #02 | No | 2.3 | 0.8 | 64 |
| #03 | Yes | 3.7 | 2.2 | 40 |
| #04 | No | 3.5 | 1.5 | 58 |
| #05 | Yes | 5.2 | 3.5 | 32 |
| #06 | No | 3.3 | 1.4 | 58 |

Figure 6-6 illustrates an example of vascular shrinkage observed immediately following the HIFU procedure.

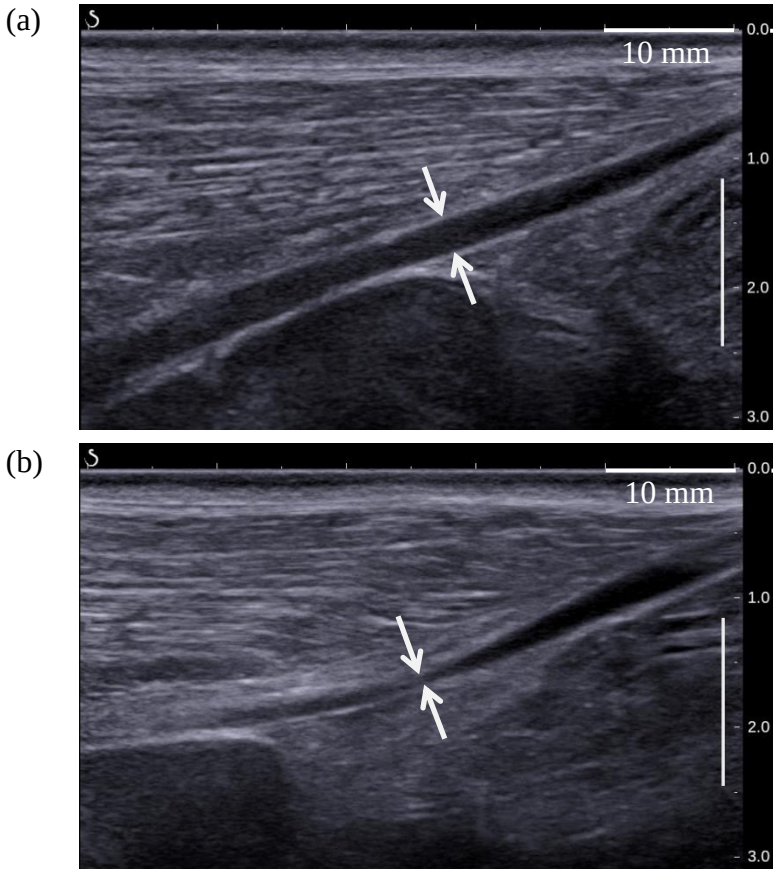


**Figure 6-6 – Ultrasound images of a sheep vein before (a) and immediately after HIFU treatment (b) showing luminal shrinkage.**

No complications occurred during exposures.

#### 6.2.2.2 Lesion sizes

On the photographs, gross lesions were distinguishable for every vein treated except for one (#05). As no gross lesion was observed at any location of the tissues in sample #05, this vein was excluded from all analysis (Figure 6-9).

For all other veins, the mean lesion sizes along $x$ and $z$ are displayed in Figure 6-7. The mean gross lesion size is respectively $4.7 \pm 1.2$ mm along $x$ and $8.0 \pm 2.9$ mm along z.

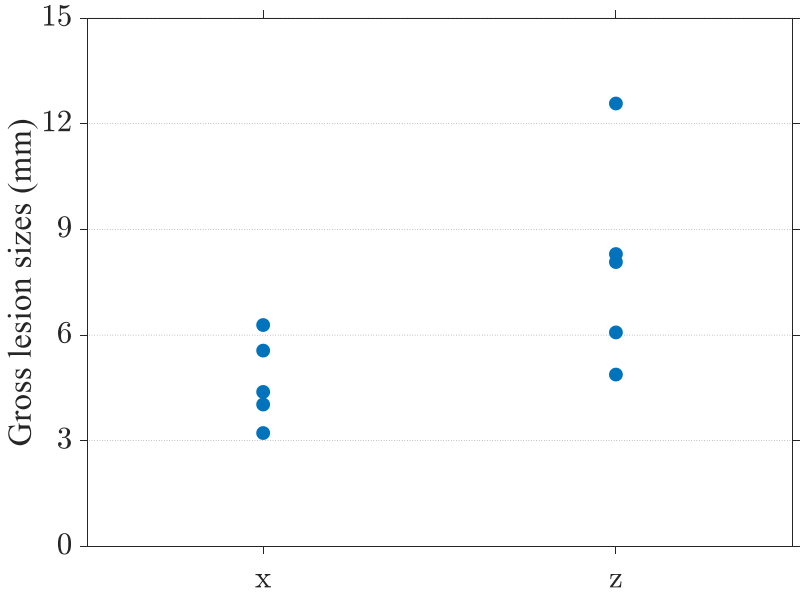


**Figure 6-7 – Mean lesion sizes along $x$ and $z$.**

Figure 6-8 illustrates the 3D reconstruction of the gross lesions, vein wall and vein lumen.

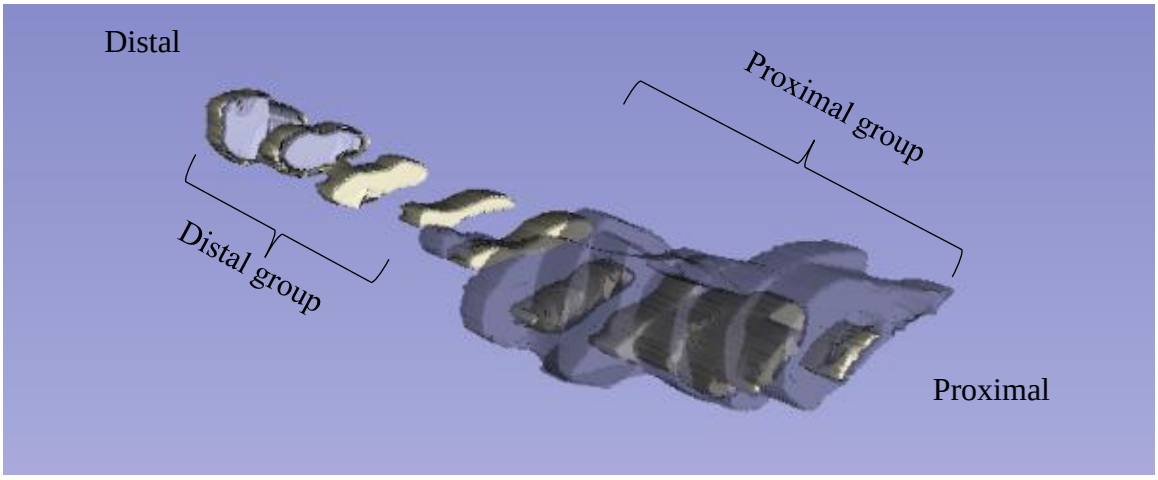


**Figure 6-8 – 3D reconstruction based on the segmentations of gross lesions (grey outlines), vein wall (white outlines) and lumen (purple outline).**

For each treated vein, the distribution of lumen areas in the $xz$ plane along $y$ is presented in Figure 6-9.

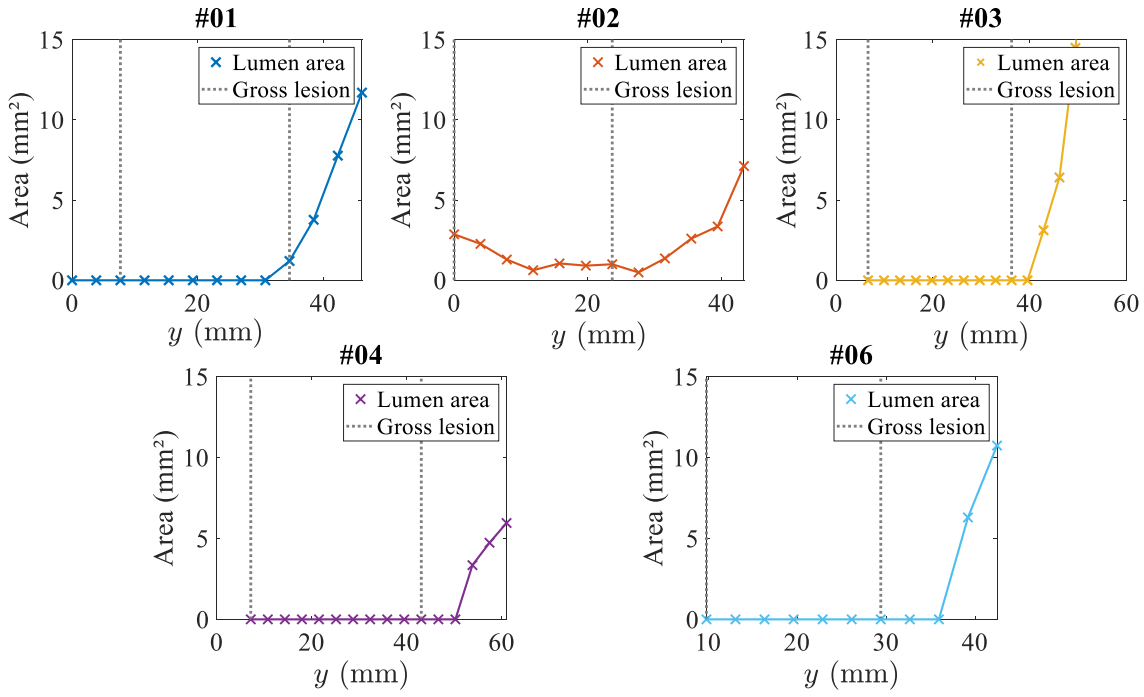


**Figure 6-9 – Distribution of the areas of vein lumen along $y$ for each vein (#01-#04 and #06).** A gross lesion was observed in the region comprised between the dotted grey lines. According to the frame of reference, $y = 0$ corresponds to the most proximal part of the vein treated.

The population of the proximal and distal vein lumen areas are displayed in Figure 6-10.

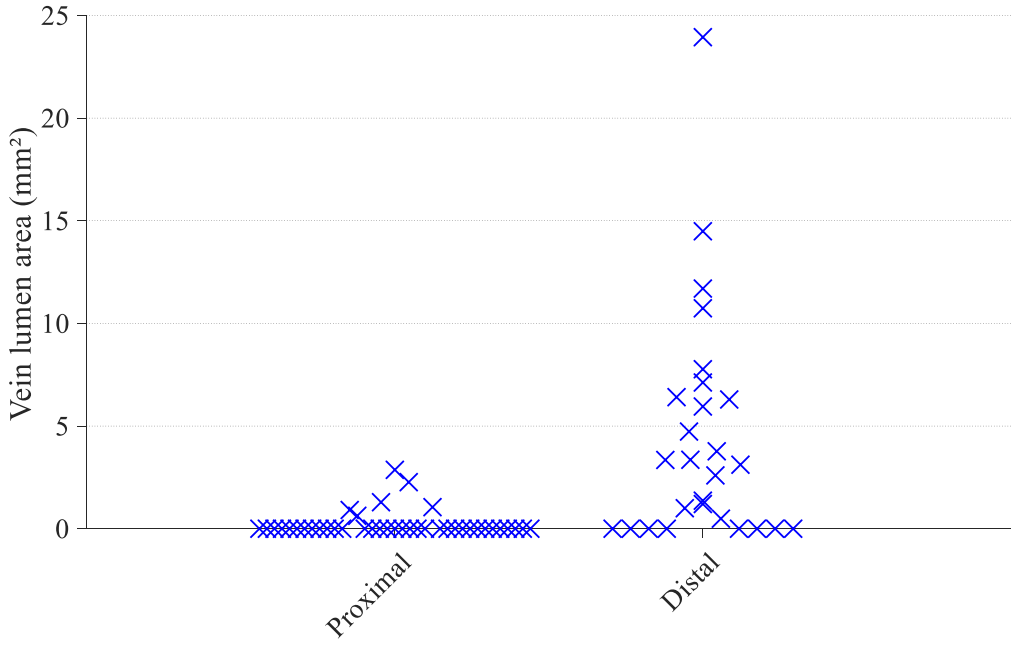


**Figure 6-10 – Vein lumen area proximally and distally to the border of the lesion.**

The mean of the two populations was significantly different ($p$ =0.0006). The vein was completely collapsed in 85 % of the slices in the proximal group. The vein was completely collapsed in 30 % of the slices in the distal group. The difference in lumen size was visible in all treatments. Examples of lumen size reduction are provided in Figure 6-11 and Figure 6-12.

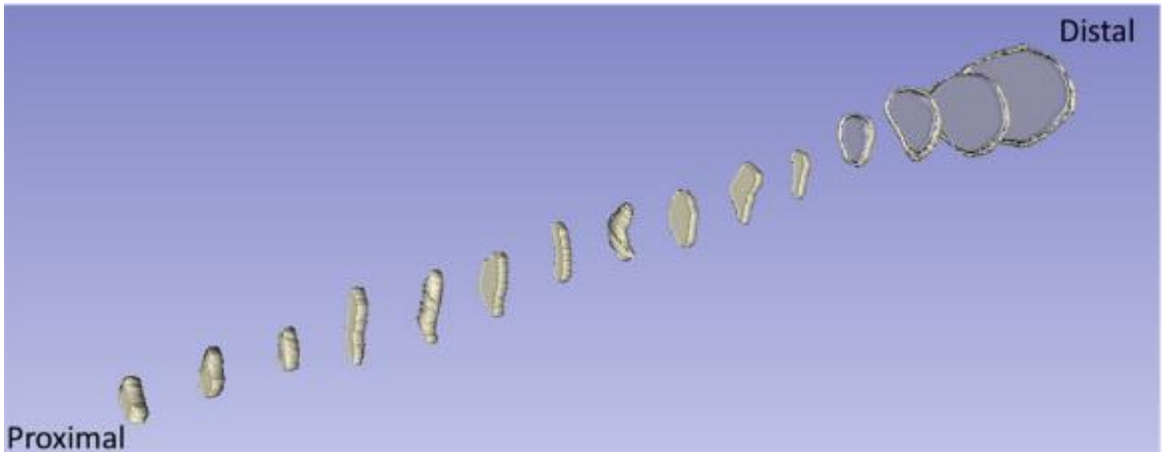


**Figure 6-11 – 3D reconstruction of a treated vein.** The vein wall and the lumen are represented by the white and purple outlines respectively. The vein is completely collapsed on the proximal side.

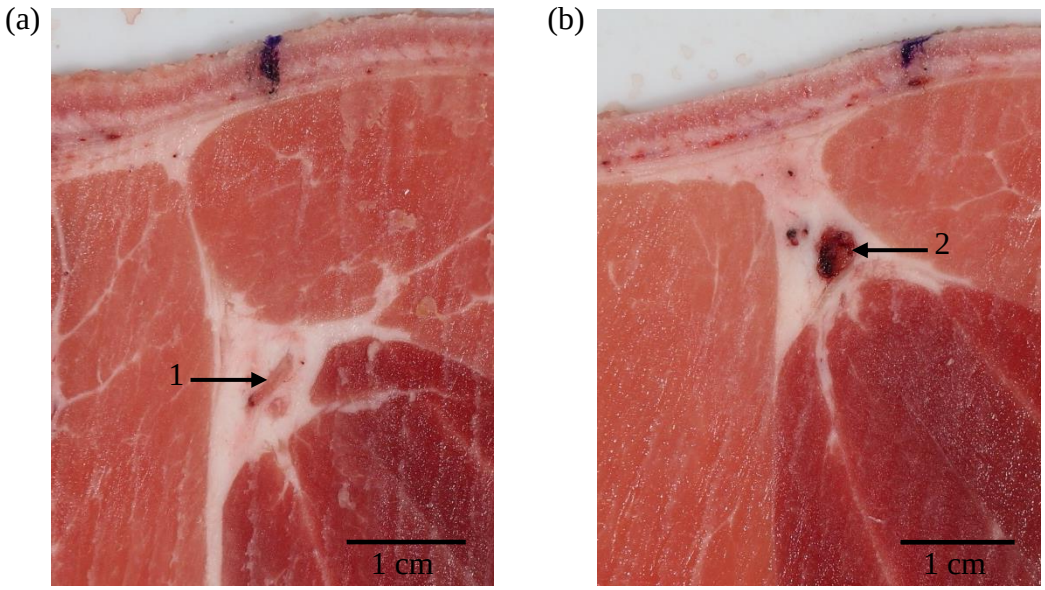


**Figure 6-12 – Macroscopic slices in proximal (a) and distal (b) zones showing respectively a collapsed vein (1) and a vein with visible lumen (2).**

### 6.2.3 Discussion

In this study, *in vivo* experiments were performed to investigate the vein wall shrinkage induced by HIFU treatments on medium-sized sheep veins. The veins were repeatedly sonicated for 8 s at a mean acoustic power of 61 W and the shrinkage was evaluated with B-mode imaging after the HIFU procedures.

At the end of the treatments, all the treated veins (6/6) showed luminal constriction. Immediate findings showed a mean vein wall contraction of 53 %. Given the amount of vein wall shrinkage achieved in this study, the treatment parameters are deemed relevant for the ablation of veins of similar diameters.

In the existing literature, only one *in vivo* study conducted by Yang *et al.* [127] investigated the shrinkage related to the application of HIFU to blood vessels with similar diameters (rabbit aorta of approximatively 3 mm in diameter). After exposure to 4 MHz for 5 s, rabbit aorta showed no evidence of lumen constriction. We hypothesize that no shrinkage was observed due to the cooling of blood flow, which acted as a heat sink.

In our study, the veins that showed a smaller shrinkage corresponded to cases where the blood flow could not have been fully stopped during pulses. On the contrary, a shrinkage of 58 % or more was observed in the veins treated with a completely interrupted blood flow

during sonications. In addition to stop the blood flow, the vein compression decreases the vein diameter, which might also contribute to a greater vein wall coverage. Vein compression with full blood flow interruption during pulses should therefore be considered for future clinical application.

In the published literature, data quantifying the vein shrinkage achieved immediately following *in vivo* endovenous thermal ablation (RF or laser) are scarce. Only one study conducted by Weiss *et al.* [123] quantified the thermally-induced shrinkage in acute after laser and RF ablation of sheep jugular veins. In their study, 26 % and 77 % of shrinkage were achieved after completion of laser and RF procedures respectively. Investigators also evaluated the evolution of the amount of shrinkage over time. They reported a shrinkage of 27 % and 50 % one week after laser and RF treatments respectively.

Irreversible occlusion following endovenous thermal ablation is thought to result from a process of shrinkage where vein lumens narrow incrementally until the vein evolves into a fibrotic cord [61], [128], [129]. However, in the study conducted by Weiss *et al.* [123] a wall relaxation was observed over time after RF treatments.

The progression over time of the shrinkage achieved with HIFU was not evaluated in the present study, but future studies will be conducted to ascertain whether a substantial shrinkage (> 50%) is maintained.

Apart from the predictive value of the amount of shrinkage for an irreversible vascular occlusion, some studies [116], [130], [131] proposed to induce a limited constriction for the management of venous reflux, just enough to restore valvular competence. The RF results were however discouraging and with varying effectiveness. The concept of functional vein restoration with RF was not reported in other studies to our knowledge.

In this study, the ablation zones induced by HIFU treatments were macroscopically assessed. Thermal lesions were observed surrounding all the treated veins except for sheep #05. Compared to the other veins, this one had a larger vein diameter (5.2 mm) and was sonicated at a lower acoustic power (50 W in mean). Moreover, this vein was not properly collapsed during treatments and was sonicated with a persistent blood flow (Table 6-1). A consequence of all this might have modified the heat deposition and prevented the cumulative temperature rise outside the focal zone. However, this vein showed reduction in lumen diameter, which is a sign of vein wall coagulation.

For all the other treatments, the mean gross lesion sizes along $x$ and $z$ were found to be 4.7 mm and 8.0 mm respectively. The shape of the lesion was similar to the shape of the HIFU-induced lesions observed in previous unreported experiments that we conducted on rabbit liver. However, the gross appearance of the lesions was different. As observed in Figure 6-12, the veins were mainly surrounded by fatty tissues. Soft tissues, like muscle or liver, are generally described in the literature to turn white when thermal damages occur. In contrast, data regarding the color change of fatty tissues are scarcer. However, it is commonly reported that necrotic fatty tissues basically turn yellow. Here, pale red-rose regions were considered as lesions. The difference between treated and untreated areas was clearly visible (Figure 6-13) and were considered to be the consequence of HIFU treatments. Moreover, a variety of tissue damages can arise and fat necrosis was not necessarily induced in this study. The impact of lesions in fatty tissues is unknown. However, in a clinical study conducted by Rouvière *et al.* [132], while treating prostate cancer with HIFU, lesions extended into surrounding fatty tissues. The patients were followed up several months after treatment and fatty lesions did not induce any bad clinical outcome. Lesions were progressively absorbed by macrophages, like prostate tissue lesions.

(a) (b)

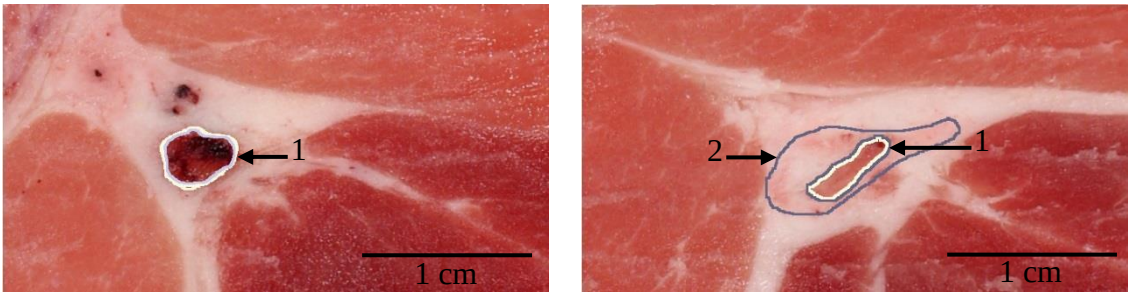


**Figure 6-13 – (a) Distal slice: no lesion observed around the vein (1) and (b) proximal slice where a lesion (2) is observed around the vein (1).**

In addition to thermal lesions surrounding the targeted veins, the vein lumens were segmented. All the veins treated showed a decrease in lumen area between the most distal slice and the most proximal. In particular, the veins were completely collapsed in 86 % of the slices located proximally to the distal borders of the lesions. No collapse has been observed in any vein with B-mode images. It may be possible that during freezing, veins were pushed away by

surrounding tissues, which might have contributed to further contraction, possibly inducing collapse.

## 6.3 Numerical modelling of the HIFU-induced vein wall shrinkage

As mentioned in the Introduction, experimental measurements of the vein wall shrinkage were used to validate a numerical model accounting for thermally-induced vein lumen reduction developed by Anthony Grisey.

### 6.3.1 Numerical model

The model was based upon a dynamic computation of the vascular thermal damage estimated from the thermal rise induced by the HIFU pulses. An overview of the methodology is presented in Figure 6-14.

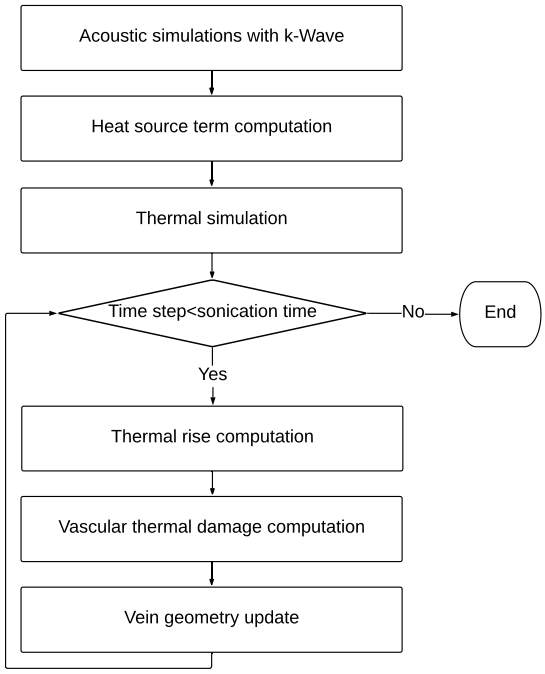


**Figure 6-14 – Flowchart of the thermally-induced vein lumen reduction model.**

#### 6.3.1.1 Simulations

The treatment configuration applied experimentally was modeled numerically: two 8 s pulses delivered in continuous wave mode at 60 W acoustic and with the focus located 16 mm under skin. This corresponds to the treatment of one transverse slice of the vein.

Because of the hole in the therapy transducer for the imaging probe, the axial symmetry of the beam is broken, and three-dimensional simulations are therefore necessary. Hereinafter, $z$ denotes the main propagation axis, pointing from the transducer to the focus towards the subject anatomy, $x$ the axis of the imaging probe, oriented from the left to the right of the image. $y$ is the cross product of $x$ and $z$, so that the $(x, y, z)$ frame is orthonormal and right-handed (Figure 6-1).

##### 6.3.1.1.1 Acoustic simulations

Acoustic simulations were first performed with the simulator presented in Chapter 3. The acoustic field was therefore computed with the k-Wave library 1.2 [83], [84] with the 'layer-by-layer' approach [87].

In this study, ultrasound propagated through the cooling fluid contained in the balloon fixed to the transducer, the superficial tissues (skin, subcutaneous fat and muscle) and the muscles successively, with the acoustic properties listed in Table 6-2. Tissue properties were assumed to remain constant during the procedure. Nonlinearities were modeled up to the fourth harmonic, with a spatial resolution of up to 62 µm. The Courant-Friedrichs-Lewy (CFL) coefficient was set to 0.5, resulting in a time step of 20 ns for the finest resolution. A perfectly matched layer was used to avoid reflections at the boundaries of the domain. The acoustic source term was computed as:

$$p^2 = \frac{2P_{ac}\rho c_s}{S_{transducer}} \tag{6.2}$$

where $p$ is the pressure amplitude, $P_{ac}$ the acoustic power, $\rho$ the acoustic density, $c_s$, the speed of sound and $S_{transducer}$ the surface area of the transducer. $P_{ac}$ and $S_{transducer}$ were respectively set to $P_{ac}$ =60 W and $S_{transducer} = 2.07 \times 10^{-3}$ m$^2$.

**Table 6-2 – Acoustic properties of tissues used for simulations.**

| | Cooling liquid | Superficial tissues | Muscles | Blood | Vein wall |
|---|---|---|---|---|---|
| Sound speed ($m.s^{-1}$) | 1495 | 1573 [95] | 1580 [58] | 1580 | 1580 |
| Density ($kg.m^{-3}$) | 1000 | 995 [95] | 1060 | 1060 [133] | 1060 |
| Attenuation at 3 MHz ($dB.cm^{-1}$) | 0.02 [134] | 2.48 [95] | 2.25 [58] | 0.5 [58] | 4.35 [135] |
| Acoustic non-linearity parameter | 5 [136] | 7.8 [95] | 7.8 [58] | 7.8 | 7.8 |

#### 6.3.1.1.2 Thermal simulation

##### 6.3.1.1.2.1 Modeling of vein contraction

As displayed in Table 6-1, there were some differences in the pre-treatment diameter of the veins. Simulations were thus run for initial pre-treatment diameters $d$ of 2.3, 3.5 and 5.2 mm.

The vein wall thickness was set to 0.5 mm for all simulations, which is the typical vein thickness reported in the literature [135], [137]. At the beginning of the treatment, the vein was modeled as an elliptic cylinder along the $y$ axis (Figure 6-1). The length of the semi-minor axis along $z$ is denoted $r_z$. It was set to 100 µm. The length of the semi-major axis $r_x$ (Figure 6-1) was computed based on the Euler approximation of the circumference of an ellipse:

$$r_x = \sqrt{\frac{d^2}{2} - r_z^2} \tag{6.3}$$

The circumference of the vein was dynamically modified to take into account the shrinkage induced by collagen denaturation. $r_z$ was kept constant and $r_x(y,t)$ was dynamically adapted to the local circumference of the vein in each plane.

As mentioned previously, we simulated here only one plane, in which two symmetrical targets were successively sonicated, yielding to asymmetric shrinkage. To model this asymmetry, the left and right halves of the vein were considered as two independent half-ellipses of semi-major axis $r_{x-}(y=0,t)$ and $r_{x+}(y=0,t)$. The continuity of the vein wall is guaranteed by the fact that $r_z$ is considered constant.

#### 6.3.1.1.2.2 Temperature rise simulation

Thermal simulations were based on the Pennes bioheat equation:

$$\rho_t C_t \frac{\partial T_t}{\partial t} = k_t \nabla^2 T_t + \omega_b \rho_b C_b (T_b - T_t) + Q \tag{6.4}$$

with $\rho, C, T$ corresponding to the density, the specific heat and the temperature respectively; the subscripts $t$ and $b$ refer to tissue and blood respectively; $\omega_b$ is the perfusion coefficient, $k_t$ the tissue conductivity, $T_b$the blood temperature and $Q$ the heat source term resulting from the power deposited by the acoustic wave.

The equation was solved in 3D using a first order Euler explicit finite difference scheme with MATLAB® R2018b. The grid size was 38 × 38 × 25 mm. The time step was 50 ms and the spatial step was 200 μm.

#### 6.3.1.1.2.3 Vascular wall damage

The extent of the thermal damage to the vessel was computed based on the vascular thermal damage model described by Agah *et al.* [77] using a general Arrhenius equation:

$$\Omega(\mathbf{x}, t) = \ln\left(\frac{c(\mathbf{x}, 0)}{c(\mathbf{x}, \tau)}\right) = A_f \int_0^{\tau} \exp\left(\frac{-E_a}{RT(\mathbf{x}, t)}\right) dt \tag{6.5}$$

where $\Omega$ $(\mathbf{x}, \mathrm{t})$ is the damage parameter, $c(\mathbf{x}, 0)$ and $c(\mathbf{x}, \tau)$ are the concentration of the undamaged molecules at the beginning of the treatment and at time $\tau$ respectively. $A_f$ is the frequency factor, $E_a$ is the activation energy $R$ the universal gas constant and $T$ the temperature.

$A_f$ and $E_a$ were set to $A_f$ =5.6 $10^{63}$ $s^{-1}$ and $E_a$ =430 kJ.$mol^{-1}$, according to [77]. The degree of vessel damage is appraised by $\Omega(\mathbf{x}, \mathrm{t})$, where $\Omega(\mathbf{x}, \mathrm{t}) = 1$ defines the first noticeable irreversible damage and formally corresponds to the denaturation of 63 % of the native proteins [77]. The threshold for vascular coagulation was set to $\Omega(\mathbf{x}, \mathrm{t}) = 5$, which formally corresponds to the denaturation of 99 % of the collagen.

### 6.3.1.2 Vein wall constriction

#### 6.3.1.2.1 Model

Shrinkage during heating brings distant parts of the vein wall towards the focal spot. Gorisch *et al.* [76] reported the relative diameter of veins after 16 seconds heating at different temperatures. These exposures were translated into vascular damage values (Ω) according to the formula reported by Agah *et al.* [77]. Data were then fitted with an exponential curve to derive an analytical formula of the diameter shrinkage with respect to Ω: $l(\Omega)$ (Figure 6-15). The fitting curve was found to be:

$$l(\Omega) = 1 - (0.83 - 0.87 \times e^{-2\Omega}) \tag{6.6}$$

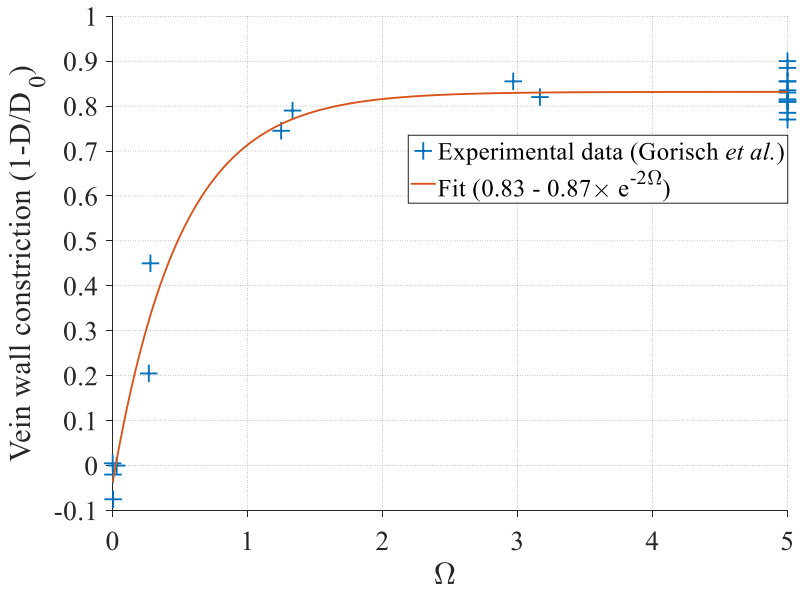


**Figure 6-15 – Evolution of the vein contraction with Ω.** $D_0$ and D represent respectively the diameter before and after the heating

#### 6.3.1.2.2 Implementation

The vein wall was considered to be made of several unitary voxels, each having a unitary length. With the parameters used in this study (vein wall thickness and spatial resolution), the initial vein wall mask consisted in three concentric rings of pixels (Figure 6-16, upper left).

The implementation of the shrinkage was based on the computation of Ω in each voxel belonging to the vein wall. The contraction of each pixel was computed and the vein diameter

for the next time step was estimated. The updated vein wall mask was then populated with interpolated values of Ω based on the curvilinear coordinates along the vein wall.

The implementation of the diameter shrinkage was based on the use of a weighted curvilinear abscissa along the cross-section denoted $s$. $s$ represents the cumulative sum of the normalized lengths of each pixel along each vein wall ring relatively to the previous time. The algorithm used for diameter shrinkage implementation is illustrated in Figure 6-16 and can be found in Appendix B.

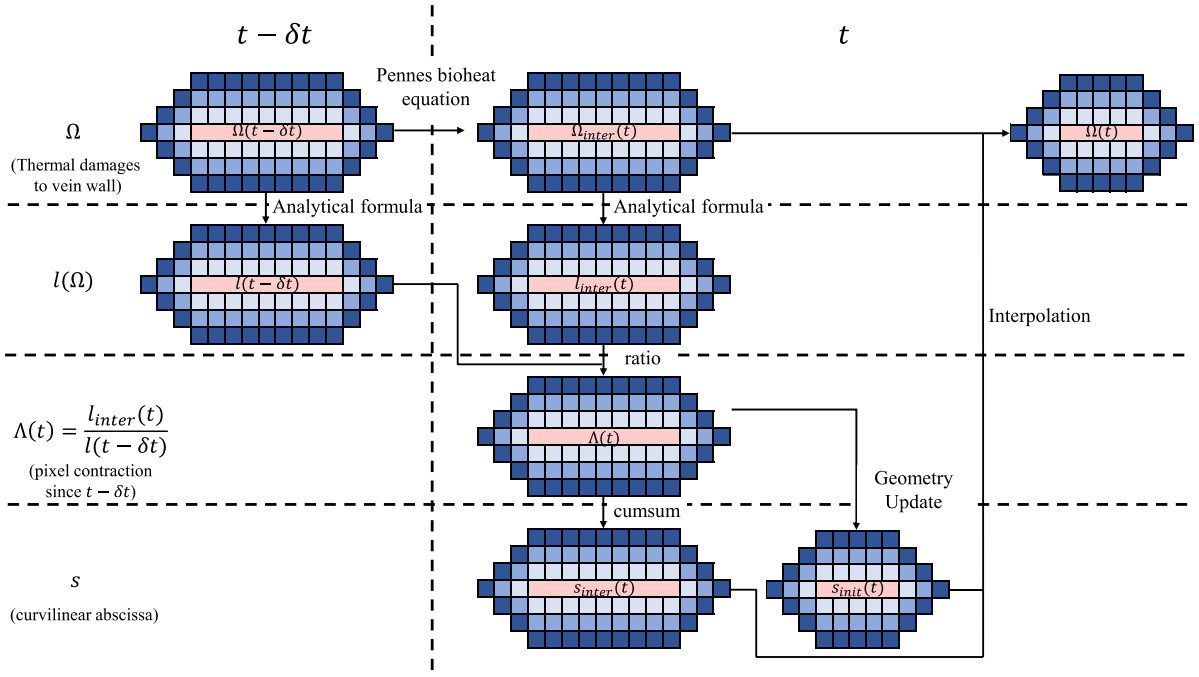


**Figure 6-16 – Illustration of the process to compute the shrinkage of the vein.**

## 6.3.2 Results

### 6.3.2.1 Simulations

Figure **6-17** shows the distribution of the root mean square acoustic pressure (Prms) field in the $xz$ plane simulated with the "layer by layer" approach.

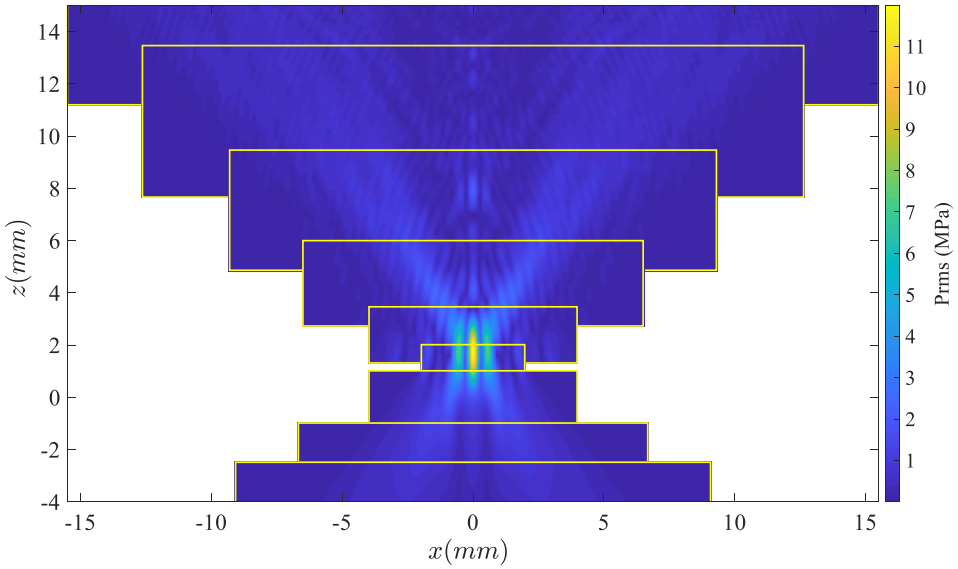


**Figure 6-17 – Simulated rms pressure field of the geometrical model in the *xz* plane.** Yellow rectangles represent the limits of the subsequent layers.

### 6.3.2.2 Estimated vein wall constrictions

Figure 6-18 shows the final shrinkage and the thermal damage on the shrunken vein wall after HIFU exposures. Figure 6-19 illustrates the comparison between the estimated and the measured vein wall shrinkage for the three initial pre-treatment diameters simulated here.

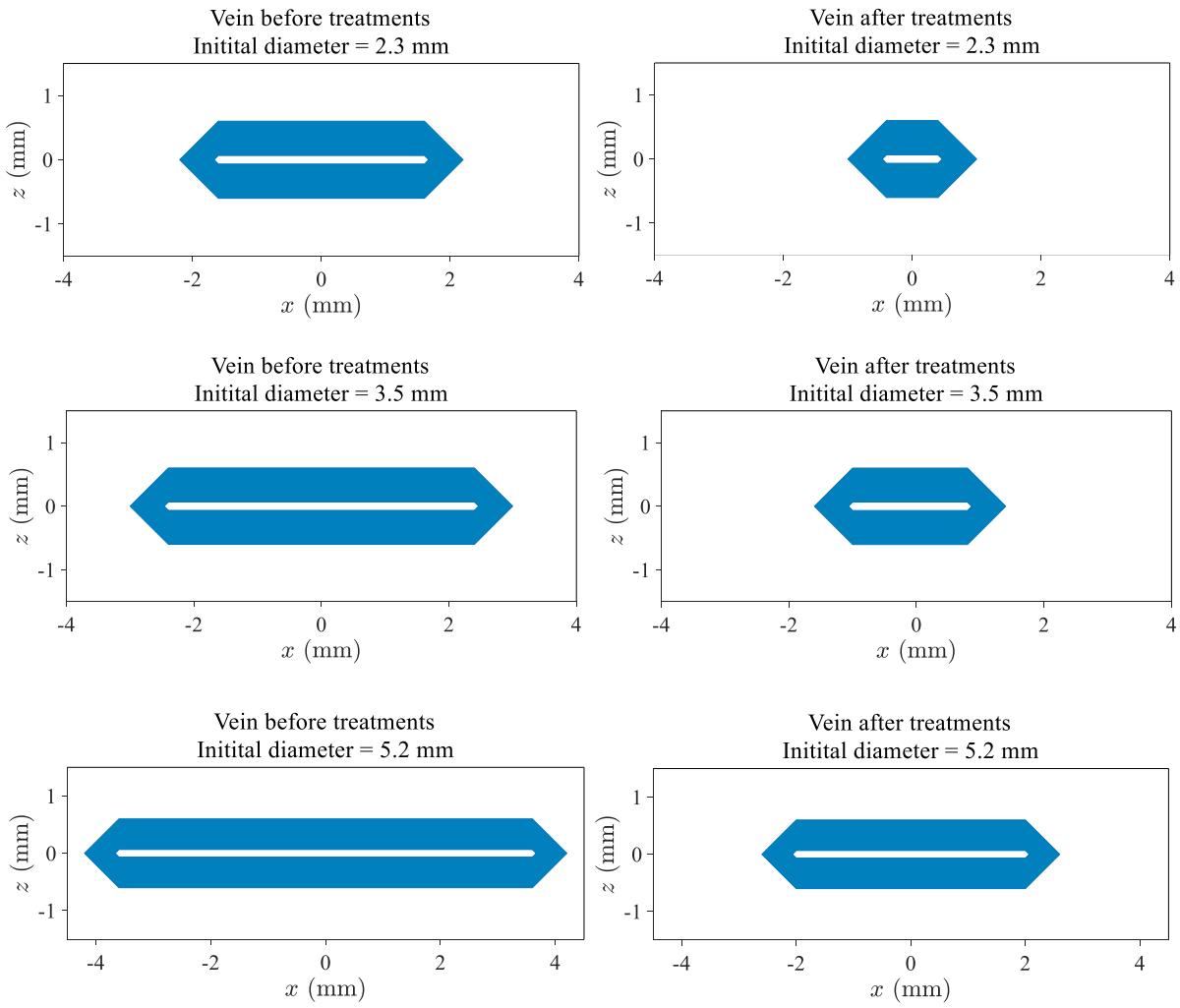


**Figure 6-18 – Shrinkage simulations for veins with an initial pre-treatment diameter of 2.3 mm (top row), 3.5 mm (middle row) and 5.2 mm (bottom raw).** Left column: before treatment. Right column: after treatment.

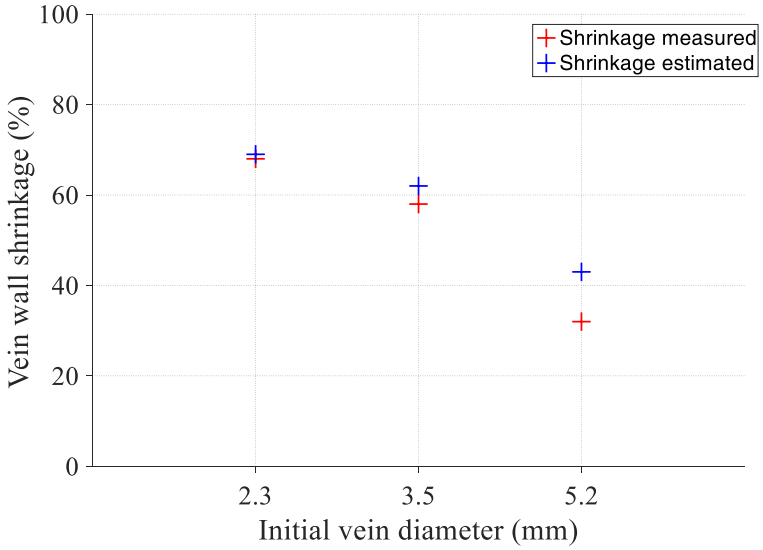


**Figure 6-19 – Comparison between the simulated (blue) and experimental (red) luminal shrinkage in a vein cross-section for the three initial pre-treatment diameters.**

### 6.3.3 Discussion

In this study, the experimental data of the HIFU-induced vein wall shrinkage were used to validate a numerical model of the shrinkage induced by HIFU treatments.

The treatment parameters of the *in vivo* experiments were simulated numerically, and the vein wall shrinkage was estimated for three pre-treatment diameters (2.3, 3.5 and 5.2 mm) reflecting the experimental variations in the sheep veins diameters. Simulated and measured vein wall shrinkages were in good agreement for the 2.3- and 3.5-mm diameters. The numerical model could therefore be a useful tool to adjust HIFU exposure parameters in function of the vein diameter to maximize the vein wall heating for small vessels. A mismatch between estimated and measured luminal constriction was observed for the 3.5- and 5.2-mm diameters. These discrepancies can be explained by the fact that veins were treated with persistent blood flow, which was not taken into account in this numerical model.

This model includes other limitations: for example, collagen denaturation was considered to be responsible of the thermally-induced shrinkage only. However, other processes may also contribute, like water losses. Moreover, this model also assumed isotropic tissue properties. However, like many other soft tissues, blood vessels are anisotropic [138]. Contraction could therefore depend on the orientation of the vein relating to the HIFU field, which was not evaluated here.

## 6.4 Conclusion

The evaluation of tissue alterations induced by HIFU treatments provided indications for both the efficacy and safety of the HIFU procedure implemented for venous ablation.
Given the amount of venous shrinkage obtained after treatment, particularly after the ablation of veins with a diameter smaller than 3.5 mm, the HIFU treatment protocol is promising. As expected, thermal lesions in perivascular tissues were induced during the treatments. Ablated lesions extended over 4.7 mm and 8.0 mm along $x$ and $z$ respectively, on average. The assessment of the lesion sizes induced by HIFU treatments helps defining safety margins with regards to sensitive structures.

To minimize perivenous tissue damage during venous thermal ablation, RF and laser techniques require tumescent infiltration. The injected liquid forms a protective layer around the vein. Similarly, tumescent infiltration could be performed before sonications to protect sensitive perivascular structures, although it would require proper degassing to avoid cavitation in the liquid.

A limitation of this study is that no microscopic examination was performed to better characterize changes in tissues and to confirm the macroscopic observations. In this study, the tissues were deep-frozen without having been previously protected for freezing, but slow freezing is known to cause distortion of tissues due to ice crystal formations and alter the tissue morphology. To protect sections from ice crystal artifacts during freezing, it would have required to cryoprotect the whole animal for freezing, which was impossible due to the size of the animal. Histological analysis of tissue damages could thus not be performed.

In the next chapter, thermal alterations of sheep veins and surrounding tissues are microscopically assessed. Long-term effects of HIFU treatments are additionally provided and animal wellbeing following HIFU procedure and adverse effects are also evaluated.

# 7

# Thermal effects induced after HIFU ablation of veins: macroscopic and microscopic characterization at 30, 60 and 90 days

## 7.1 Introduction

In chapter 6, the vascular and perivascular tissue response were macroscopically estimated after HIFU ablation of sheep veins. Gross evaluation of the targeted vessels and the surrounding tissues after HIFU treatment showed evidence of vein wall coagulation and perivenous injury.

The objective of our HIFU procedure is to achieve a safe and efficient vascular coagulation. Follow-up studies were therefore conducted to evaluate the impact of the thermal damages induced by HIFU treatments and are reported here. Healing of the treated vein was additionally characterized to assess if fibrotic occlusion could be achieved.

In the study reported in this chapter, 18 medium-sized sheep veins were exposed to HIFU. The animals were followed up to 30, 60 and 90 days post-treatment. During the follow-up duration, the sheep's wellbeing and their health condition were monitored.

The short and long-term tissue response of the targeted vessels and perivascular tissues were histologically characterized. The microscopic venous changes were additionally compared to what is reported after conventional endovenous thermal ablation.

## 7.2 Materials and methods

### 7.2.1 Animal experiments

Nine female sheep, 18 to 32 months old (21 $\pm$ 6) and weighing 46 to 65 kg (55 $\pm$ 8 kg) were used in this study. The animals were split into three groups of three animals each and were followed up 30, 60 and 90 days after treatments. The experiments were carried out according to the guidelines of the French National Committee for animal trials C.N.R.E.E.A (Comité national de réflexion éthique sur l'expérimentation animale) and were approved by the institutional ethics committee for animal experiments (agreement number CE16/2017022116542356).

As in previous animal studies, experiments were conducted on the lateral sheep saphenous vein. In addition to present close similarities to human's saphenous vein, the sheep lateral saphenous vein is a medium-sized vein of the superficial venous system (average 3 mm diameter), which makes chronic experiments feasible.

The sheep were initially anesthetized with intravenous injection of ketamine (5 mg/kg, Ketamine 1000, Virbac, France) and Diazepam (0.5 –1 mg/kg, Diazepam TVM5, TVM Lab, France). Anesthesia was maintained by endotracheal intubation of oxygen (100 %) and Isoflurane (2-2.5 %, Vetflurane, Virbac, France). The arterial blood pressure, heart rate, body core temperature and respiratory rates and pattern were monitored and were kept within physiological range throughout the treatments. The animals were installed on the surgical table in lateral decubitus position to access the targeted vein.

Once the sheep was anesthetized, hair of both hind limbs was first shaved with a hair trimmer (Aesculap® Favorita II, B-Braun, Germany). The remaining hair was then removed with a commercial depilatory cream (Klorane, France). Prior to the treatments, ultrasound examinations including B-mode and Duplex imaging were performed to identify the portion of the vein to be treated and to evaluate post-sonications venous changes. Approximatively five minutes before the beginning of the HIFU procedure, intravenous morphine (0.1-0.2 mg/kg, Chlorhydrate de Morphine, Renaudin, France) was administrated for additional analgesia.

Each animal had both lateral saphenous veins treated with HIFU. All experiments were performed with a HIFU system and a transducer similar to the ones presented in chapter 3. A total of eighteen saphenous veins with a mean diameter of 3.2 $\pm$ 1.0 mm were exposed to HIFU. Each vein was treated with a sequence of HIFU sonications distributed in a row of multiple spots along the vein with a 3.5 mm spacing between subsequent spots. In each spot, two sonications were delivered to the vein cross-section, as was modeled in the previous chapter (chapter 6). A minimum cooling time of 30 s was set between sonications for the skin to cool down. Continuous HIFU sonications were applied for 8 s with a mean acoustic power of 84 $\pm$ 6 W. During each treatment, the hind limb of interest was slightly elevated to reduce vein caliber and maximize thermal damage of the vein wall. Before each exposure, the vein was compressed until no blood flow was visible on color Doppler in order to limit the heat sink effect of the blood flow and help vein wall coagulation.

The effects of the HIFU treatments were first evaluated with post-treatment ultrasound imaging. At the end of the treatment, the sheep were recovered from anesthesia and were returned to their pen. From day one to the day of euthanasia, the animals were closely observed (food and drink consumption, behavior, posture…) and regular physical examinations were performed to detect any possible abnormalities post-treatment. Prior to sacrifice, the sheep were anesthetized as described above and ultrasound images were performed to assess clinically the targeted venous segment. Animals were then euthanized by an intravenous injection of 25 mL of Pentobarbital 18 % (Dolethal, Vetoquinol, France).

### 7.2.2 Histopathological assessment

Venous tissues along with the perivenous muscle tissues in direct contact with the veins or with the connective tissue surrounding the veins were harvested and fixed by immersion in a 10 % buffered formalin solution containing 4 % of formaldehyde. The tissues were then sent for histologic processing and histopathological analysis. The muscle tissues extracted were 5-mm thick and the harvested vein segments averaged 3 cm in length (Figure 7-1).

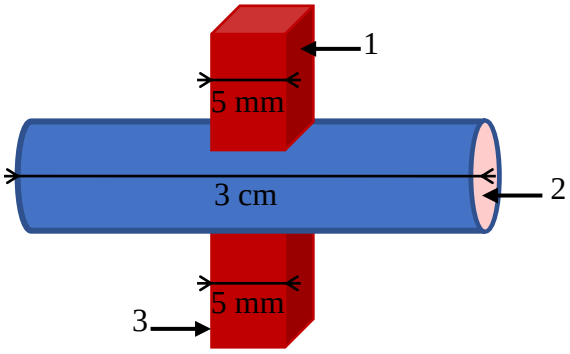


**Figure 7-1 – Illustration of the harvested samples.** 1. Superficial muscle tissue; 2. Vein segment; 3. Deep muscle tissue.

The muscle tissues were deposited in histocassettes. They were trimmed parallel to the bottom of the cassette into 3-µm thick slices and were deposited on slides (Figure 7-2).

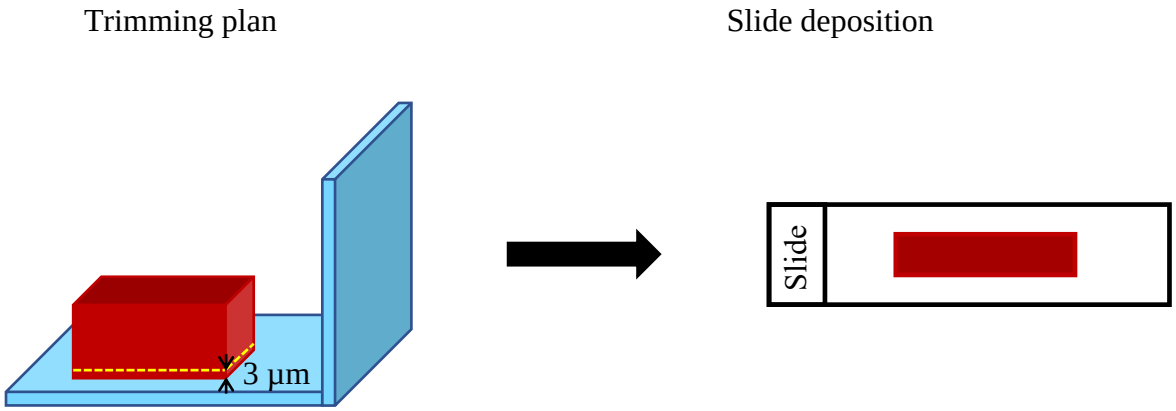


**Figure 7-2 – Muscle trimming plan (a) and slide deposition (b).**

Vein samples were cross-sectioned into four regularly spaced sections and were embedded in paraffin. Subsections of 3 to 5 µm thick were then cut and were deposited on glass slides (Figure 7-3).

Both muscle and venous slides were stained with Hematoxylin and Eosin (H&E) and Gomori's Elastin Trichrome (GET). GET was performed to identify changes in collagenous fibers and differentiate the collagen fibers from the smooth muscle fibers.

(a) Vein trimming step

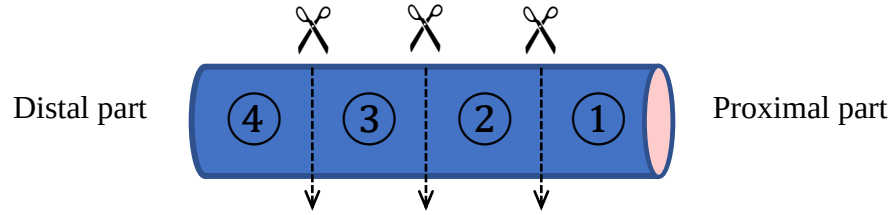


(b) Slide deposition


**Figure 7-3 – Illustration of the vein trimming plan (a) and the slide deposition (b).**

Thermal changes and subsequent healing changes were pathologically assessed by an experienced pathologist (ACVP board certified). For vein tissues, microscopic features evaluated during histopathological analysis included vein mural injury, vein thrombosis, vein fibrosis and potential occurrence of vein perforation and blood extravasation.

## 7.3 Results

### 7.3.1 Macroscopic and imaging assessment

No adverse events occurred during exposures and all animals recovered well after HIFU treatments. None of the sheep showed complications during the follow-up. Sheep continued their normal pattern of feeding and lived normally until the end of the scheduled sacrifice.

Immediately following HIFU exposures, hyperechoic marks and vein lumen reduction were typically observed (Figure 7-4 (b)), as compared to images acquired before the treatment (Figure 7-4 (a)). After the procedure, all targeted vein segments showed sonographically blurred vascular contours as well as vein wall constriction. Figure 7-5 illustrates a typical vein shrinkage observed after the procedure. Before sacrifice, occlusion was also observed 30, 60 and 90 days post-treatment, as evidenced by the incompressibility of the vein with ultrasound probe pressure (Figure 7-6), the interruption of color Doppler signals (Figure 7.**7**) or the presence of a hyperechoic cord filling the lumen (Figure **7-7**). In total, 83 % of the veins

showed before sacrifice interruption or reduction of the blood flow as judged by the color Doppler ultrasound. Table 7-1 summarizes the imaging results of the treated sheep saphenous veins.

**Table 7-1 – Imaging findings synthesis.**

| Animal group | D30 | D60 | D90 |
|---|---|---|---|
| Number of veins showing lack of Doppler signal | 6/6 | 5/6 | 4/6 |
| Number of veins showing echogeneicity | 4/6 | 5/6 | 2/6 |

During tissue samples harvesting, HIFU-treated regions were observable as whitened and indurated zones. Neither perforation nor charring were reported for any of the targeted veins.

(a) (b)

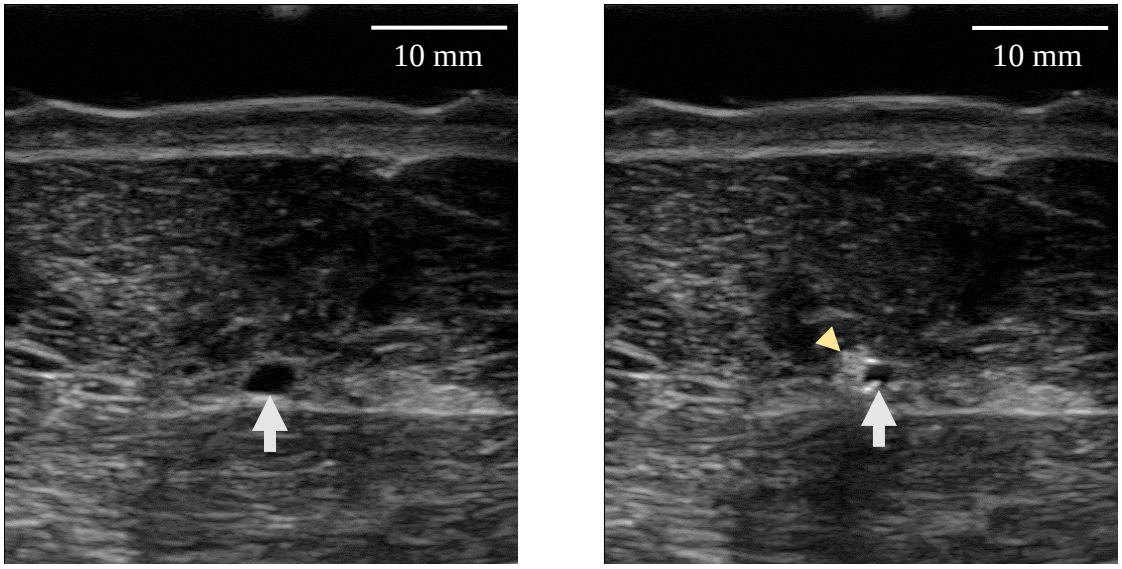


**Figure 7-4 – Ultrasound images of the lateral saphenous vein (pointed by a white arrow) of a sheep before exposure (a) and immediately after exposure (b).** The exposed vein has a reduced lumen and a hyper-echoic mark (pointed by a yellow arrowhead) is visible.

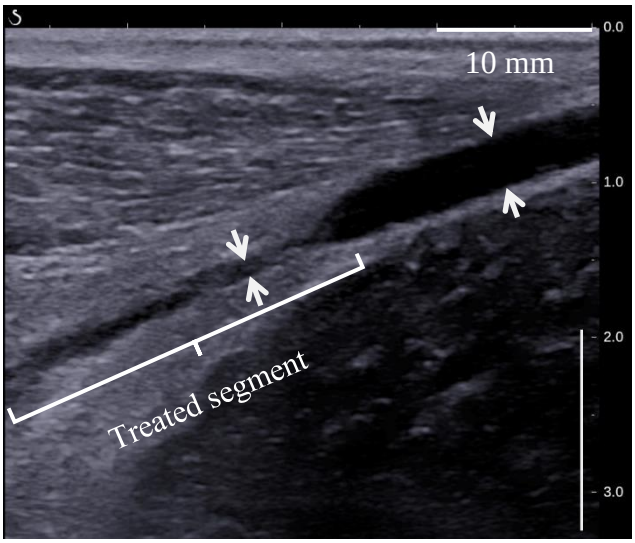


**Figure 7-5 – B-mode image after HIFU procedure showing a vein diameter constriction and blurred vascular contours.**

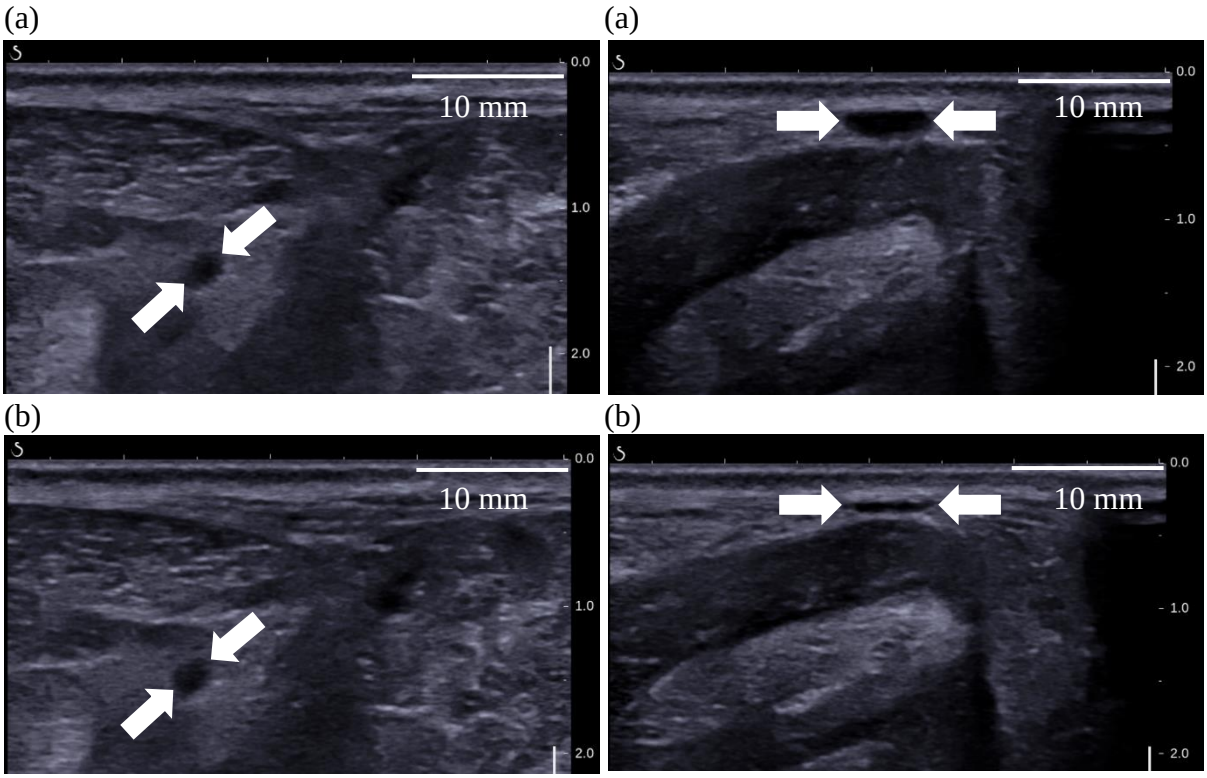


**Figure 7-6 – Ultrasound images showing a non-compressible treated vein at 30 days post-treatment (left column) and a compressible untreated vein (right column).** Veins are pointed by white arrows. (a) and (b) represent respectively the sheep veins before and after external ultrasound compression.

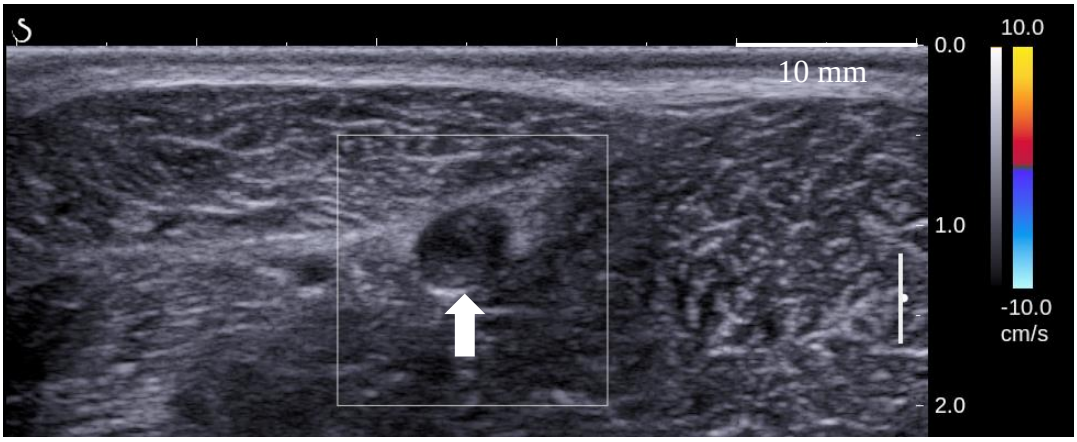


**Figure 7.7 – Color Doppler ultrasound image showing the absence of flow in a sheep vein (white arrow) 60 days after treatments.**

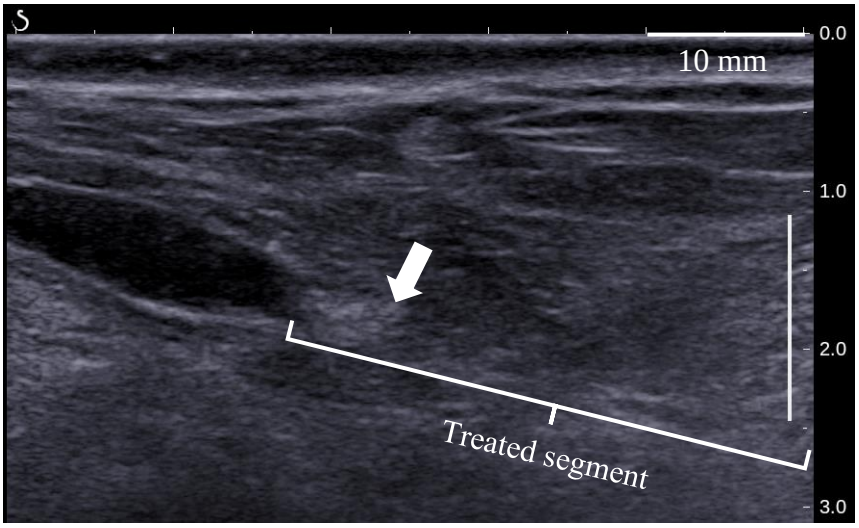


**Figure 7-7 – B-mode image of a sheep vein (white arrow) taken 90 days after sonications and showing complete fibrosis of the treated segment.**

### 7.3.2 Histological findings

Histological evaluation of venous tissues harvested 30, 60 or 90 days post treatment showed typical changes due to thermal injury as can be seen on Figure 7-8.

Microscopic changes were characterized at 30 days by coagulative necrosis of the vein wall (Figure 7-8 (a)). Smooth muscle cells showed coagulation necrosis. The mural, adventitial and perivascular collagen showed thermal denaturation characterized by a loss in microfibrillar structure and collagen hyalinization. Vein thrombosis and occlusion were observed. In addition, histiocytes and foreign-body giant cells were found in the HIFU-affected vascular tissues. At 60 days after the treatment, vein thrombosis and occlusion associated with vein wall fibrosis were observed. Residual hyalinization was also found in the tunica media (Figure 7-8 (b)). Treatment-induced vein changes at 90 days presented occlusive thrombosis, characterized by organized fibrocellular thrombus, and vein wall fibrosis (Figure 7-8 (c)). No vein lacerations and no subsequent blood extravasation were observed in any of the evaluated veins.

Microscopic evidence of thermal damage was also found in perivenous tissues. At 30 days, perivascular fat necrosis and limited muscle necrosis in the superficial perivenous skeletal muscle were observed. Perivascular fat necrosis was detected in the form of local and demarcated steatonecrosis with the presence of macrophages and giant cells into the necrotic tissue (Figure 7-9 (a)). Muscle necrosis was observed as delimited areas of coagulative necrosis with fibrous healing (Figure 7-9 (a)). Perivenous collateral changes at 60 days post-treatment

included perivascular fibrosis and confined muscle necrosis that was limited to the superficial perivenous muscle exclusively. Muscle-affected tissues presented regenerating myofibers and muscle fibrosis (Figure 7-9 (b)). No fat necrosis was observed at 60 days. Surrounding tissue changes at 90 days after HIFU treatment were primarily found in perivenous connective tissue and were characterized by perivascular fibrosis (Figure 7-9 (c)). No fat necrosis neither residual necrotic adipose tissue was observed at 90 days post-treatment. Histological findings are summarized in Table 7-2.

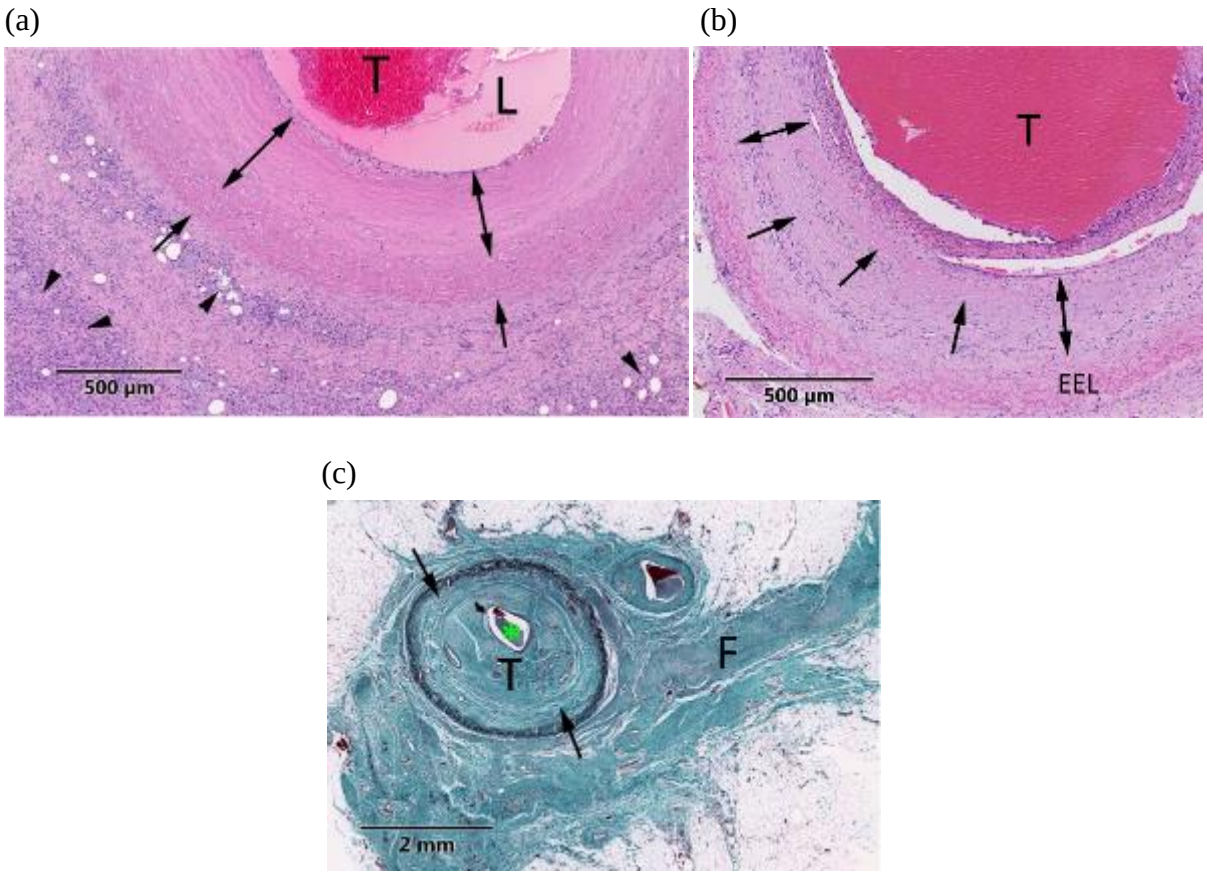


**Figure 7-8 – Representative illustrations of HIFU lesions in vascular tissue.** (a): H&E-section of a vein extracted 30 days after treatment. HIFU lesion shows vein wall hyalinization (arrows), thrombus (T) and necrotic perivascular adipose tissue (arrowheads). (b): H&E-section of a vein extracted at 60 days. Thrombus (T), fibroblast infiltration (double arrows) and residual media hyalinization (arrows) are observed. (c): GET-section of a vein extracted at 90 days and presenting fibrocellular thrombus (T), media fibrosis (arrows) and perivascular fibrosis (F).

(a) (b)

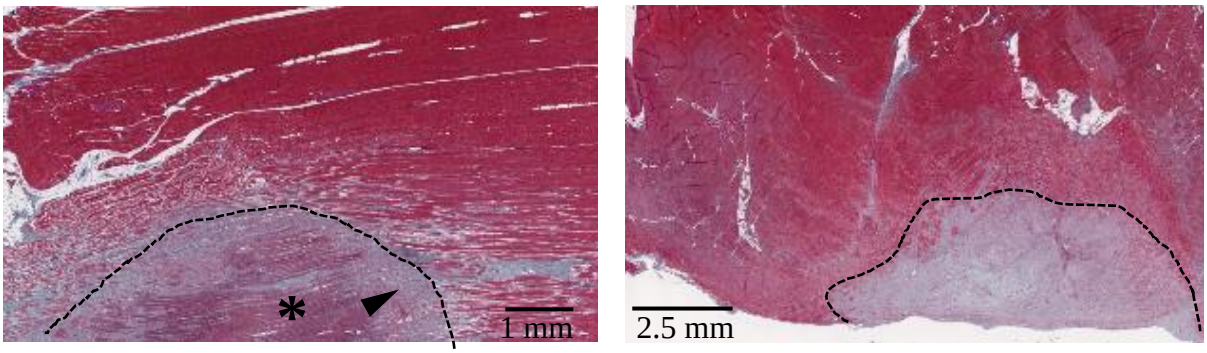


**Figure 7-9 – Typical HIFU lesions in perivenous collateral tissues.** (a): GET-section of a superficial perivenous muscle extracted at 30 days; the area under the dotted line presents focal muscle necrosis with fibrosis (arrowhead) and residual necrotic muscle tissue (asterisk). (b): GET-section of a superficial perivenous muscle harvested 60 days post-treatment (GET); the area above the dotted line shows necrosis and regeneration with fibrosis in the muscle.

**Table 7-2 – Histopathological findings synthesis.**

| | HISTOPATHOLOGICAL FINDINGS | | | | | | | | | | | |
|---|---|---|---|---|---|---|---|---|---|---|---|---|
| | Vascular changes | | | | | | | Perivenous changes | | | Inflammatory signals | |
| Animals group | Vein wall hyalinization | Adventitial collagen hyalinization | Vein wall fibrosis | Vein thrombosis | Vein occlusion | Vein wall perforation | Vein charring | Perivascular fibrosis | Perivascular fat necrosis | Superficial or deep Muscle necrosis | Histiocytes | Foreign body giant cells |
| D30 | 3/6 | 3/6 | 6/6 | 6/6 | 6/6 | 0/6 | 0/6 | 6/6 | 6/6 | 7/12 | 6/6 | 6/6 |
| D60 | 1/6 | 0/6 | 4/6 | 4/6 | 4/6 | 0/6 | 0/6 | 5/6 | 0/6 | 5/12 | 1/6 | 1/6 |
| D90 | 0/6 | 0/6 | 5/6 | 1/6 | 1/6 | 0/6 | 0/6 | 4/6 | 0/6 | 1/12 | 0/6 | 0/6 |

## 7.4 Discussion

This chapter evaluated long-term tissue response in and around veins after HIFU treatment. In particular, the histological profile of HIFU-treated veins and perivenous tissues were studied at 30, 60 and 90 days post-treatment.

Microscopic evaluation of HIFU-treated veins revealed evidence of thermal damages as demonstrated by coagulation necrosis of the vein wall, venous thrombosis and fibrosis.
At 30 days, thermal coagulation was primarily associated with media hyalinization, thermal denaturation of collagen fibers, collagen hyalinization and fibrin thrombus. Similar histologic changes consecutive to high temperature elevation have been reported on veins treated by EVLA or RF and examined at 21 to 42 days after treatment [116], [139]–[142].

At 60 days, vascular wall still showed residual vein wall hyalinization but additionally exhibited fibroblasts infiltration. Likewise, fibrin thrombus was observed at 60 days but organized fibrous thrombi were also found. These changes are characteristic of gradual and ongoing fibrous healing, as evidenced by the presence of fibroblasts reportedly engaged in tissue repair [143]. Injured tissues were gradually replaced by granulation and fibrous connective tissues.

At 90 days, treated veins showed complete healing with transformation of heat-affected sections to scar tissues. Fibrous healing and vein damages were considered stable at 90 days after HIFU treatment. The desired therapeutic effect has thus been achieved: vein fibrotic closure. The ultrasound setting used in this study is effective. To the best of our knowledge, no other study reported fibrotic vein occlusion after extracorporeal HIFU application on non-bleeding medium-sized veins.

We additionally reported changes in the perivascular tissues and the collateral muscles. They were primarily characterized by localized areas of coagulation necrosis. Surrounding connective tissues showed fat necrosis with chronic inflammatory response at 30 days post-treatment exclusively. Healing reaction to adipose tissue necrosis as evidenced by inflammatory cells infiltration resolved over time since perivascular fat necrosis (steatonecrosis) was no longer observed at 60 nor at 90 days. From a pathology standpoint, steatonecrosis was not considered to represent a safety concern as it fully healed and resorbed over time.

Surrounding muscles also showed evidences of prior thermal injury. At 30 days, it was evidenced by local necrotic areas with gradual fibrous healing confined to the superficial perivenous muscle exclusively. One can also note here that the presence of hyperechoic marks at focus resulting from boiling could have impeded the propagation of the HIFU beam beyond focus. At 60 days, evidences of prior thermal injury were also confined to superficial perivenous muscle and were characterized by demarcated areas of coagulation, myofiber regeneration and fibrous healing. Fibrous healing was complete and stable at 90 days and substantial muscle regeneration was observed.

Based on these results, thermal collateral damages to perivenous tissues were limited and completely healed over time. The treatment setup used in this study thus appears to be safe regarding perivascular tissues. No hemorrhage was observed following HIFU exposures, contrary to previous studies [19], [22], [27], [28], [74]. This supports the choice of the ultrasound parameters used in this study in terms of safety and efficiency for treating medium-sized veins.

Microscopic evaluation of treated veins and surrounding tissues helps understanding clinical findings. Vein occlusion assessed by ultrasound imaging could be explained by the histologic findings: the transformation of the treated vein segment into a hyperechoic cord visible on the ultrasound images could be attributed to fibrotic sealing of the veins. Fibrotic scars are indeed mainly composed of collagen, as determined by histologic examinations. The collagen content in fibrotic tissues is known to increase the acoustic impedance and increase echogenicity [144].

Macroscopic and microscopic features reported here inside and around the vein after HIFU treatment have also been observed following thermoablation procedures like RFA or EVLA. The primary changes after radiofrequency and laser treatments include vein shrinkage, vein induration, medial and adventitial lesions, vein thrombosis and perivenous tissue damages [116], [123], [140], [141], [145]–[152]. Tissue repair response has also been reported in RF or laser chronic studies and were characterized by gradual replacement of injured tissue components by granulation and fibrous connective tissue [139], [146], [153], [154]. HIFU-induced vascular and perivascular changes as well as subsequent healing changes are hence similar to that reported after endovenous thermotherapies. In particular, according to the analysis of our experienced pathologist in the evaluation of RF-affected veins, HIFU and RF

create lesions with identical features, to the extent that HIFU lesions were deemed indistinguishable from the lesions that can be induced by radiofrequency.

## 7.5 Conclusion

In this study, the HIFU ablation of veins was demonstrated to induce comparable tissue responses to those obtained after endovenous thermal treatments. In these experiments, no adverse effects or complications occurred and complete and stable healing of perivenous lesions caused by HIFU treatments was observed at 90 days. The safety of the ablation procedure regarding perivenous muscles and adipose tissue was therefore validated. The ability to achieve non-invasively fibrotic closure of veins was also demonstrated.

The HIFU treatment implemented in this study was therefore demonstrated to be both safe and effective. These results have been used to support a first-in-human clinical study for the treatment of pathologic leg veins.

# 8

# Conclusions and perspectives

The experimental work presented in this thesis was aimed at the identification of HIFU parameters capable of coagulating veins with an extracorporeal HIFU system. In order to foster clinical translation, a medical system developed by Theraclion (the Echopulse ®) was used for all the studies presented in this manuscript. The treatment of varicose veins with HIFU would be a new and completely non-invasive alternative to current clinical practice.

Initially, numerical simulations were used to identify an effective treatment approach. The objective was to induce continuous vascular thermal damage that covers the entire vein circumference. The simulation results provided the required number of sonications and the spacing (1.2 mm or 0.6 mm according to the pulse trajectory) between the HIFU pulses. These treatment parameters were first used to irreversibly coagulate small veins (2 mm in diameter) in a lagomorph model and were able to induce a persistent vascular occlusion in the sub-chronic setting. Thermal coagulation of the vessel wall was evidenced by histology. These animal experiments highlighted the importance of sonicating the vein without the presence of blood flow in order to damage the complete vein circumference. Based on this work, a patent application detailing the method necessary to effectively coagulate blood vessels with HIFU was filled.

The next step, in order to develop a clinically relevant sonication method, was to demonstrate the ability to coagulate larger vein diameters. For this purpose, a sheep model was chosen as it presents veins dimensions closer to human varicose veins, and a new set of HIFU parameters with longer sonication time (8 seconds) was selected.

Experimental temperature measurements during HIFU ablation were used as inputs to determine the spacing between these new HIFU pulses in order to obtain confluent regions of tissue coagulation. This thermal study additionally demonstrated that HIFU ablation induces a peak temperature similar to that generated by endo-venous radiofrequency ablation.

In order to assess the performance and refine our understanding of the treatment, macroscopic studies were performed and tissue damage post-HIFU ablation were evaluated by both gross pathology and ultrasound imaging. The relevance of the treatment parameters used for vein ablation was ascertained according to the amount of vein wall shrinkage achieved immediately after sonication.

In order to ensure a successful translation to clinics, the safety and performance of the HIFU protocol were then validated. For this purpose, preclinical trials were conducted on sheep with various lengths of follow-up: 30, 60 and 90 days. A physical examination of the animals' wellbeing as well as the histological analysis of the venous and peri-venous tissues demonstrated the safety of the ablation procedure, and confirmed the similarity with the effects induced by RF.

This thesis triggered Theraclion's decision to initiate a clinical trial and provided data to support regulatory submissions. A clinical trial was launched in Austria and led to the CE-marking of Theraclion's HIFU system for this new indication. The results are very encouraging, as can be seen with an interesting clinical case presented hereunder.

A 72-year-old woman presented with a non-healing venous ulcer (Figure 8-1 (a)) secondary to neovascularization and a refluxing sapheno-femoral stump post stripping of the great saphenous vein (GSV). HIFU treatments were delivered in the same way as in the preclinical trials presented in this manuscript (8-s pulses at 85 W acoustic).

(a) (b)

**Figure 8-1 – Appearance of the leg before (a) and 3 months after treatment (b).** (a) Active ulcer (white dotted circle) caused by sapheno-femoral reflux; (b) Same leg 3 months after treatments, healing of the ulcer.

Three months after the treatments, the recurrent flow was abolished and the ulcer was healed (Figure 8-1 (b)). Figure 8-2 shows the color Doppler appearance of the stump before and 3 months after sonication.

(a) (b)

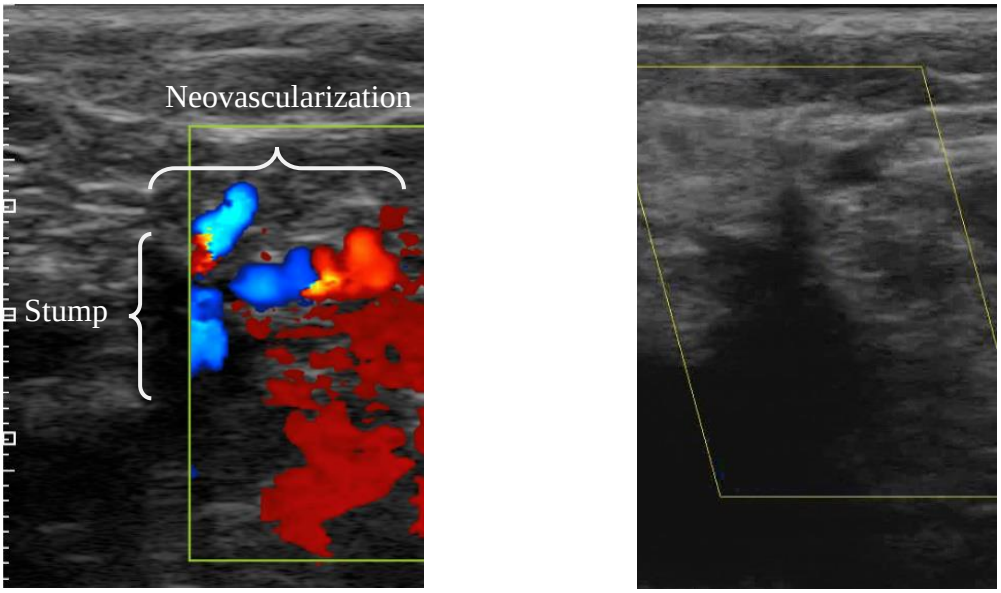


**Figure 8-2 – Color Doppler examinations (transverse views) of the stump and the neovascularization at the sapheno-femoral junction demonstrating reflux abolition.** (a) Pretreatment evaluation shows stump with reflux; (b) 3 months follow-up examination showing occlusion of the treated stump.

The outstanding challenge for HIFU treatments, which is essential in order to gain clinical acceptance, will be to shorten treatment times to enable them to be as fast as endovenous thermal ablation techniques. In this thesis, only the thermal effects of HIFU were investigated. However, based on the work of Hynynen *et al.* [19], a synergy between thermal ablation and cavitation could allow for reduced treatment time, whilst permitting selective coagulation and minimizing perivascular changes.

Lastly, one could imagine a project for the non-invasive treatment of all leg vein pathologies with ultrasound, allowing both the coagulation of incompetent superficial veins and the dissolution of thromboses in the deep veins.

# Appendix A.

# Spatial registration of the temperature curves

This appendix provides a description of the process used to register spatially the temperature curves acquired by the thermocouples.

For each subset of 5 temperature curves, a series of optimizations was performed as follows:

- 35 values of the coordinate of the center of the gaussian were tested with a spatial spacing of 0.2 mm:

$$Y_{center}^{k} = -3.4 + k \times 0.2 \text{ with } k = 0,1,2 \dots 34$$

- Then, for each $Y_{center}^{k}$, a gaussian curve centered on $Y_{center}^{k}$was fitted for each time step $t_i$ at the five data points. The fitting error for each time step, denoted $e_i^k$, was calculated. Finally, the fitting errors for all time steps, $J^k$, were then summed: $J^k = \sum_i e_i^k$.

The best $Y_{center}^{k}$, denoted $Y_{center}$ was selected as the value minimizing the temporal sum of fitting errors $J^k$.

The centers of the corresponding gaussian profiles were then spatially translated by $-Y_{center}$.

The spatial registration process is depicted on Figure 8-3.

Subset of five curves acquired by a given thermocouple for a given treatment

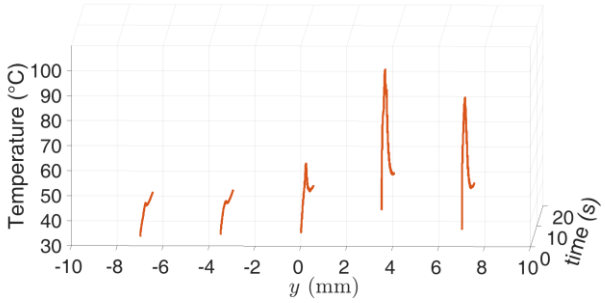


- Test 35 values of $Y_{center}^{k}$
- For each $Y_{center}^{k}$, perform a gaussian fit for every time with the gaussian function centered on $Y_{center}^{k}$
- For each $Y_{center}^{k}$ , quantify the goodness of fit

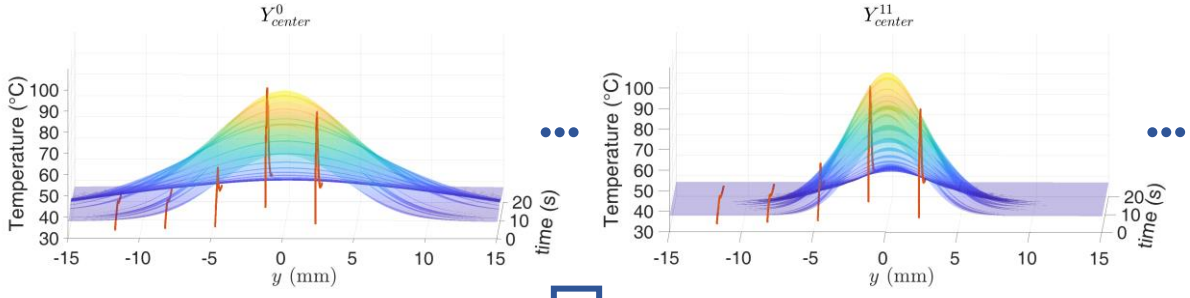


- Define $Y_{center}$ the $Y_{center}^{k}$ with the best fitting score (Here, $Y_{center}^{11}$)
- Translate the subset of five curves by -$Y_{center}$

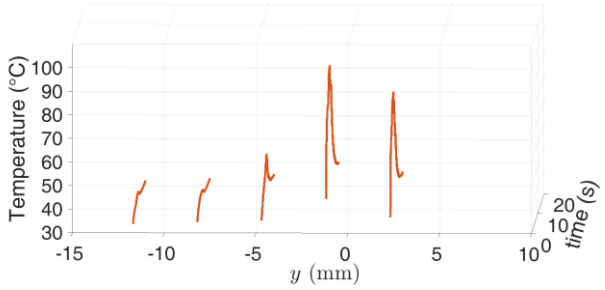


**Figure 8-3 – Illustration of the spatial registration process.**

# Appendix B.

# Algorithm for the implementation of the vein shrinkage

This appendix contains the algorithm[2] used for the implementation of the vein shrinkage in the chapter 6.

At a time $t$:

- Let $U(t) = \{u(\mathbf{x}) \in vein\}$ be the set of voxels ($u(\mathbf{x})$) of the vein wall and $R_k(t) = \{u(\mathbf{x}) \in ring\ k\}$ the set of voxels of the $k^{\text{th}}$ vein wall ring. Therefore, $U(t) = \cup_k R_k(t)$.
- Let $T_{inter}(\mathbf{x}, t)$ represent the updated temperature field computed based on $T(\mathbf{x}, t - \delta t)$ and the bioheat equation
- Based on the updated temperature field, the thermal damage within each voxel of the vein wall is updated and is denoted $\Omega_{inter}(u(\mathbf{x}) \in U(t - \delta t), t)$. the thermal damage. At this stage, the vein has not yet been shrunken and $\Omega_{inter}(u(\mathbf{x}), t)$ and $\Omega(u(\mathbf{x}), t)$ are defined on the same vein geometry. The vein wall constriction in each voxel during the current time step can be computed as:

$$\Lambda(u(\mathbf{x}) \in U(t - \delta t), t) = \frac{l(\Omega_{inter}(u(\mathbf{x}), t))}{l(\Omega(u(\mathbf{x}), t))}$$

- In each cross-section planed:
  - For each vein wall ring, the weighted curvilinear abscissa is updated and is calculated as a spatial cumulative sum along the cross-section:

$$s_{inter}\big(u(\mathbf{x}) \in U(t - \delta t)\big) = \underset{u(\mathbf{x}) \in R_k(t - \delta t)}{cumsum}\big(\Lambda(u(\mathbf{x}) \in U(t - \delta t), t)\big)$$

  - Based on the spatial mean of the contracted pixel length, the new vein circumference is computed as follow:

[2] This algorithm was developed by Anthony Grisey (Theraclion)

$$circumference(t) = \underset{u(\mathbf{x})\in U(t-\delta t)}{circumference}(t-\delta t) \times mean\left(\Lambda(u(\mathbf{x}),t)\right)$$

A new geometry of the vein wall $U(t)$ is then computed.

- On the updated geometry, the weighted curvilinear abscissa is computed for each vein wall ring considering all voxels of unitary length.
- $\Omega(u(\mathbf{x}) \in U(t))$ is finally computed by interpolation within each ring $R_k(t)$ of the updated vein wall $U(t)$ with:
  - $s_{inter}(u(\mathbf{x}) \in R_k(t-\delta t),t)/\max\limits_{u(\mathbf{x})\in R_k(t-\delta t)}(s_{inter}(t))$ the initial sample points
  - $\Omega_{inter}(u(\mathbf{x}) \in R_k(t-\delta t),t)$ the initial sample (thermal damage) values
  - $s_{init}(u(\mathbf{x}) \in R_k(t),t)/\max\limits_{u(x,y,z)\in R_k(t)}\left(s_{init}(u(\mathbf{x}),t)\right)$ the query points
  - $T(\mathbf{x} \in U(t),t)$ is similarly computed by interpolation within each ring $R_k(t)$ of the updated vein wall $U(t)$
  - $s_{inter}(u(\mathbf{x}) \in R_k(t-\delta t),t)/\max\limits_{u(\mathbf{x})\in R_k(t-\delta t)}(s_{inter}(t))$ the initial sample points
  - $\mathrm{T}_{inter}(u(\mathbf{x}) \in R_k(t-\delta t),t)$ the initial sample values
  - $s_{init}(u(\mathbf{x}) \in R_k(t),t)/\max\limits_{u(\mathbf{x})\in R_k(t)}(s_{init}(u(\mathbf{x}),t))$ the query points

# References


[1] C. Janbon, J. C. Laborde and I. Quere, “History of the treatment of varices,” *Journal des maladies vasculaires*, vol. 19, pp. 210–215, 1994.

[2] P. Gloviczki, *Handbook of venous disorders: Guidelines of the American venous forum third edition*. CRC Press, 2008.

[3] M. Perrin, “History of venous surgery,” *Phlebolymphology*, vol. 18, no. 3, pp. 123–129, 2011.

[4] M. P. Goldman and R. A. Weiss, *Sclerotherapy E-book: Treatment of Varicose and Telangiectatic Leg Veins*. Elsevier Health Sciences, 2016.

[5] K. Myers and P. Hannah, *Manual of Venous and Lymphatic Diseases*. CRC Press, 2017.

[6] J. J. Bergan and N. Bunke-Paquette, *The Vein Book*. Oxford University Press, 2014.

[7] T. M. Proebstle, J. Alm, O. Gckeritz, C. Wenzel, T. Noppeney, C. Lebard, O. Pichot, C. Sessa and D. Creton, “Three-year European follow-up of endovenous radiofrequency-powered segmental thermal ablation of the great saphenous vein with or without treatment of calf varicosities,” *Journal of Vascular Surgery*, vol. 54, no. 1, pp. 146–152, 2011.

[8] R. J. Min and N. M. Khilnani, “Endovenous Laser Treatment of Saphenous Vein Reflux,” *Techniques in Vascular and Interventional Radiology*, vol. 6, no. 3, pp. 125–131, 2003.

[9] R. Van den Bos, L. Arends, M. Kockaert, M. Neumann and T. Nijsten, “Endovenous therapies of lower extremity varicosities: A meta-analysis,” *Journal of Vascular Surgery*, vol. 49, no. 1, pp. 230–239, Jan. 2009.

[10] R. J. Min, S. E. Zimmet, M. N. Isaacs and M. D. Forrestal, “Endovenous Laser Treatment of the Incompetent Greater Saphenous Vein,” *Journal of Vascular and Interventional Radiology Interv Radiol*, vol. 12, pp. 1167–1171, 2001.

[11] F. Lurie, D. Creton, B. Eklof, L. S. Kabnick, R. . Kistner, O. Pichot, S. Schuller-Petrovic and C. Sessa, “Prospective randomized study of endovenous radiofrequency obliteration

(closure procedure) versus ligation and stripping in a selected patient population (EVOLVeS Study)," *Journal of Vascular Surgery*, vol. 38, no. 2, pp. 207–214, Aug. 2003.

[12] P. Quehe, Z. Alavi, T. Kurylo-Touz, A.-H. Saliou, A. Badra, L. Baudino, S. Gestin, R. Haudebourg, L. Bressollette, G. Gladu, F. Ledan, R. Haudebourg, S. Gestin and L. Bressollette, "Endovenous Celon radiofrequency-induced thermal therapy of great saphenous vein: A retrospective study with a 3-year follow-up," *SAGE Open Medicine*, vol. 6, pp. 1–8, 2018.

[13] E. Mowatt-Larssen, S. S. Desai, A. Dua and C. E. Shortell, *Phlebology, Vein Surgery and Ultrasonography: Diagnosis and Management of Venous Disease*. Springer, 2013.

[14] B. Braithwaite, L. Hnatek, U. Zierau, M. Camci, G. Akkersdijk, D. Nio, M. Sarlija, M. Ajduk, P. Santoro and E. Roche, "Radiofrequency-induced thermal therapy: results of a European multicentre study of resistive ablation of incompetent truncal varicose veins," *Phlebology*, vol. 1, pp. 38–46, 2013.

[15] J. Lohr and A. Kulwicki, "Radiofrequency Ablation: Evolution of a Treatment," *Seminars in vascular surgery*, vol. 23, pp. 90–100, 2010.

[16] G. Ter Haar and C. Coussios, "High intensity focused ultrasound: Physical principles and devices," *International Journal of Hyperthermia*, vol. 23, no. 2, pp. 89–104, 2007.

[17] C. R. Hill, J. C. Bamber and G. R. Ter Haar, *Physical principles of medical ultrasonics*. ASA, 2004.

[18] J. E. Kennedy, "High-intensity focused ultrasound in the treatment of solid tumours," *Nature Reviews Cancer*, vol. 5, no. 4, pp. 321–327, 2005.

[19] K. Hynynen, V. Colucci, A. Chung and F. Jolesz, "Noninvasive arterial occlusion using MRI-guided focused ultrasound," *Ultrasound in Medicine & Biology*, vol. 22, no. 8, pp. 1071–1077, 1996.

[20] S. Vaezy, M. L. Noble, A. Keshavarzi, M. Paun, A. F. Prokop, C. Cornejo, S. Sharar, E. Y. Chi, L. A. Crum and R. W. Martin, "Liver Hemostasis With High-Intensity Ultrasound," *Ultrasound in Medicine & Biology*, vol. 23, pp. 217–225, 2004.

[21] K. Ichizuka, S. Ando, M. Ichihara, T. Ishikawa, N. Uchiyama, K. Sasaki, S. Umemura, R. Matsuoka, A. Sekizawa, T. Okai, T. Akabane and M. Kushima, "Application of high-intensity focused ultrasound for umbilical artery occlusion in a rabbit model," *Ultrasound in obstetrics & gynecology*, vol. 30, no. 1, pp. 47–51, 2007.

[22] M. Ichihara, K. Sasaki, S. Umemura, M. Kushima and T. Okai, "Blood flow occlusion via ultrasound image-guided high-intensity focused ultrasound and its effect on tissue perfusion," *Ultrasound in Medicine & Biology*, vol. 33, pp. 452–459, 2007.

[23] T. Okai, K. Ichizuka, J. Hasegawa, R. Matsuoka, M. Nakamura, K. Shimodaira, A. Sekizawa, M. Kushima and S. Umemura, "First successful case of non-invasive in-utero treatment of twin reversed arterial perfusion sequence by high-intensity focused

ultrasound," *Ultrasound in Obstetrics and Gynecology*, vol. 42, no. 1, pp. 112–114, 2013.

[24] S. Vaezy, R. Martin, H. Yaziji, P. Kaczkowski, G. Keilman, S. Carter, M. Caps, E. Y. E. Y. Chi, M. Bailey and L. Crum, "Hemostasis of punctured blood vessels using high-intensity focused ultrasound," *Ultrasound in Medicine & Biology*, vol. 24, no. 6, pp. 903–910, Jul. 1998.

[25] R. W. Martin, S. Vaezy, P. Kaczkowski, G. Keilman, S. Carter, M. Caps, K. Beach, M. Plett and L. Crum, "Hemostasis of punctured vessels using Doppler-guided high-intensity ultrasound," *Ultrasound in Medicine and Biology*, vol. 25, no. 6, pp. 985–990, 1999.

[26] S. Vaezy, R. Martin, P. Kaczkowski, G. Keilman, B. Goldman, H. Yaziji, S. Carter, M. Caps and L. Crum, "Use of high-intensity focused ultrasound to control bleeding," *Journal of Vascular Surgery*, vol. 29, pp. 533–542, 1999.

[27] I. H. Rivens, I. J. Rowland, M. Denbow, N. M. Fisk, G. R. Ter Haar and M. O. Leach, "Vascular occlusion using focused ultrasound surgery for use in fetal medicine," *European Journal of Ultrasound*, vol. 9, pp. 89–97, 1999.

[28] M. L. Denbow, I. H. Rivens, I. J. Rowland, M. O. Leach, N. M. Fisk and G. R. ter Haar, "Preclinical development of noninvasive vascular occlusion with focused ultrasonic surgery for fetal therapy," *American journal of obstetrics and gynecology*, vol. 182, pp. 387–392, 2000.

[29] R. Fujiwara, K. Sasaki, T. Ishikawa, M. Suzuki, S. Umemura, M. Kushima and T. Okai, "Arterial blood flow occlusion by high intensity focused ultrasound and histologic evaluation of its effect on arteries and surrounding tissues," *Journal of Medical Ultrasonics*, vol. 29, pp. 85–90, 2002.

[30] J. H. Hwang, S. Vaezy, R. W. Martin, M.-Y. Y. Cho, M. L. Noble, L. A. Crum and M. B. Kimmey, "High-intensity focused US: a potential new treatment for GI bleeding," *Gastrointestinal endoscopy*, vol. 58, no. 1, pp. 111–115, 2003.

[31] T. Ishikawa, T. Okai, K. Sasaki, S. Umemura, R. Fujiwara, M. Kushima, M. Ichihara and K. Ichizuka, "Functional and histological changes in rat femoral arteries by HIFU exposure," *Ultrasound in Medicine and Biology*, vol. 29, no. 10, pp. 1471–1477, 2003.

[32] S. A. Goss, R. L. Johnston and F. Dunn, "Comprehensive compilation of empirical ultrasonic properties of mammalian tissues," *The Journal of the Acoustical Society of America*, vol. 64, no. 2, pp. 423–457, 1978.

[33] H. Schultz-Haakh, J. K. Li, W. Welkowitz and N. Rosenberg, "Ultrasonic treatment of varicose veins," *Angiology*, vol. 40, no. 2, pp. 129–137, 1989.

[34] C. Delon-Martin, C. Vogt, E. Chignier, C. Guers, J. Y. Chapelon and D. Cathignol, "Venous thrombosis generation by means of high-intensity focused ultrasound," *Ultrasound in Medicine & Biology*, vol. 21, no. 1, pp. 113–119, 1995.

[35] J. H. Hwang, Y. Zhou, C. Warren, A. A. Brayman and L. A. Crum, “Targeted venous occlusion using pulsed high-intensity focused ultrasound,” *IEEE transactions on biomedical engineering*, vol. 57, no. 1, pp. 37–40, 2010.

[36] Y. Zhou, J. Zia, C. Warren, F. L. Starr, A. A. Brayman, L. A. Crum and J. H. Hwang, “Targeted long-term venous occlusion using pulsed high-intensity focused ultrasound combined with a pro-inflammatory agent,” *Ultrasound in Medicine & Biology*, vol. 37, no. 10, pp. 1653–1658, 2011.

[37] D. E. Goertz, “An overview of the influence of therapeutic ultrasound exposures on the vasculature: High intensity ultrasound and microbubble-mediated bioeffects,” *International Journal of Hyperthermia*, vol. 31, no. 2, pp. 134–144, 2015.

[38] A. Napoli, M. Anzidei, B. C. Marincola, G. Brachetti, V. Noce, F. Boni, L. Bertaccini, R. Passariello and C. Catalano, “MR Imaging–guided Focused Ultrasound for Treatment of Bone Metastasis,” *RadioGraphics*, vol. 33, no. 6, pp. 1555–1568, 2013.

[39] J.-F. Aubry and M. Tanter, “MR-Guided Transcranial Focused Ultrasound,” in *Therapeutic Ultrasound*, Springer, Cham, 2016, pp. 97–111.

[40] G. ter Haar, “Therapeutic applications of ultrasound,” *Progress in Biophysics and Molecular Biology*, vol. 93, no. 1–3, pp. 111–129, 2007.

[41] P. E. Hube, M. J. Mann, L. G. Melo, A. Ehsan, D. Kong, L. Zhang, M. Rezvani, P. Peschke, F. Jolesz, V. J. Dzau and K. Hynynen, “Focused ultrasound (HIFU) induces localized enhancement of reporter gene expression in rabbit carotid artery,” *Gene Therapy*, vol. 10, no. 18, pp. 1600–1607, 2003.

[42] C. Wright, K. Hynynen and D. Goertz, “In vitro and in vivo high-intensity focused ultrasound thrombolysis,” *Investigative radiology*, vol. 47, no. 4, pp. 217–25, 2012.

[43] C. J. Shaw, G. R. Ter Haar, I. H. Rivens, D. A. Giussani and C. C. Lees, “Pathophysiological mechanisms of high- intensity focused ultrasound-mediated vascular occlusion and relevance to non-invasive fetal surgery,” *Journal of The Royal Society Interface*, vol. 11, no. 95, 2014.

[44] J.-F. Aubry, “High-intensity therapeutic ultrasound: Metrological requirements versus clinical usage,” *Metrologia*, vol. 49, no. 5, 2012.

[45] W. D. O’Brien Jr, “Ultrasound-biophysics mechanisms,” *Progress in biophysics and molecular biology*, vol. 93, pp. 212–255, 2007.

[46] S. D. Nandlall, “Monitoring cell and tissue damage during ablation by high-intensity focussed ultrasound,” 2011.

[47] J. N. Tjotta and S. Tjotta, “Nonlinear equations of acoustics, with application to parametric acoustic arrays,” *The Journal of the Acoustical Society of America*, vol. 69, no. 6, pp. 1644–1652, 1981.

[48] F. A. Duck, “Acoustic properties of tissue at ultrasonic frequencies,” in *Physical*

*properties of tissues: a comprehensive reference book*, Academic press, 1990, pp. 73–135.

[49] S. A. Sapareto and W. C. Dewey, "Thermal dose determination in cancer therapy," *International Journal of Radiation Oncology Biology Physics*, vol. 10, pp. 787–800, 1984.

[50] P. S. Yarmolenko, E. J. Moon, C. Landon, A. Manzoor, D. W. Hochman, B. L. Viglianti and M. W. Dewhirst, "Thresholds for thermal damage to normal tissues: An update," *International Journal of Hyperthermia*, vol. 27, no. 4, pp. 320–343, 2011.

[51] C. C. Coussios, C. H. Farny, G. ter Haar and R. A. Roy, "Role of acoustic cavitation in the delivery and monitoring of cancer treatment by high-intensity focused ultrasound (HIFU)," *International Journal of Hyperthermia*, vol. 23, no. 2, pp. 105–120, 2007.

[52] J. Gateau, N. Taccoen, M. Tanter and J.-F. Aubry, "Statistics of Acoustically Induced Bubble-Nucleation Events in inVitro Blood: A Feasibility Study," *Ultrasound in Medicine and Biology*, vol. 39, no. 10, pp. 1812–1825, 2013.

[53] J. Gateau, J.-F. Aubry, D. Chauvet, A.-L. Boch, M. Fink and M. Tanter, "In vivo bubble nucleation probability in sheep brain tissue," *Physics in Medicine and Biology*, vol. 56, no. 22, pp. 7001–7015, 2011.

[54] E. E. Konofagou and K. Hynynen, "Localized harmonic motion imaging: therory, simulations and experiments," *Ultrasound in Medicine & Biology*, vol. 29, pp. 1405–1413, 2003.

[55] F. L. Lizzi, R. Muratore, C. X. Deng, J. A. Ketterling, S. Kaisar Alam, S. Mikaelian and A. Kalisz, "Radiation-force technique to monitor lesions during ultrasonic therapy," *Ultrasound in Medicine and Biology*, vol. 29, pp. 1593–1605, 2003.

[56] P. M. Morse and K. U. Ingard, *Theoretical acoustics*. Princeton university press, 1986.

[57] M. F. Hamilton and D. T. Blackstock, *Nonlinear acoustics*. Academic press San Diego, 1998.

[58] F. A. Duck, *Physical properties of tissues: a comprehensive reference book*. Academic Press, 1990.

[59] M. J. Callam, "Epidemiology of varicose veins," *British Journal of Surgery*, vol. 81, pp. 167–173, 1994.

[60] A.-A. Ramelet, M. Perrin and H. Kern, P Bounameaux, *Phlebology*. Elsevier Masson, 2008.

[61] M. Vuylsteke, "Endovenous laser ablation," 2012.

[62] K. Burnand and A. Wadoodi, "The physiology and hemodynamics of chronic venous insufficiency of the lower limb," in *Handbook of venous disorders:Guidelines of the American venous forum third edition*, CRC Press, 2009, pp. 47–55.

[63] C. Allegra, P.-L. Antignani, J. J. Bergan, P. H. Carpentier, P. Coleridge-Smith, A. Cornu-Thénard, B. Eklof, H. Partsch, E. Rabe, J.-F. Uhl and M.-T. Widmer, "The 'C' of CEAP: suggested definitions and refinements: an international union of phlebology conference of experts," *Journal of vascular surgery*, vol. 37, pp. 129–131, 2003.

[64] R. Kolluri, "Interventional management of varicose veins," in *Practical peripheral vascular intervention*, Lippincott Williams & Wilkins, 2011.

[65] N. Labropoulos, M. A. Mansour, S. S. Kang, P. Gloviczki and W. H. Baker, "New insights into perforator vein incompetence," *European journal of vascular and endovascular surgery*, vol. 18, pp. 228–234, 1999.

[66] A. J. Tafur and S. Rathbun, "Chronic venous disorders," in *Vascular Medicine: A Companion to Braunwald's Heart Disease*, Elsevier Health Sciences, 2012, pp. 639–650.

[67] R. J. Beale and M. J. Gough, "Treatment options for primary varicose veins—a review," *European journal of vascular and endovascular surgery*, vol. 30, pp. 83–95, 2005.

[68] M. Alam, T. H. Nguyen and J. S. Dover, *Treatment of leg veins*. Elsevier Health Sciences, 2006.

[69] S. Vaidyanathan, R. R. Menon, P. Jacob and B. John, *Chronic Venous Disorders of the Lower Limbs: A surgical approach*. Elsevier Health Sciences, 2015.

[70] J. G. Chandler, O. Pichot, C. Sessa, S. Schuller-Petrovic, L. S. Kabnick and J. J. M. Bergan, "Treatment of Primary Venous Insufficiency by Endovenous Saphenous Vein Obliteration," *Vascular and Endovascular Surgery*, vol. 34, no. 3, pp. 685–685, 2000.

[71] L. S. Kabnick, "Varicose veins: endovenous treatment," in *Rutherford's vascular surgery*, 2010, pp. 871–888.

[72] M. Heger, R. F. Van Golen, M. Broekgaarden, R. R. Van Den Bos, H. A. M. Neumann, T. M. Van Gulik and M. J. C. Van Gemert, "Endovascular laser-tissue interactions and biological responses in relation to endovenous laser therapy," *Lasers in Medical Science*, vol. 29, no. 2, pp. 405–422, 2014.

[73] S. M. Roth, "Endovenous Radiofrequency Ablation of Superficial and Perforator Veins," *Surgical Clinics of North America*, vol. 87, pp. 1267–1284, 2007.

[74] K. Mahoney, H. Martin and K. Hynynen, "Focused ultrasound effects on blood vessels in vivo-limits for vascular interventions," *IEEE Ultrasonics Symposium Proceedings*, vol. 2, pp. 1405–1408, 2000.

[75] J. Serrone, H. Kocaeli, T. D. Mast, M. T. Burgess and M. Zuccarello, "The potential applications of high-intensity focused ultrasound (HIFU) in vascular neurosurgery," *Journal of Clinical Neuroscience*, vol. 19, pp. 214–221, 2012.

[76] W. Gorisch and K.-P. Boergen, "Heat-induced contraction of blood vessels," *Lasers in Surgery and Medicine*, vol. 2, no. 1, pp. 1–13, 1982.

[77] R. Agah, J. A. Pearce, A. J. Welch and M. Motamedi, “Rate process model for arterial tissue thermal damage: Implications on vessel photocoagulation,” *Lasers in Surgery and Medicine*, vol. 15, no. 2, pp. 176–184, 1994.

[78] K. Hynynen, “The threshold for thermally significant cavitation in dog’s thigh muscle in vivo,” *Ultrasound in Medicine & Biology*, vol. 17, no. 2, pp. 157–169, Jan. 1991.

[79] S. L. Poliachik, W. L. Chandler, P. D. Mourad, R. J. Ollos and L. A. Crum, “Activation, aggregation and adhesion of platelets exposed to high-intensity focused ultrasound,” *Ultrasound in medicine & biology*, vol. 27, pp. 1567–1576, 2001.

[80] S. L. Poliachik, W. L. Chandler, R. J. Ollos, M. R. Bailey and L. a. Crum, “The relation between cavitation and platelet aggregation during exposure to high-intensity focused ultrasound,” *Ultrasound in Medicine and Biology*, vol. 30, no. 2, pp. 261–269, 2004.

[81] K. Sakariassen, P. Holme, U. Orvim, R. Barstad, N. Solum and F. Brosstad, “Shear-induced platelet activation and platelet microparticle formation in native human blood,” *Thrombosis Research*, vol. 92, pp. 33–41, 1998.

[82] A. Grisey, “Modeling and optimisation of heat deposition for HIFU thermal ablations,” 2015.

[83] B. E. Treeby and B. T. Cox, “k-Wave: MATLAB toolbox for the simulation and reconstruction of photoacoustic wave fields,” *Journal of Biomedical Optics*, vol. 15, pp. 021314-1: 021314-12, 2010.

[84] B. E. Treeby, J. Jaros, A. P. Rendell and B. T. Cox, “Modeling nonlinear ultrasound propagation in heterogeneous media with power law absorption using a *k* -space pseudospectral method,” *The Journal of the Acoustical Society of America*, vol. 131, no. 6, pp. 4324–4336, 2012.

[85] B. Treeby, B. Cox and J. Jaros, “k-Wave: A MATLAB toolbox for the time domain simulation of acoustic wave fields,” *A MATLAB toolbox for the time domain simulation of acoustic wave field*, vol. 1, p. 75, 2012.

[86] K. Wang, E. Teoh, J. Jaros and B. E. Treeby, “Modelling nonlinear ultrasound propagation in absorbing media using the k-Wave toolbox: Experimental validation,” *IEEE International Ultrasonics Symposium, IUS*, pp. 523–526, 2012.

[87] A. Grisey, S. Yon, V. Letort and P. Lafitte, “Simulation of high-intensity focused ultrasound lesions in presence of boiling,” *Journal of Therapeutic Ultrasound*, vol. 4, pp. 1–14, 2016.

[88] C. Constans, P. Mateo, M. Tanter and J.-F. Aubry, “Potential impact of thermal effects during ultrasonic neurostimulation : retrospective numerical estimation of temperature elevation in seven rodent setups,” *Physics in Medicine & Biology*, vol. 63, pp. 1–12, 2018.

[89] G. Maimbourg, A. Houdouin, T. Deffieux, M. Tanter and J.-F. Aubry, “3D-printed

adaptive acoustic lens as a disruptive technology for transcranial ultrasound therapy using single-element transducers," *Physics in Medicine & Biology*, vol. 63, no. 2, p. 025026, Jan. 2018.

[90] B. E. Treeby and B. T. Cox, "Modeling power law absorption and dispersion for acoustic propagation using the fractional Laplacian," *The Journal of the Acoustical Society of America*, vol. 127, no. 5, pp. 2741–2748, 2010.

[91] H. H. Pennes, "Analysis of tissue and arterial blood temperatures in the resting human forearm.," *Journal of applied physiology*, vol. 1, pp. 93–122, 1948.

[92] N. Barnat, A. Grisey, B. Lecuelle, J. Anquez, B. Gerold, S. Yon and J.-F. Aubry, "Noninvasive vascular occlusion with HIFU for venous insufficiency treatment: Preclinical feasibility experience in rabbits," *Physics in Medicine and Biology*, vol. 64, no. 2, p. 12, 2019.

[93] M. Hahn, R. Fugunt, B. Schoenfisch, E. Oberlechner, I. V. Gruber, U. Hoopmann, C. Roehm, G. Helms, F. A. Taran, A. D. Hartkopf, H. Warzecha, B. Wiesinger, S. Y. Brucker and B. Boeer, "High intensity focused ultrasound (HIFU) for the treatment of symptomatic breast fibroadenoma," *International Journal of Hyperthermia*, vol. 35, no. 1, pp. 463–470, 2018.

[94] R. D. Kovatcheva, J. D. Vlahov, J. I. Stoinov and K. Zaletel, "Benign solid thyroid nodules: US-guided high-intensity focused ultrasound ablation—initial clinical outcomes," *Radiology*, vol. 276, pp. 597–605, 2015.

[95] A. Grisey, M. Heidmann, V. Letort, P. Lafitte and S. Yon, "Influence of skin and subcutaneous tissue on High-intensity focused ultrasound beam: Experimental quantification and numerical modeling," *Ultrasound in Medicine and Biology*, vol. 42, pp. 2457–2465, 2016.

[96] S. H. Weisbroth, R. E. Flatt and A. L. Kraus, *The biology of the laboratory rabbit*. Academic Press, 2013.

[97] K. Pankhurst, "Incipient Shrinkage of Collagen and Gelatin," *Nature*, vol. 159, p. 538, 1947.

[98] L. N. Dorr and K. Hynynen, "The effects of tissue heterogeneities and large blood vessels on the thermal exposure induced by short high-power ultrasound pulses," *International Journal of Hyperthermia*, vol. 8, no. 1, pp. 45–59, 1992.

[99] L. Chent, G. ter Haar, C. R. Hill, M. Dworkint, P. Carnochant, H. Young and J. P. M. Benstedt, "Effect of blood perfusion on the ablation of liver parenchyma with high-intensity focused ultrasound," *Physics in Medicine & Biology*, vol. 38, pp. 1661–1673, 1993.

[100] J. Heisterkamp, R. van Hillegersberg, P. G. H. Mulder, E. L. Sinofsky and J. N. M. Ijzermans, "Importance of eliminating portal flow to produce large intrahepatic lesions with interstitial laser coagulation," *British Journal of Surgery*, pp. 1245–1248, 1997.

[101] E. J. Patterson, C. H. Scudamore, E. Eng, D. A. Owen, A. G. Nagy and A. K. Buczkowski, “Radiofrequency ablation of porcine liver in vivo: effects of blood flow and treatment time on lesion size,” *Annals of surgery*, vol. 227, pp. 559–565, 1998.

[102] S. N. Goldberg, M. C. Stein, G. S. Gazelle, R. G. Sheiman, J. B. Kruskal and M. E. Clouse, “Percutaneous radiofrequency tissue ablation: optimization of pulsed-radiofrequency technique to increase coagulation necrosis,” *Journal of vascular and interventional radiology*, pp. 907–916, 1999.

[103] R. Loffroy, B. Guiu, J.-P. Cercueil and D. Krause, “Endovascular therapeutic embolisation: an overview of occluding agents and their effects on embolised tissues,” *Current Vascular Pharmacology*, vol. 7, pp. 250–263, 2009.

[104] K. Hynynen, A. H. Chung, V. Colucci and F. A. Jolesz, “Potential adverse effects of high-intensity focused ultrasound exposure on blood vessels in vivo,” *Ultrasound in Medicine and Biology*, vol. 22, pp. 193–201, 1996.

[105] R. A. Weiss and M. P. Goldman, “Controlled Radiofrequency - Mediated endovenous shrinkage and occlusion,” in *Varicose Veins and Telangiectasias: Diagnosis and Treatment (second editon)*, Thieme medical publishers, 2000, pp. 217–224.

[106] R. A. Weiss and M. A. Weiss, “Controlled radiofrequency endovenous occlusion using a unique radiofrequency catheter under duplex guidance to eliminate saphenous varicose vein reflux: A 2-year follow-up,” *Dermatologic Surgery*, vol. 28, no. 1, pp. 38–42, 2002.

[107] J. E. Newman, L. Meecham, R. J. Walker and I. K. Nyamekye, “Optimising treatment parameters for radiofrequency induced thermal therapy (RFiTT): A comparison of the manufacturer’s treatment guidance with a locally developed treatment protocol,” *European Journal of Vascular and Endovascular Surgery*, vol. 47, pp. 664–669, 2014.

[108] G. Plaut, “Extracellular and supporting structures (Vol 26C),” in *Comprehensive biochemistry*, M. Florkin and E. H. Stotz, Eds. Amsterdam: Elesevier, 1971.

[109] K. Hynynen and D. K. Edwards, “Temperature measurements during ultrasound hyperthermia,” *Medical Physics*, vol. 16, no. 4, pp. 618–626, Jul. 1989.

[110] H. Morris, I. Rivens, A. Shaw and G. Ter Haar, “Investigation of the viscous heating artefact arising from the use of thermocouples in a focused ultrasound field,” *Physics in Medicine and Biology*, vol. 53, no. 17, pp. 4759–4776, 2008.

[111] H. A. S. Kamimura, C. Aurup, E. Bendau, N. Saharkhiz, M. G. Kim and E. E. Konofagou, “Iterative curve fitting of the bioheat transfer equation for thermocouple-based temperature estimation in vitro and in vivo,” *IEEE Transactions on Ultrasonics, Ferroelectrics, and Frequency Control*, vol. 3010, no. c, pp. 1–1, 2019.

[112] T. Tiennot, H. A. S. Kamimura, S. A. Lee, C. Aurup and E. E. Konofagou, “Numerical modeling of ultrasound heating for the correction of viscous heating artifacts in soft tissue temperature measurements,” *Applied Physics Letters*, vol. 114, no. 20, 2019.

[113] V. L. Martinot, S. R. Mordon, V. A. Mitchell, P. N. Pellerin and J. M. Brunetaud, “Determination of Efficient Parameters for Argon Laser-Assisted Anastomoses in Rats: Macroscopic, Thermal, and Histological Evaluation,” *Lasers in Surgery and Medicine*, vol. 15, pp. 168–175, 1994.

[114] W. Gorisch and K.-P. Boergen, “Laser related heat effects on blood vessels,” in *Lasers in Biology and Medicine*, Boston: Springer Science & Business Media, 1980, pp. 99–109.

[115] G. A. Gorisch W., Boergen KP., “Thermal collagen shrinkage promotes laser-induced vessel occlusion,” in *Laser optoelectronics in medicine: proceedings of the 7th congress International society for laser surgery and medicine in connection with laser 87 optoelectronics*, Springer Science & Business Media, 1982.

[116] S. Manfrini, V. Gasbarro, G. Danielsson, L. Norgren, J. G. Chandler, A. F. Lennox, Z. a. Zarka and A. N. Nicolaides, “Endovenous management of saphenous vein reflux,” *Journal of Vascular Surgery*, vol. 32, pp. 330–342, 2000.

[117] A. W. Zikorus, M. S. Mirizzi and S. Jose, “Evaluation of setpoint temperature and pullback speed on vein adventitial temperature during endovenous radiofrequency energy delivery in an in-vitro model,” *Vascular and Endovascular Surgery*, vol. 38, no. 2, 2004.

[118] S. Kaspar, J. Siller, Z. Cervinkova and T. Danek, “Standardisation of parameters during endovenous laser therapy of truncal varicose veins - Experimental ex-vivo study,” *European Journal of Vascular and Endovascular Surgery*, vol. 34, no. 2, pp. 224–228, Aug. 2007.

[119] T. M. Proebstle, B. Vago, J. Alm, O. Göckeritz, C. Lebard and O. Pichot, “Treatment of the incompetent great saphenous vein by endovenous radiofrequency powered segmental thermal ablation: First clinical experience,” *Journal of Vascular Surgery*, vol. 47, pp. 151–6, 2008.

[120] T. J. Beck, C. Burgmeier, R. Blagova, B. Steckmeier, V. Hecht, C. G. Schmedt and R. Sroka, “Thermal-induced effects on vein tissue - A basic ex-vivo investigation for EVLT,” *Medical Laser Application*, vol. 22, no. 4, pp. 238–241, 2008.

[121] R. Sroka, K. Weick, M. Sadeghi-Azandaryani, B. Steckmeier and C. G. Schmedt, “Endovenous laser therapy - application studies and latest investigations,” *Journal of Biophotonics*, vol. 3, no. 5–6, pp. 269–276, 2010.

[122] B. Disselhoff, A. I. Rem, R. Verdaasdonk, D. der Kinderen and F. L. Moll, “Endovenous laser ablation: An experimental study on the mechanism of action,” *Phlebology*, vol. 23, pp. 69–76, 2008.

[123] R. A. Weiss, “Comparison of endovenous radiofrequency versus 810 nm diode laser occlusion of large veins in an animal model,” *Dermatologic Surgery*, vol. 28, no. 1, pp. 56–61, 2002.

[124] C. Garcia, J. O. P. Manrique, V. A. Sanchez and E. Sala-Planell, “Endovenous

radiofrequency ablation (Venefit procedure): Impact of different energy rates on great saphenous vein shrinkage," *Annals of Vascular Surgery*, vol. 27, pp. 314–21, 2013.

[125] T. M. Proebstle, "Endovenous laser (EVL) for saphenous vein ablation," in *The Vein Book*, Academic Press, 2007, pp. 267–273.

[126] C.-G. Schmedt, O. A. Meissner, K. Hunger, G. Babaryka, V. Ruppert, M. Sadeghi-Azandaryani, B. M. Steckmeier and R. Sroka, "Evaluation of endovenous radiofrequency ablation and laser therapy with endoluminal optical coherence tomography in an ex vivo model," *Journal of Vascular Surgery*, vol. 45, pp. 1047–1058, 2007.

[127] R. Yang, S. Griffith and F. Rescorla, "Feasibility of using high intensity focused ultrasound for the treatment of unresectable retroperitoneal malignancies," *Journal of ultrasound in medicine*, 1992.

[128] M. Goldman, J. Bergan and J.-J. Guex, "Intravascular Approaches to the Treatment of Varicose Veins: Radiofrequency and Lasers," in *Sclerotherapy: Treatment of Varicose and Telangiectatic Leg Veins*, 4th ed., Elesevier, 2007, pp. 301–314.

[129] R. J. Min, N. Khilnani and S. E. Zimmet, "Endovenous laser treatment of saphenous vein reflux: long-term results.," *Journal of vascular and interventional radiology*, vol. 14, no. 8, pp. 991–996, 2003.

[130] S. Pichardo, R. Milleret, L. Curiel, O. Pichot and J.-Y. Chapelon, "In vitro experimental study on the treatment of superficial venous insufficiency with high-intensity focused ultrasound," *Ultrasound in Medicine & Biology*, vol. 32, pp. 883–891, 2006.

[131] L. Petrusca, R. Salomir, R. Milleret, O. Pichot, M. Rata, F. Cotton and J.-Y. Y. Chapelon, "Experimental investigation of thermal effects in HIFU-based external valvuloplasty with a non-spherical transducer, using high-resolution MR thermometry," *Physics in Medicine & Biology*, vol. 54, no. 17, pp. 5123–5138, 2009.

[132] O. Rouviere, D. Lyonnet, A. Raudrant, C. Colin-Pangaud, J. Y. Chapelon, R. Bouvier, J. M. Dubernard and A. Gelet, "MRI Appearance of prostate following transrectal HIFU ablation of localized cancer," *European Urology*, vol. 40, pp. 265–274, 2003.

[133] F. Xu, T. J. Lu, K. A. Seffen and E. Y. K. Ng, "Mathematical modeling of skin bioheat transfer," *Applied Mechanics Reviews*, vol. 62, no. 5, p. 050801, 2009.

[134] S. Wang, V. Frenkel and V. Zderic, "Preliminary optimization of non-destructive high intensity focused ultrasound exposures for hyperthermia applications," *Proceedings of the 31st Annual International Conference of the IEEE Engineering in Medicine and Biology Society*, pp. 3055–3059, 2009.

[135] M. Kim, J.-Y. Kim, S.-C. Noh and H.-H. Choi, "Thermal characteristics of non-biological vessel phantoms for treatment of varicose veins using high-intensity focused ultrasound," *PLoS ONE*, vol. 12, no. 4, pp. 1–17, 2017.

[136] G. F. Pinton, *Numerical methods for nonlinear wave propagation in ultrasound*. Duke University, 2007.

[137] J. P. Travers, C. E. Brookes, J. Evans, D. M. Baker, C. Kent, G. S. Makin and T. M. Mayhew, "Assessment of wall structure and composition of varicose veins with reference to collagen, elastin and smooth muscle content," *European journal of vascular and endovascular surgery*, vol. 11, pp. 230–237, 1996.

[138] P. R. Hoskins, "Physical properties of tissues relevant to arterial ultrasound imaging and blood velocity measurement," *Ultrasound in Medicine and Biology*, vol. 33, no. 10, pp. 1527–1539, 2007.

[139] R. Weiss, C. Feied and M. Weiss, "RF-mediated endovenous occlusion," in *Vein diagnosis and treatment*, McGraw-Hill Medical Publishing Division, 2001, pp. 211–221.

[140] M. Vuylsteke, J. Van Dorpe, J. Roelens, T. De Bo, S. Mordon and I. Fourneau, "Intraluminal fibre-tip centring can improve endovenous laser ablation: A histological study," *European Journal of Vascular and Endovascular Surgery*, vol. 40, no. 1, pp. 110–116, 2010.

[141] M. Vuylsteke, J. Van Dorpe, J. Roelens, T. De Bo and S. Mordon, "Endovenous laser treatment: A morphological study in an animal model," *Phlebology*, vol. 24, no. 4, pp. 166–175, 2009.

[142] R. G. Bush, H. N. Shamma and K. Hammond, "Histological changes occurring after endoluminal ablation with two diode lasers (940 and 1319 nm) from acute changes to 4 months," *Lasers in Surgery and Medicine*, vol. 40, no. 10, pp. 676–679, 2008.

[143] B. M. Delavary, W. M. van der Veer, M. van Egmond, F. B. Niessen and R. H. J. Beelen, "Macrophages in skin injury and repair," *Immunobiology*, vol. 216, no. 7, pp. 753–762, 2011.

[144] S. Fields and F. Dunn, "Correlation of echographic visualizability of tissue with biological composition and physiological state," *The Journal of the Acoustical Society of America*, vol. 54, no. 3, pp. 809–812, Sep. 1973.

[145] H. Bedi, N. Calton, K. Kwatra and V. Tewarson, "Histopathological findings of the human great saphenous vein treated with endoluminal radio frequency ablation," *International Surgery Journal*, vol. 1, no. 1, pp. 3–5, 2014.

[146] K. Brachmann and U. Gütz, "Histologische veränderungen nach endoluminaler varizenbehandlung durch die zirkuläre thermoablation (ClosureFast™)," *Phlebologie*, vol. 41, no. 2, pp. 73–76, 2012.

[147] C.-G. Schmedt, R. Sroka, S. Steckmeier, O. a. Meissner, G. Babaryka, K. Hunger, V. Ruppert, M. Sadeghi-Azandaryani and B. M. Steckmeier, "Investigation on radiofrequency and laser (980 nm) effects after endoluminal treatment of saphenous vein insufficiency in an ex-vivo model," *European Journal of Vascular and Endovascular Surgery*, vol. 32, no. 3, pp. 318–325, 2006.

[148] S. Thomis, P. Verbrugghe, R. Milleret, E. Verbeken, I. Fourneau and P. Herijgers, “Steam ablation versus radiofrequency and laser ablation: An in vivo histological comparative trial,” *European Journal of Vascular and Endovascular Surgery*, vol. 46, no. 3, pp. 378–382, 2013.

[149] R. Blagova, C. Burgmeier, S. Steckmeier, B. Steckmeier, G. Barbaryka, T. J. Beck, V. Hecht, C. G. Schmedt and R. Sroka, “Ex-vivo investigations on endoluminal laser therapy of varicosis - An optimization process,” *Medical Laser Application*, vol. 22, no. 4, pp. 242–247, 2008.

[150] O. A. Meissner, C. G. Schmedt, K. Hunger, H. Hetterich, R. Sroka, J. Rieber, G. Babaryka, B. M. Steckmeier, M. Reiser, U. Siebert and U. Mueller-Lisse, “Endovascular optical coherence tomography ex vivo: Venous wall anatomy and tissue alterations after endovenous therapy,” *European Radiology*, vol. 17, no. 9, pp. 2384–2393, 2007.

[151] L. Jelev, K. Guirov, M. Minkov and W. Ovtscharoff, “Morphological changes in the wall of great saphenous vein after radiofrequency ablation,” *Scripta Scientifica Medica*, vol. 45, pp. 60–62, 2013.

[152] E. V. Shaidakov, A. G. Grigoryan, D. E. Korzhevskii, E. A. Ilyukhin, D. A. Rosukhovski, V. L. Bulatov and O. I. Tsarev, “Morphologic changes in the vein after different numbers of radiofrequency ablation cycles,” *Journal of Vascular Surgery: Venous and Lymphatic Disorders*, vol. 3, no. 4, pp. 358–363, 2015.

[153] M. E. Vuylsteke and S. R. Mordon, “Endovenous laser ablation: A review of mechanisms of action,” *Annals of Vascular Surgery*, vol. 26, no. 3, pp. 424–433, 2012.

[154] X. Wang, X. Wang, W. Su and Y. Yuan, “Microwave ablation versus laser ablation in occluding lateral veins in goats,” *Journal of Huazhong University of Science and Technology*, vol. 36, no. 1, pp. 106–110, 2016.

[155] R. Kovatcheva, J.-N. Guglielmina, M. Abehsera, L. Boulanger, N. Laurent and E. Poncelet, “Ultrasound-guided high-intensity focused ultrasound treatment of breast fibroadenoma-a multicenter experience,” *Journal of Therapeutic Ultrasound*, vol. 3, p. 1, 2015.

[156] A. Chapman and G. ter Haar, “Thermal ablation of uterine fibroids using MR-guided focused ultrasound-a truly non-invasive treatment modality,” *European Radiology*, vol. 17, no. 10, pp. 2505–2511, 2007.

[157] S. Crouzet, J. Y. Chapelon, O. Rouvière, F. Mege-Lechevallier, M. Colombel, H. Tonoli-Catez, X. Martin and A. Gelet, “Whole-gland Ablation of Localized Prostate Cancer with High-intensity Focused Ultrasound: Oncologic Outcomes and Morbidity in 1002 Patients,” *European Urology*, vol. 65, no. 5, pp. 907–914, May 2014.

[158] M. Greiner, *Thérapeutiques endovasculaires des pathologies veineuses*. Springer Science & Business Media, 2012.

[159] T. M. Proebstle, B. Vago, J. Alm, O. Göckeritz, C. Lebard and O. Pichot, “Treatment of

the incompetent great saphenous vein by endovenous radiofrequency powered segmental thermal ablation: First clinical experience," *Journal of Vascular Surgery*, vol. 47, no. 1, pp. 151–157, 2008.

# Résumé de thèse

## Introduction générale

Les varices des membres inférieurs sont une des affections veineuses les plus fréquentes dans les pays occidentaux, touchant 25 % de la population adulte [59]. Les varices sont définies comme des veines superficielles anormalement dilatées et tortueuses, de diamètre égal ou supérieur à 3 mm en orthostatisme [63]. Elles sont le siège d'un reflux sanguin et entraînent une circulation veineuse pathologique. Les varices peuvent toucher les veines saphènes (grande et petite veine saphène), leurs collatérales ou n'importe quelle veine superficielle (Figure 8-4).

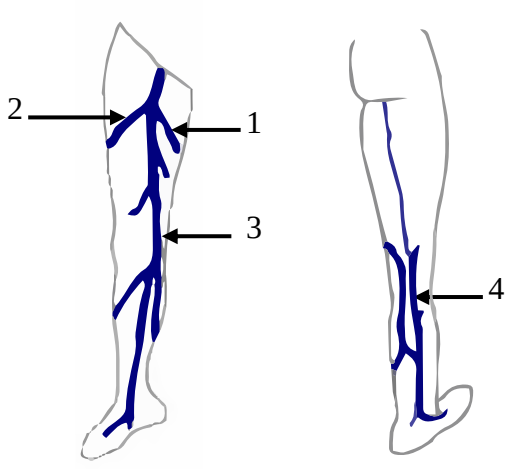


**Figure 8-4 – Principales veines superficielles des membres inférieurs.** 1. Veine saphène accessoire postérieure de cuisse ; 2. Veine saphène accessoire antérieure ; 3. Grande veine saphène (GVS) ; 4. Petite veine saphène (PVS)

Les varices des membres inférieurs peuvent être primaires (idiopathiques) ou secondaires, acquises à la suite d'un syndrome post-thrombotique par exemple. En dehors de

leur aspect inesthétique, les varices peuvent être symptomatiques et, en l'absence de traitement, s'accompagner de complications graves comme la survenue d'une thrombose veineuse profonde ou la formation d'un ulcère. Plusieurs options thérapeutiques existent pour améliorer la qualité de vie des sujets présentant des varices et prévenir la survenue de complications.

Parmi les principales modalités de traitements interventionnelles des varices figurent la chirurgie traditionnelle et l'ablation, qui peut être soit chimique (sclérothérapie), soit thermique (par radiofréquence, ou par laser). Ces techniques de traitement visent toutes à supprimer les veines pathologiques ou incompétentes de la circulation sanguine. L'intervention chirurgicale classiquement réalisée repose sur la technique de *stripping* également appelée éveinage. Elle consiste à retirer la veine pathologique à l'aide d'un *stripper*, guide flexible inséré préalablement dans la veine. Les traitements endovasculaires, moins traumatisants que la chirurgie, visent à oblitérer la veine incompétente en y injectant un agent sclérosant qui entraînera une thrombose (sclérothérapie) ou en introduisant dans la lumière veineuse un dispositif (cathéter ou fibre) délivrant une énergie thermique qui entraînera sa destruction. Ces méthodes thermiques reposent sur l'échauffement local de la paroi vasculaire afin d'entraîner une rétraction de la veine et plus tard à sa transformation en cordon fibreux.

Des études ont montré que ces méthodes thermiques sont aussi efficaces et sûres qu'une chirurgie traditionnelle [7]–[11]. Toutefois, ces méthodes thermiques ne sont pas applicables à toutes les veines pathologiques. De plus, l'insertion du cathéter ou de la fibre dans la veine peut être longue, complexe et engendrer des perforations de la paroi veineuse [12].

Tout comme ces méthodes thermiques, les ultrasons focalisés de haute intensité, connus sous l'acronyme HIFU issu de l'anglais *High-Intensity Focused Ultrasound*, permettent de réaliser des ablations thermiques. En focalisant une onde acoustique sur une cible tissulaire, l'absorption du faisceau ultrasonore à cet endroit crée une augmentation rapide de la température conduisant à la destruction des cellules dans la cible. Les ultrasons focalisés de haute intensité sont aujourd'hui utilisés en routine pour de nombreuses applications cliniques comme le traitement des adénofibromes du sein [155], des fibromes utérins [156] ou du cancer de la prostate [157].

L'utilisation des HIFU a également été explorée pour de nombreuses autres pathologies comme pour le traitement des varices [33]–[36], [130]. En effet, l'absorption élevée des ultrasons par les parois veineuses [32] ainsi que l'environnement anatomique de la plupart des

varices des membres inférieurs (absence d'os et d'air sur le chemin des ultrasons) rendent les HIFU adaptés pour le traitement des varices. De plus, les traitements par ultrasons focalisés de haute intensité peuvent être extracorporels, ce qui permettrait d'offrir une alternative non-invasive pour l'ablation thermique des varices et de s'affranchir ainsi de toute ponction transcutanée et risque de perforation.

La possibilité d'occlure des vaisseaux sains in vivo par traitements HIFU a été investiguée dans plusieurs travaux précliniques [19], [21], [22], [27]–[29], [31], [34]–[36], [74]. Dans ces études, différentes méthodes de traitement et paramètres d'exposition ont été évalués. Tous ont permis d'occlure des petits vaisseaux (0.5-1.5 mm de diamètre). Toutefois, aucune étude n'a démontré la possibilité d'induire, par HIFU uniquement, sans injection de produits de contraste, pro-inflammatoire ou sclérosant, un scellement fibreux du vaisseau de manière non-invasive, efficace et sûre.

Le but de cette thèse était de développer une méthode d'ablation thermique non-invasive pour le traitement des varices avec le dispositif HIFU commercialisé par Theraclion.

La possibilité d'occlure des vaisseaux de petits diamètres (2 mm) avec des tirs HIFU de 4 secondes a d'abord été évaluée et démontrée expérimentalement sur des veines de lapin. Afin de proposer une méthode de traitement pertinente pour l'ablation des varices (de plus large diamètre), une nouvelle procédure d'ablation thermique basée sur l'utilisation de tirs plus longs (8 secondes) a été conçue. L'espacement entre les tirs ultrasonores permettant d'induire une coagulation continue de la paroi vasculaire le long de la veine a été déterminé numériquement sur la base de mesures intravasculaires de température lors de traitements HIFU sur veines de brebis.

Afin d'évaluer l'efficacité de la procédure et de mieux comprendre les effets des traitements HIFU, la réaction des tissus après traitement a été étudiée par imagerie ultrasonore et par examen pathologique macroscopique. L'efficacité immédiate du traitement HIFU a été établie sur la base du pourcentage de réduction du calibre veineux obtenu après les tirs ultrasonores, sortants d'expériences *in vivo* sur des veines de brebis. Enfin, dans le but d'obtenir une autorisation d'essai clinique, des expérimentations *in vivo* sur brebis avec suivi distant jusqu'à 90 jours ont été conduites afin de valider l'efficacité et la sécurité du traitement à long terme.

# Identification et validation des paramètres de traitement pour occlure des veines de 2 mm de diamètre

L'objet de cette étude a consisté à évaluer la possibilité de boucher des veines de 2 mm de diamètre de façon définitive et reproductible avec le dispositif HIFU de Theraclion (Echopulse® présenté dans le chapitre 3).

Des simulations numériques ont d'abord été réalisées afin d'ajuster le nombre de pulses à délivrer et le pas de tir pour coaguler uniformément des segments de veine de 2 mm de diamètre et 2 cm de long. Des expériences *in vivo* sur veines de lapins avec suivi distant ont ensuite été conduites pour évaluer l'occlusion des vaisseaux dans les semaines suivant le traitement.

## Simulations numériques

Les simulations ont été effectuées pour deux types de tirs HIFU : (1) des tirs stationnaires et (2) des tirs en mouvement au cours desquels le point focal suit une trajectoire rectiligne à un vitesse de 0.75 $mm.s^{-1}$. Quelle que soit la trajectoire étudiée, des tirs continus de 4 secondes à une puissance acoustique de 85 W et à 3 MHz ont été considérés.

La propagation acoustique dans les tissus, l'élévation de température induite, ainsi que les dommages thermiques à la paroi vasculaire ont été successivement simulés. Les simulations acoustiques ont été effectuées à l'aide de k-Wave, un code basé sur une méthode de résolution pseudo-spectrale [85]. La Figure 8-5 montre les champs de pics de pression positive et négative simulés dans les tissus avec k-Wave.

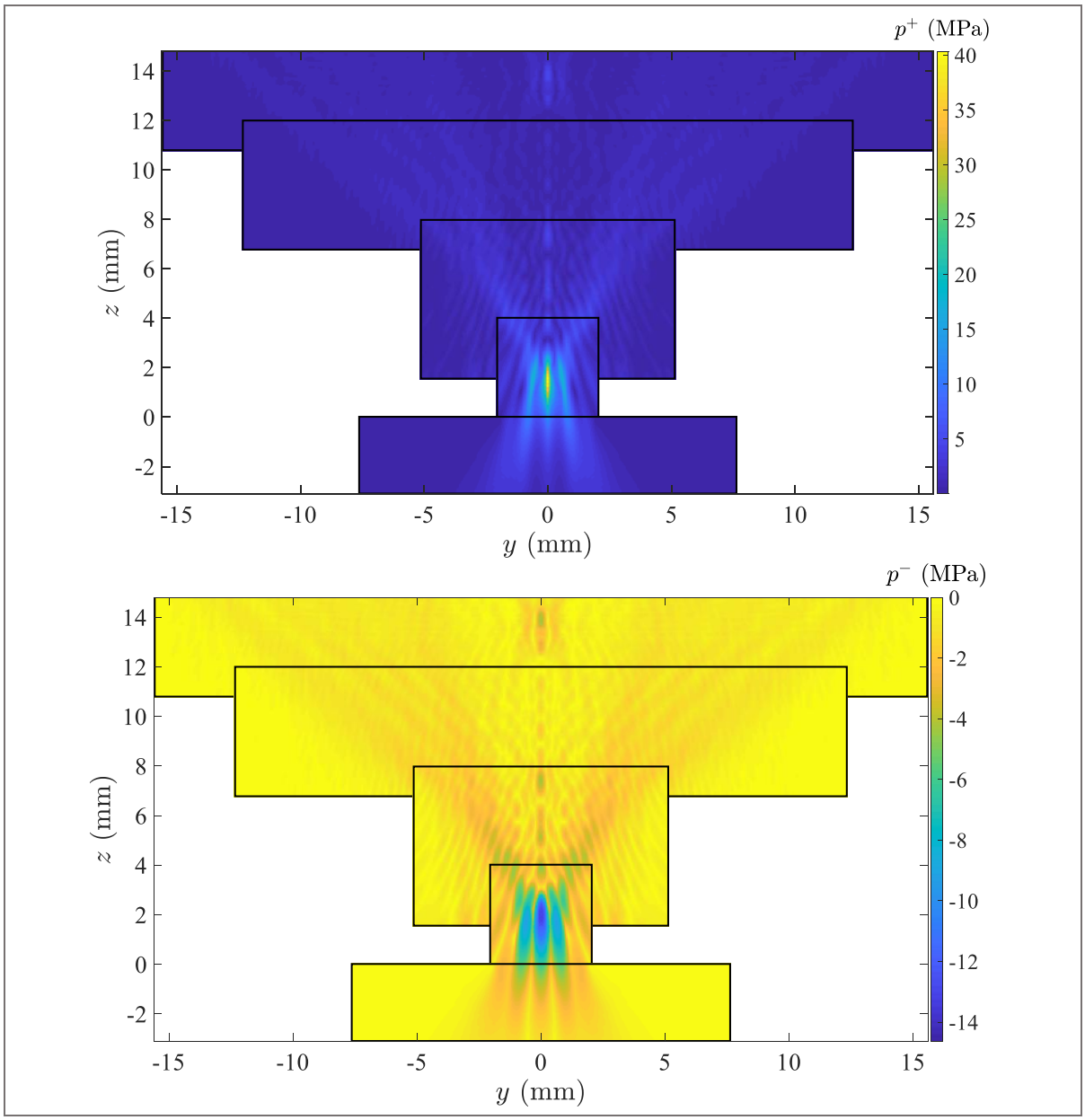


**Figure 8-5 − Champs de pics de pression positifs et négatifs issus des simulations à 3 MHz**. La pression est exprimée en MPa.

Une fois le champ de pression obtenu, l'élévation de température dans les tissus a été calculée à partir de l'équation de chaleur de Pennes [91]:

$$\rho C \frac{\partial T(\mathbf{x},t)}{\partial t} = k\nabla^2 T(\mathbf{x},t) + Q(\mathbf{x},t) + \omega_b \rho_b C_b (T_b - T(\mathbf{x},t))$$

où $\rho, C, T$ et $k$ désignent respectivement la masse volumique, la capacité thermique massique, la température du tissu et la conductivité thermique du tissu, $\omega_b, \rho_b, C_b$ et $T_b$ désignent respectivement le taux de perfusion, la masse volumique du sang, la capacité thermique

massique du sang, et la température du sang. $Q$ correspond au terme source de chaleur, proportionnel à l'intensité acoustique.

A partir des cartographies de températures dans les tissus, les dommages thermiques induits à la paroi veineuse lors des traitements HIFU ont été déterminés en utilisant un modèle dédié de dommages thermiques vasculaires formalisé par Agah *et al.* [77] et basé sur l'équation d'Arrhenius. Ce modèle suggère que le dommage thermique à la paroi de la veine est corrélé à la dénaturation des fibres de collagène des parois vasculaires. Il est exprimé par Ω et donné par :

$$\Omega(\mathbf{x},t) = A_f \int_0^{\tau} \exp\left(\frac{-E_a}{RT(\mathbf{x},t)}\right) dt$$

où Ω désigne l'endommagement de la paroi vasculaire, $A_f$ le facteur de fréquence, $E_a$ l'énergie d'activation, $R$ la constante des gaz parfaits et $T$ la température. Les paramètres $E_a$ et $A_f$ ont été fixés à $E_a =$ 430 kJ.mol$^{-1}$ et $A_f = 5.6 \times 10^{63}$ s$^{-1}$ conformément à Agah *et al.* [77].
Le seuil des dommages a été fixé à $\Omega$=5, correspondant formellement à la dénaturation de 99 % du collagène.

Pour les deux types de tirs considérés, les résultats des simulations ont montré que : (1) 13 tirs stationnaires espacés de 1.5 mm le long de la veine et (2) 37 tirs en mouvement distants de 0.5 mm permettraient d'endommager de manière homogène et irréversible le vaisseau sur une longueur de 2 cm. Les Figure 8-6 et Figure 8-7 montrent les distributions des dommages thermiques à l'intérieur des tissus pour les deux types de tirs.

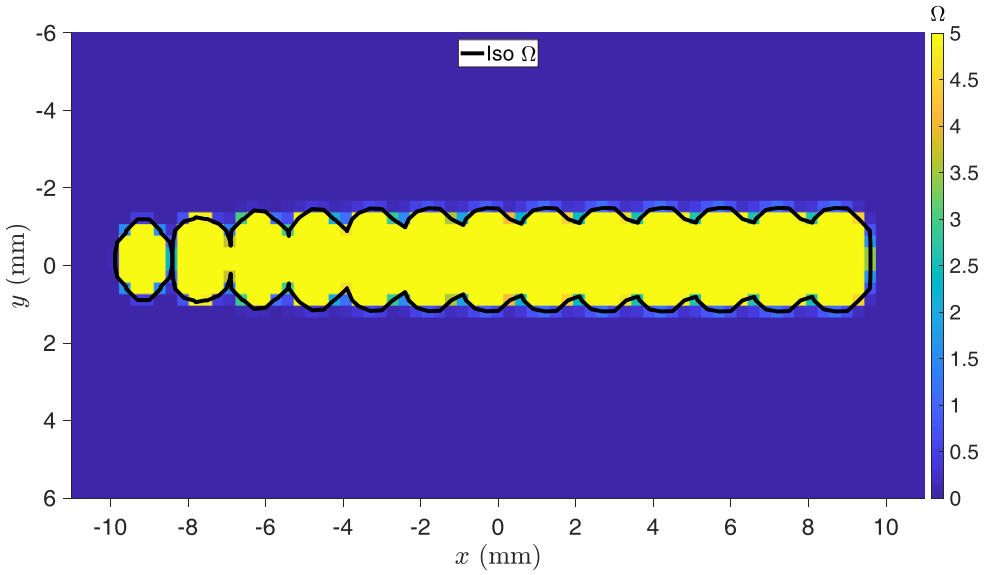


**Figure 8-6 – Distribution du dommage thermique après un traitement HIFU composé de 13 tirs HIFU stationnaires espacés de 1.5 mm et délivrés pendant 4 s à une puissance acoustique de 85 W.**

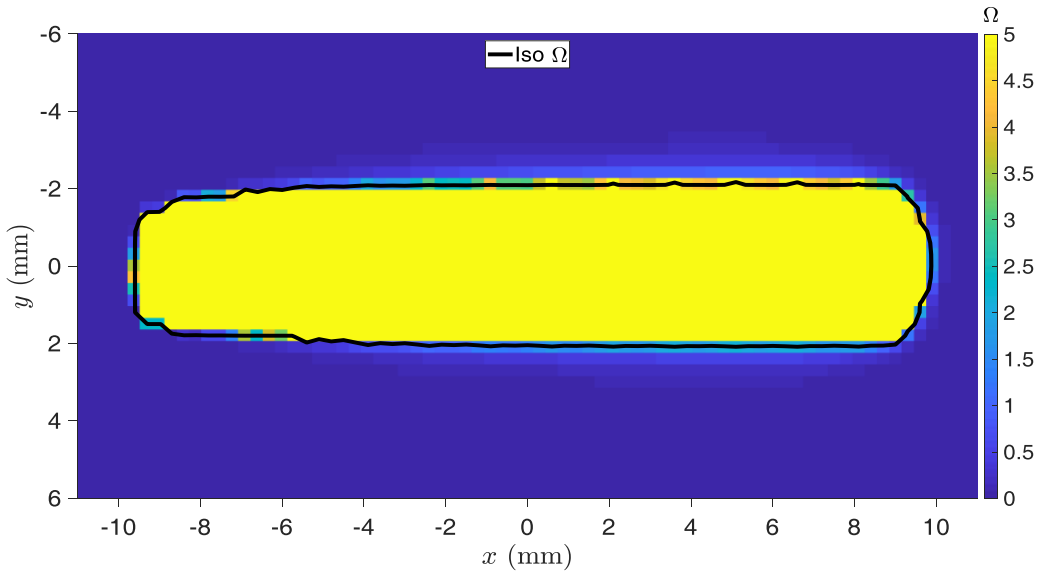


**Figure 8-7 – Distribution du dommage thermique après un traitement HIFU composé de 37 tirs HIFU en mouvement vertical, espacés horizontalement de 0.5 mm et délivrés pendant 4 s à une puissance acoustique de 85 W.**

## Expérimentations animales

Sur la base des résultats des simulations, les agencements de tirs ont été évalués *in vivo* sur veines saphènes de lapins. Au total 27 veines saphènes de 2 ± 0.6 mm de diamètre ont été exposées à des tirs HIFU à 3 MHz. Pour 30 % des traitements, le flux sanguin était arrêté

pendant les tirs par compression mécanique. Après traitement, les animaux ont été réveillés et maintenus en vie pendant une durée moyenne de 15 jours. A la fin du suivi, les animaux ont été sacrifiés et les vaisseaux ont été prélevés pour analyse histologique. D'après les données histologiques, 82 % des veines étaient fermées. Les vaisseaux traités avec compression pendant les tirs affichaient un taux d'occlusion de 100 %. La Figure 8-8 montre des exemples de coupes histologiques typiques des vaisseaux traités avec des tirs fixes et en mouvement.

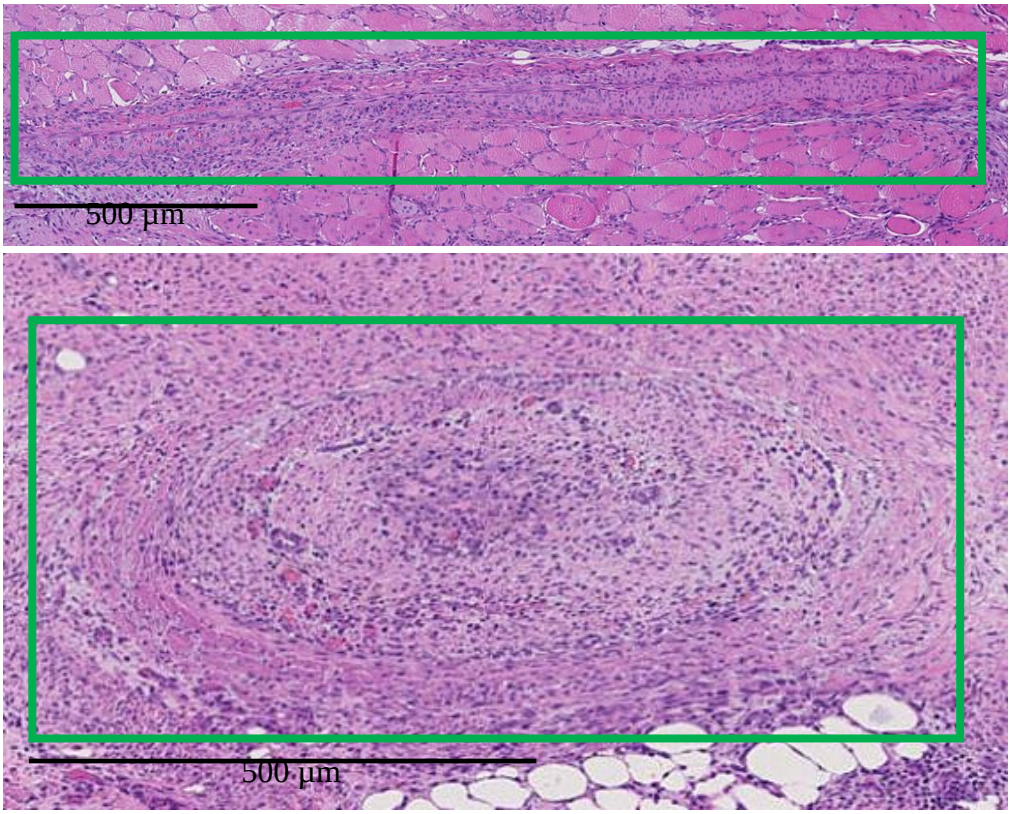


**Figure 8-8 – Coupes HE de veines saphènes de lapin traitées avec tirs stationnaires (haut) et des tirs en mouvement (bas), affichant une occlusion.**

Ces études animales ont démontré la possibilité d'occlure des petits vaisseaux de façon durable par dommages thermiques avec le dispositif HIFU de Theraclion. Ces études ont de plus souligné l'importance de la compression de la veine pendant les tirs pour arrêter le flux sanguin. Ces travaux ont enfin donné lieu au dépôt d'un brevet, et à la publication d'un article dans le journal Physics in Medicine and Biology [92].

## Caractérisation de l'échauffement thermique lors de l'insonification d'une veine de diamètre égal ou supérieur à 4 mm

L'objet de cette étude était d'évaluer une nouvelle méthode d'ablation thermique par HIFU basée sur l'utilisation de pulses de durée plus longue (8 secondes).

Afin de définir une technique de traitement pertinente et efficace pour le traitement des varices, nous nous sommes basés sur les recommandations de traitement des méthodes thermiques endovasculaires.

Pour qu'un traitement soit efficace, il est préconisé d'endommager la paroi vasculaire de façon homogène le long de la veine [73], [105], [106]. Pour ce faire, le traitement par radiofréquence (RF), dont la méthode est la plus codifiée [158], recommande de chauffer la veine entre 70 °C et 120 °C (les températures variant suivant le dispositif RF).

Nous avons dans cette étude déterminé l'espacement maximal le long de la veine entre deux tirs HIFU consécutifs de 8 secondes, pour coaguler de façon continue un segment veineux. Pour ce faire, le profil de température généré par ce nouveau tir a d'abord été estimé grâce à des données de températures obtenues *in vivo* sur des veines saphènes de brebis (diamètre moyen de 5 mm). Des thermocouples, insérés dans la veine saphène, ont mesuré l'élévation de température à la paroi à différentes positions par rapport au point focal lors de l'émission de plusieurs tirs HIFU de 8 secondes à 85 W acoustique.

Les mesures de températures ont été recalées en temps et en espace (Figure 8-9). A chaque pas de temps, les courbes de températures ont été ajustées avec une fonction gaussienne. Le profil final spatiotemporel de la distribution de température générée par un tir HIFU a été estimé (Figure 8-9, Bas).

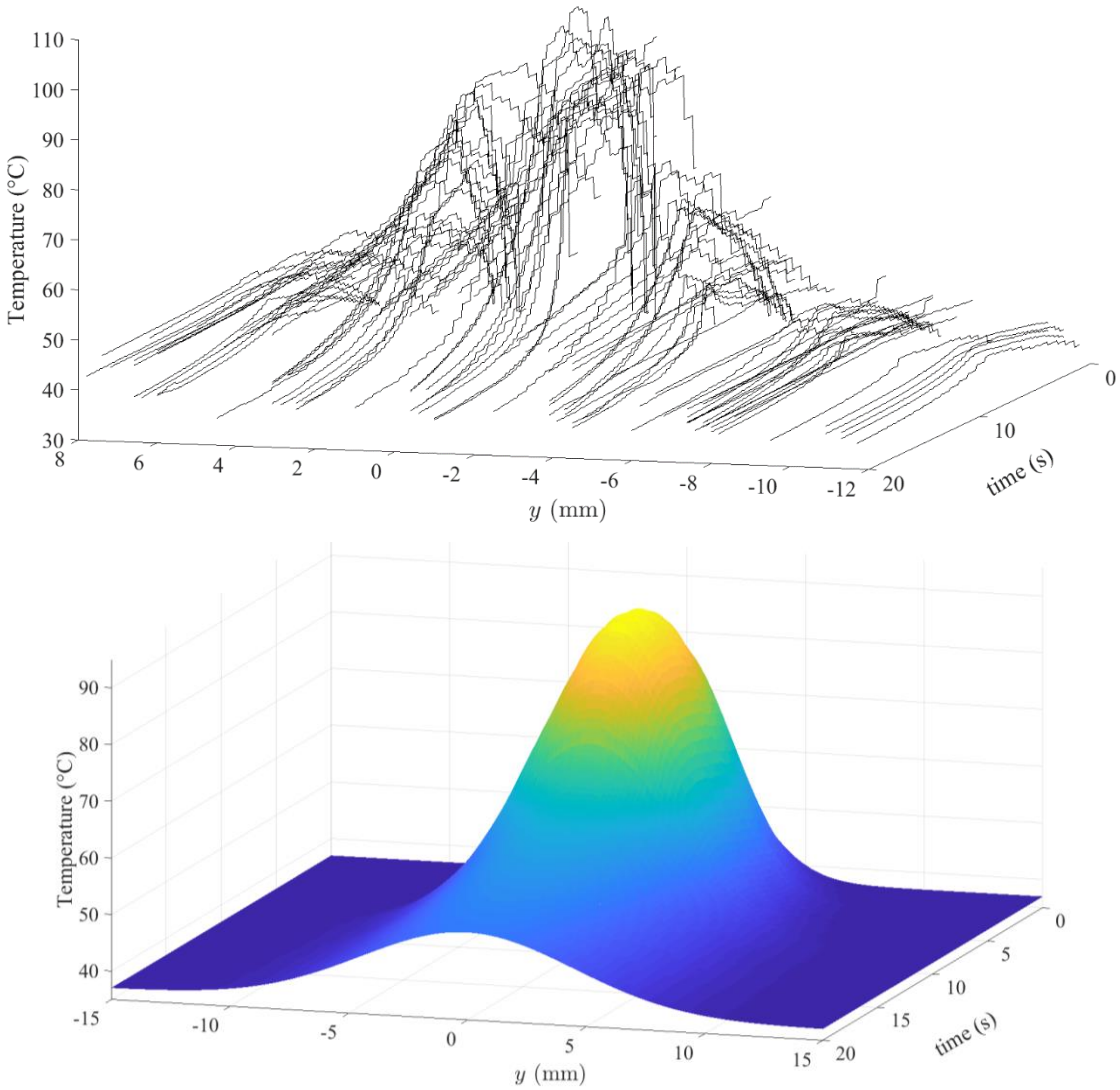


**Figure 8-9 – Recalage dans le temps et dans l'espace des courbes de température (Haut), Profil estimé de la distribution spatiotemporelle de la température (Bas).**

Sur la base de cette distribution spatiotemporelle de la température et en utilisant le modèle de dommages vasculaires décrit par Agah *et al* [77], l'étendue des dommages thermiques le long de la veine a été estimée.

Nous avons montré que les tirs HIFU devaient être espacés les uns des autres de 3.6 mm au maximum pour obtenir un dommage thermique continu le long de la veine (Figure 8-10).

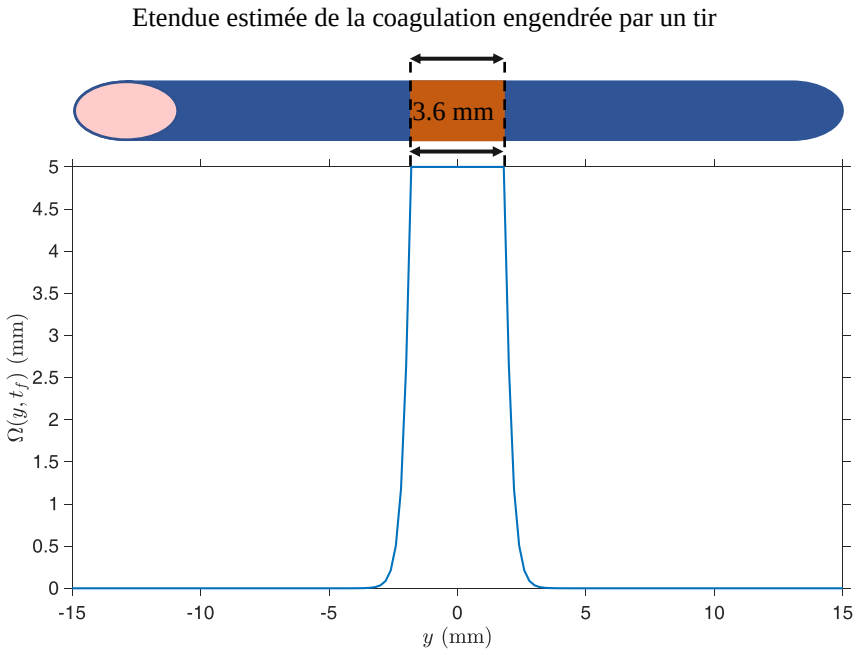


**Figure 8-10 – Estimation de l'endommagement ($\Omega(y,t_f)$) engendré par un tir HIFU.**

Dans cette étude, les maximums de températures enregistrées lors des traitements HIFU ont été comparés à celles atteintes lors de traitement par radiofréquence. La température engendrée à la paroi lors de nos traitements HIFU est située dans la même plage de températures que celle induite avec les dispositifs actuels de traitement par radiofréquence ClosurePlus®, ClosureFast®, Venclose®, Celon® (Figure 8-11).

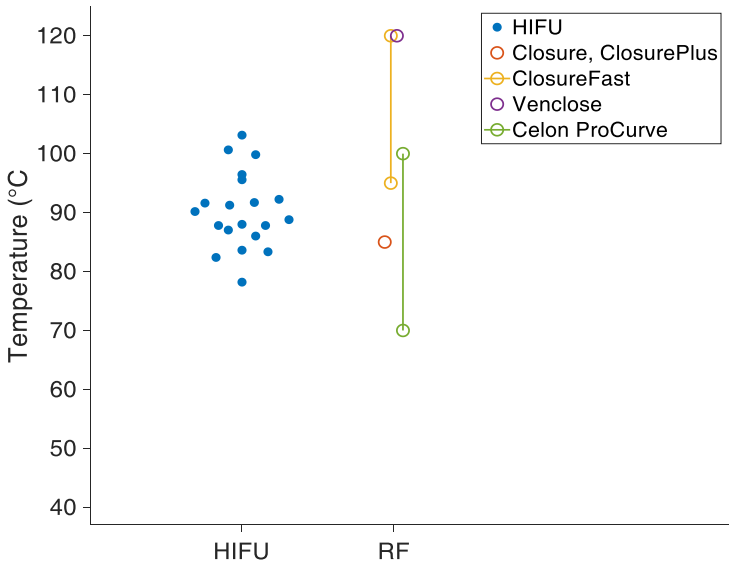


**Figure 8-11 – Comparaison des températures entre les traitements HIFU et les traitements par radiofréquence.**

# Effets immédiats des traitements HIFU sur les tissus : quantification des dommages et validation d'un modèle de rétrécissement de la veine

Nous avons étudié ici la réaction immédiate des tissus après traitements HIFU. Nous avons en particulier évalué le rétrécissement de la paroi veineuse survenant à la suite d'un échauffement intense.

La rétraction de la veine a une valeur prédictive de succès pour le traitement des varices, d'après l'expérience clinique dans l'utilisation des méthodes thermiques endovasculaires [76], [116]–[122]. Une réduction du calibre veineux d'au moins 50 % est un signe garant d'un succès, ainsi qu'un marqueur de durabilité à long-terme [125], [158], [159]. L'efficacité de notre technique d'ablation thermique HIFU a donc été établie sur la base du pourcentage de constriction de la veine obtenu immédiatement après traitements.

Compte-tenu de la nécessité de traverser des tissus superficiels (gras, muscle) pour atteindre la veine et des coefficients d'absorption élevés des ultrasons dans ces tissus, des dommages péri-veineux sont attendus. Nous avons ici évalué les tailles des lésions engendrées après traitement HIFU.

Cette étude a été menée sur six brebis. Des traitements HIFU ont été délivrés sur la veine saphène latérale de la patte gauche de chaque brebis. Des tirs HIFU de 8 secondes à une puissance acoustique moyenne de 61 ± 15 W ont été délivrés.

A la fin de la procédure, la constriction veineuse a été quantifiée par imagerie mode B. En fin de traitement, toutes les veines étaient rétractées. Elles affichaient en moyenne une réduction de 53 ± 14 % de leur calibre initial. Figure 8-12 montre un exemple de rétraction veineuse observé immédiatement après traitements HIFU.

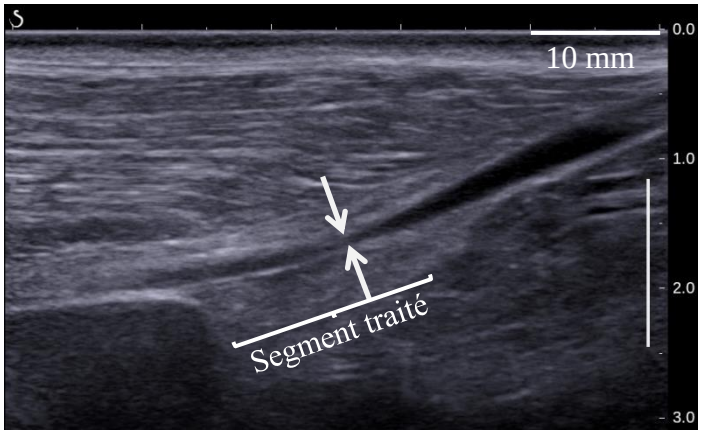


**Figure 8-12 – Imagerie échographique d'une veine saphène de brebis affichant après traitements HIFU un rétrécissement de son calibre.**

Les données quantitatives des rétractions veineuses ont également été utilisées pour valider un modèle numérique pour prédire le rétrécissement veineux engendré après traitements HIFU. La constriction veineuse a été estimée à partir de différents diamètres initiaux des veines de brebis (2.3, 3.5 et 5.2 mm). Les valeurs estimées par le modèle corrélaient bien avec celles mesurées (Figure 8-13). Les résultats ont donc permis de valider le modèle.

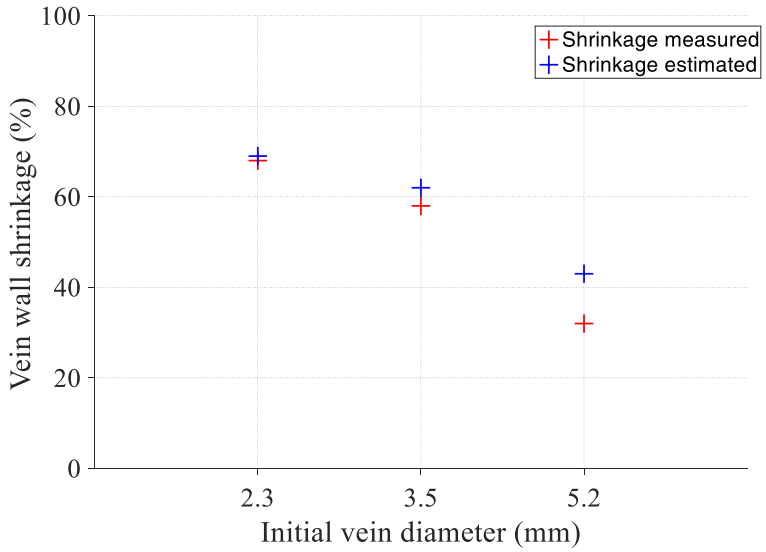


**Figure 8-13 – Comparaison des simulations avec les résultats expérimentaux.**

Après euthanasie, les animaux, en position de traitement, ont été emmenés en chambre froide et congelés à -17 °C pendant 48 heures minimum. Les pattes d'intérêt ont été extraites et des sections millimétriques de la région d'intérêt ont été découpées à la scie à ruban. Chaque section a été photographiée et la lésion, la paroi et la lumière veineuse ont été manuellement segmentées avec l'outil Slicer 3D (Figure 8-14).

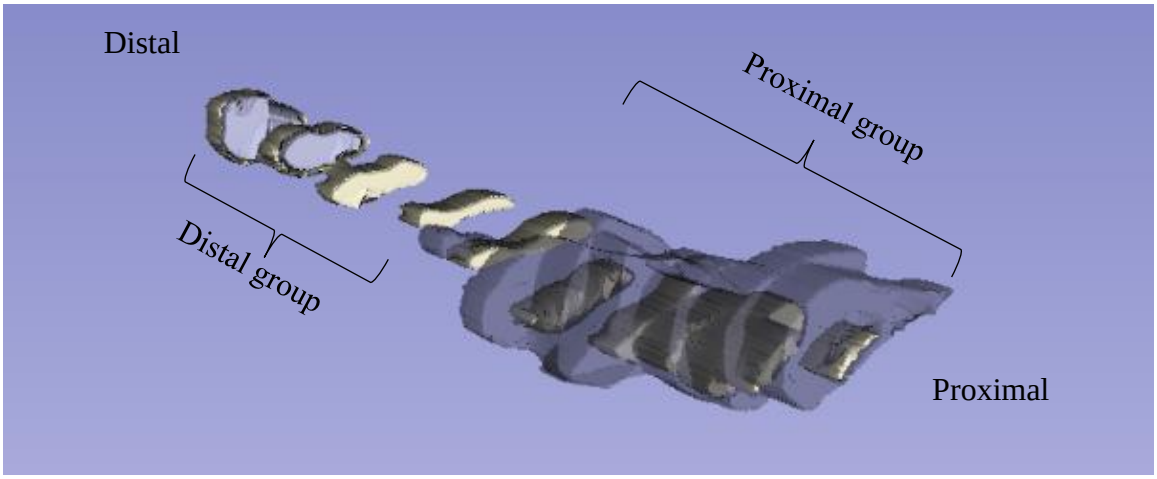


**Figure 8-14 – Reconstruction 3D des dommages thermiques (contours gris foncé), de la paroi (contours blancs) et lumière veineuse (contours mauves).**

En moyenne les lésions s'étendaient sur 8.0 ± 2.9 mm dans la direction de propagation des ultrasons et sur 4.7 ± 1.2 mm perpendiculaire à la direction de propagation des ultrasons (et transverse à la veine).

## Caractérisation macroscopique et microscopique des dommages thermiques 30, 60 et 90 jours après traitements HIFU

Dans le but d'obtenir une autorisation d'essai clinique, nous avons cherché à démontrer ici que notre méthode de traitement par HIFU permettait de coaguler des veines de manière efficace et sûre. Pour étudier la formation de fibrose veineuse conduisant à l'occlusion définitive de la veine, des études pré-cliniques avec suivi distant ont été menées.

Les expérimentations animales ont été réalisées chez la brebis sur les veines saphènes latérales. Cette veine, de diamètre compris entre 3 et 6 mm, présente des similitudes avec la veine saphène humaine. Tout comme chez l'humain, elle est entourée d'un fascia. De plus, cette veine fait partie du système veineux superficiel, et son occlusion n'engendrera donc pas de problèmes fonctionnels.

Dans cette étude, neuf brebis et dix-huit veines ont été traitées par HIFU. Les veines ont été exposées au même traitement HIFU. Pour chaque veine, une séquence de plusieurs sites de tirs distants de 3.5 mm le long de la veine (conformément aux simulations précédentes) a été délivrée. Les ultrasons focalisés, à la fréquence de 3 MHz, ont été délivrés pendant 8 secondes à une puissance acoustique de 85 W. Après traitement, les animaux ont été réveillés pour que le processus de fibrose puisse avoir lieu. Afin d'étudier la cinétique de la fibrose veineuse, les brebis ont été euthanasiées après différentes durées : 30, 60 et 90 jours après traitement. Le bien-être animal a été évalué pendant la durée de suivi. Aucune complication ni gêne fonctionnelle n'a été observée chez aucune brebis. Après traitement et juste avant euthanasie, les veines traitées ont été observées par imagerie ultrasonore. Une réduction du diamètre a été observée pour toutes les veines traitées.

Les veines traitées ainsi que les tissus environnants ont été prélevés *post-mortem* et analysés par histologie. Lors de l'extraction des échantillons, aucune perforation pariétale ni carbonisation de la veine traitée n'a été observée.

A 30 jours, les lésions histologiques observées ont mis en évidence une nécrose de coagulation de la paroi veineuse ainsi qu'une nécrose localisée des tissus adipeux et musculaires environnants. A 60 jours, une évolution vers la fibrose a été observée dans toutes les régions lésées (paroi veineuse, tissus adipeux et musculaires). A 90 jours, la fibrose était complète et considérée stable dans tous les sites examinés.

La Figure 8-15 montre une image échographique et une coupe histologique d'une veine saphène de brebis 90 jours après traitements HIFU.

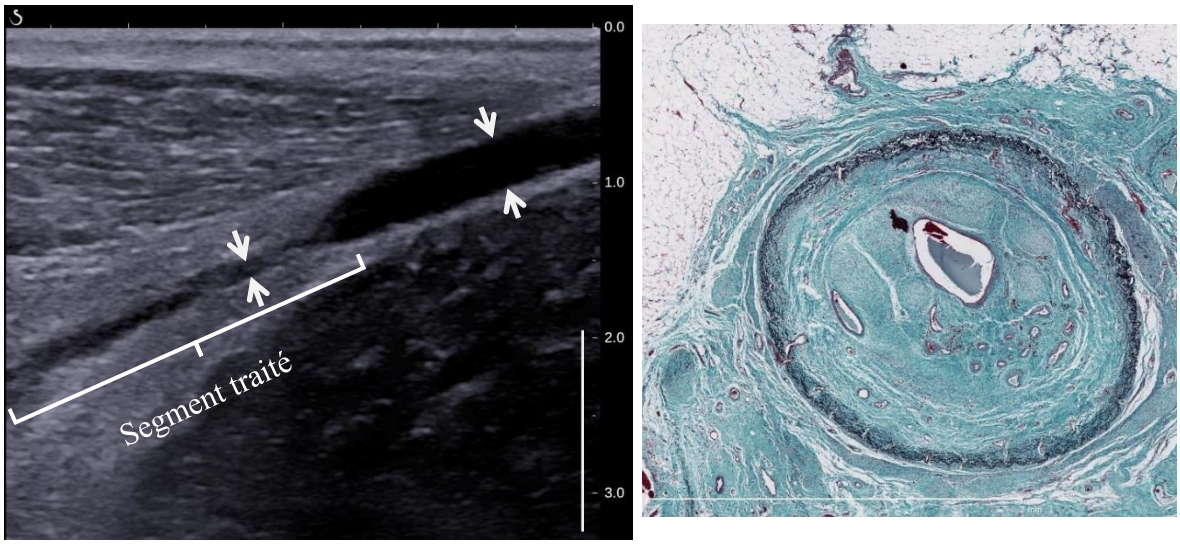


**Figure 8-15 – Image B-mode (gauche) et coupe histologique (Droite) d'une veine saphène de brebis 90 jours après traitements HIFU.**

Selon l'histopathologiste, aucune lésion histologique observée à 30,60 et 90 jours ne pose de problème sur le plan de la sécurité. Toujours selon l'histopathologiste, les dommages tissulaires après traitement HIFU sont similaires à ceux observés après traitement par radiofréquence. Notre méthode d'ablation par HIFU induit les mêmes effets aux tissus que la technique endovasculaire par radiofréquence, mais de façon non invasive.

Les résultats de cette étude ont démontré et validé sur la brebis l'efficacité et la sécurité de notre technique d'ablation thermique extracorporelle par ultrasons focalisés de haute intensité.

# Conclusion

L'ensemble de ces travaux a permis à Theraclion d'obtenir l'autorisation de conduire un essai chez l'homme, visant à valider le traitement des veines pathologiques par ultrasons focalisés de haute intensité. Cette investigation clinique, réalisée en Autriche, a abouti à des résultats très positifs et a permis, en sus des résultats précliniques de cette thèse, l'obtention du marquage CE du dispositif HIFU de Theraclion pour cette indication clinique.

# Scientific output

## Publications in peer-reviewed journals

### Published

N. Barnat, A. Grisey, B. Lecuelle, J. Anquez, S. Yon, J-F. Aubry. **Noninvasive vascular occlusion with HIFU for venous insufficiency treatment: preclinical feasibility experience in rabbits.** *Physics in Medicine and Biology. 2019.*

N. Barnat, A. Grisey, B. Gerold, S. Yon, J. Anquez, J-F. Aubry. **Efficacy and safety assessment of an ultrasound-based thermal treatment of varicose veins in a sheep.** *International Journal of Hyperthermia. 2020.*

### Submitted

N. Barnat, A. Grisey, J. Anquez, B. Gerold, S. Yon, J-F. Aubry. **Vein wall shrinkage induced by thermal coagulation with HIFU: numerical modelling and *in vivo* experiments in sheep.** *Submitted, International Journal of Hyperthermia.*

## Presentations

N. Barnat*, A. Grisey, B. Lecuelle, J. Anquez, S. Yon, J-F. Aubry. **Vascular occlusion by HIFU for treating venous insufficiency: feasibility study in rabbits**. *Oral presentation, ISTU 2018, Nashville, USA.*

N. Barnat, A. Grisey, J. Anquez, B. Gerold, S. Yon, J-F. Aubry[+]. **Controlled luminal shrinkage with thermal HIFU for venous insufficiency treatment**. *Oral presentation, FUS 2018, Virginia, USA.*

N. Barnat, A. Grisey, J. Anquez, B. Gerold, S. Yon, J-F. Aubry[+]. **Sub-chronic venous occlusion with thermal HIFU for venous insufficiency treatment: a preliminary study on rabbit saphenous veins**. *Oral presentation, FUS 2018, Virginia, USA.*

N. Barnat*, A. Grisey, B. Gerold, J. Anquez, S. Yon, J-F. Aubry. **Macroscopic and microscopic evaluation of HIFU thermal ablations of sheep veins at 30, 60 and 90 days.** *Oral presentation, ISTU /EUFUS 2019, Barcelona, Spain.*

[+] Presented by Jean-François Aubry due to visa's problems. I trumped all other problems and despite of this finished my thesis.

## RÉSUMÉ

Cette thèse avait pour objectif le développement d'une méthode d'ablation thermique non-invasive des veines par ultrasons focalisés de haute intensité (HIFU). Elle a pour but de démontrer la preuve de concepts et permettre à terme le traitement des varices des membres inférieurs avec le dispositif de Theraclion.
La possibilité d'occlure des vaisseaux de petits calibres a tout d'abord été investiguée. Deux procédures de traitement candidates ont été évaluées par simulations numériques puis *in vivo* sur des veines de lapin. L'analyse histologique a démontré l'efficacité des traitements, en particulier lorsque les vaisseaux étaient comprimés lors des tirs.
Une nouvelle procédure d'ablation thermique a ensuite été conçue pour coaguler des veines de plus gros calibres, de diamètre plus proche des varices humaines. Des mesures de températures *in vivo* sur des veines de brebis lors de tirs HIFU ont permis d'estimer le pas de tir permettant d'obtenir une coagulation continue le long de la veine. Des essais en aigu sur des veines saphènes de brebis ont permis de quantifier les dommages thermiques et de valider l'efficacité immédiate de notre méthode de traitement. Enfin, une étude avec suivis distants jusqu'à 90 jours a été conduite chez la brebis afin d'étudier l'efficacité et la sécurité à long terme de notre méthode de traitement. L'analyse histologique des dommages thermiques a validé sur la brebis la performance et la sécurité de notre méthode d'ablation thermique. D'un point de vue histopathologique, les dommages engendrés par nos traitements HIFU se sont également révélés similaires à ceux observés après traitement par radiofréquence, une technique endovasculaire d'ablation thermique des varices.
L'ensemble de ces travaux a permis à Theraclion d'obtenir l'autorisation de conduire un essai clinique sur 50 patients. Les résultats très positifs de cette étude ont conduit à l'obtention du marquage CE du dispositif HIFU pour cette indication thérapeutique.



## MOTS CLÉS

HIFU, ultrasons focalisés, varices, veines, ablation thermique, simulations numériques, essais précliniques, essais cliniques.



## ABSTRACT

A novel thermal approach to treat non-invasively incompetent veins with high-intensity focused ultrasound (HIFU) is presented in this thesis.
The ability to occlude small veins was first investigated. Two different sonication procedures were evaluated by numerical simulations and tested *in vivo* on rabbit veins. The histologic examination of the treated veins demonstrated the efficacy of the treatments, especially when the vein was compressed during ultrasonic exposures.
A new procedure was then designed in order to coagulate larger veins, closer to human vein diameters. Experimental temperature measurements at the vein wall during HIFU pulses were used as inputs to determine numerically the optimum spacing between the pulses in order to induce a continuous coagulation along the vein. Acute animal trials on sheep veins were conducted to quantify tissue damages following such treatments. Finally, chronic studies up to 90 days were conducted on sheep in order to evaluate the long-term safety and efficacy of our treatment procedure. The histological findings validated the performance and safety of our HIFU thermal method, in a sheep model. From a pathology standpoint, the HIFU lesions are similar to those observed after radiofrequency ablation (an endovenous thermal modality used for the treatment of varicose veins).
The results presented in this thesis allowed Theraclion to get the authorization to conduct first-in-human clinical trials for varicose vein treatments. The results were very encouraging and led to the CE-marking of the HIFU system.



## KEYWORDS

HIFU, focused ultrasound, varicose veins, veins, thermal ablation, numerical simulations, preclinical trials, clinical trials.